TLR7/8 AGONIST ENCAPSULATING POLYMERIC NANOPARTICLES FOR CANCER IMMUNOTHERAPY

A DISSERTATION
SUBMITTED TO THE FACULTY OF
UNIVERSITY OF MINNESOTA
BY

HYUNJOON KIM

IN PARTIAL FULFILLMENT OF THE REQUIREMENTS
FOR THE DEGREE OF
DOCTOR OF PHILOSOPHY

JAYANTH PANYAM
ADVISOR

OCTOBER 2018

ACKNOWLEDGEMENTS

‘Flower road’ is a metaphor in South Korea, to describe a person’s journey filled with happiness and joy that guide traveling to the destination. I am very fortunate that my five years in graduate school were like walking on the flower road. I appreciate the many blooms of support that were along my journey along.

I would first like to thank my advisor Dr. Jayanth Panyam. He has been a great mentor and a good friend over the years. I appreciate his encouragement to me to become an independent researcher. Instead of telling me what to do and what to not to, which would have been much easier, he let me think on my own and speak up my ideas. I also appreciate his patience as a mentor. I walked to his office at least twice a day to discuss the research, future career, and to chat about the Vikings and Timberwolves. Although he was busy with meetings and writing grants, he always greeted with me with a smile and was willing to listen and address my concerns. To me, his office was an oasis of answers and rests.

I would like to express my deep gratitude to Dr. Thomas Griffith and his group members. As a pharmaceutical student majoring in nanoscience, I faced many challenges when starting the immunology based nanovaccine project. However, Dr. Griffith has enhanced my training and perspective in immunology. I particularly appreciate his time as a chaperone when we traveled to MD Anderson Cancer Center in Houston for my training. Besides the scientific discussions, he was a great person to talk about the baseball and Marvel comics. I also thank Tammy for helping me with the experiments and greeting me with warm welcome. I thank Dr.Katie Murphy who taught me how to do 10+ color flow cytometry and Frankie and Whitney for being great friends

I would like to acknowledge Dr. Timothy Wiedmann and Dr. Ronald Siegel for being my committee members. Their critical reviews and feedbacks in my oral preliminary exam was invaluable, which led to significant improvements in my research. Besides committee members, I would like to thank Dr.William Elmquist and Dr.Cheryl Zimmerman for the great lectures on Pharmacokinetics. I also appreciate Dr.Raj Suryanarayanan, Dr. Calvin Sun, Dr. Karunya Kandimalla and Dr. Carolyn Fairbanks for helpful feedbacks in the department seminars.

I also want to thank Pharmaceutics administrative staff; Candy McDermott, Katie James, Amanda Hokanson, and Jody Tracy. You were like magical genies, who made my life a lot easier. I could focus on my research because you handled everything else.

The research staff at University of Minnesota also deserves recognition. I appreciate John Oja and Guillermo Marques at the University Imaging Center for the training on multiple imaging instruments and Elizabeth Lundstrom at the Geochemical lab for assistance on ICP-MS analysis. I also appreciate Hanseung Lee at the CharFac for the SEM and TEM imaging. I thank RAR staff; Brenda Koniar and Felicia Boynton for the assistance on the animal studies.

For the past five years, I have met wonderful people in the lab. I spend more time with them than my family, which made me feel like brothers and sisters. I first would like to thank lab alumni Dr. Tanmoy Sadhukha, Dr. Lin Niu, Dr. Ameya Kirtane, Dr. Garvey Liu and Dr. Stephen Kalscheuer. You shared your precious time to teach me experiments and helped me to be a part of the laboratory. I also thank my current lab members Dr.Gopi Moku, Dr. Buddhadev Layek, Vidhi Khanna, Drishti Sehgal, Wenqiu Zhang, Yafan Su and

Jiawei Wang. It has been a wonderful time working with you. Special thanks to Vidhi, Drishti and Wenqiu for their contributions in completing my thesis projects.

I also thank mentors in Korea, who encouraged me to pursue Ph.D in the US. I thank Dr. Kyungho Moon, for his endless support and trust in me to become a scholar. I appreciate Dr.Kwangmeyung Kim and Dr.Juhee Ryu for giving me the opportunity to work at the best research institute in Korea. Special thanks to Sun-ah Kim, for teaching me all the experimental techniques that I know today.

I also thank my friends for their support. I could have not completed the graduate school, if there was no 'fun' in my life, which you brought. I wish you all the best as well.

I want to thank my special one, Seenae. She painted colors and added the flavors to my boring life. My life in Minnesota changed 180º, since I met you. I would have been much more cranky and grouchy person, if you didn't make me smile. Thank you for believing in me and loving me.

Finally, I have to express my deepest gratitude to my parents. Their unconditional love and support made what I am today. I appreciate them for being good role models. I always admire their diligence, faithfulness and sincere attitude built up successful careers. I appreciate my father, Dr. Kim, for being the perfect role model as a scholar. I thank my mother for her endless passion and professionalism in her career, which inspires me to work harder. Many thanks to you and wish you to be healthy.

DEDICATION

This thesis is dedicated to my parents Dr. Byungmin Kim and Hyunjoo Choi.

ABSTRACT

The immune system is important for the prevention of cancer and formed the basis of cancer immunotherapy. That is, enhancement of the immune response for the treatment of malignant cancer cells. The field has undergone significant progress to include the use of checkpoint inhibitors, monoclonal antibodies and cytokine therapies. In addition, a cancer vaccine, composed of tumor associated antigens (TAAs) and vaccine adjuvant, is particularly promising. Effective vaccines can mobilize tumor-specific CD8 T cells to kill selectively tumor cells with cytotoxic granules and secrete IFN-ɣ that sensitize tumors to be susceptible to effector immune cells. Additionally, activated CD8 T cells become memory cells and can respond to same TAA-epitopes, which can be effective for long-term protective immunity to inhibit cancer recurrence.

Activation of dendritic cells (DCs), which are the main antigen-presenting cells (APCs), is critical for T cell immunity. To an elicit tumor-specific CD8 T cell response, DCs have to process and present TAAs to CD8 T cells through the major histocompatibility complex (MHC) I. Moreover, co-stimulatory signals and pro-inflammatory cytokines are required to stimulate CD 8 T cells. However, CD8 T cell anergy and exhaustion will occur if TAA treatment is not sufficiently immunogenic to trigger DC activation. Therefore, development of immunostimulatory adjuvant that can trigger DC activation can enhance therapeutic efficacy of cancer vaccines.

Imidazoquinoline-structured synthetic toll-like receptor (TLR) 7/8 agonists are strong cytokine inducers that can be a potent vaccine adjuvant. TLR7/8 ligation can

activate MyD88 signaling pathways and stimulate DCs to upregulate co-stimulatory molecules and secrete pro-inflammatory cytokines and type I interferons. However, TLR7/8 agonists lack prominent efficacy *in vivo* due to the rapid clearance from the injection site. Following subcutaneous (SC) injection, small molecules enter the systemic circulation via blood capillaries and only small portion can reach the draining lymph nodes. Therefore, our goal was to develop a SC injectable drug carrier that can more efficiently deliver as well as prolong duration of at the site of action of TLR7/8 agonists.

In this study, we fabricated poly(lactide-co-glycolide) (PLGA) nanoparticles (NPs) containing TLR7/8 agonists. Nanoparticulate delivery of TLR7/8 agonist showed enhanced DC activation and antigen-presentation compared to the soluble form of TLR7/8 agonists. When combined with peptide/tumor cell lysate-based antigens, NPs potentiated the antigen-specific CD8 T cell expansion and increased cytotoxic functions, which resulted in enhanced efficacy in both prophylactic and therapeutic tumor models.

To further enhance endo/lysosomal delivery of TLR7/8 agonists in PLGA NPs, we included a sodium bicarbonate-mediated gas-generating system that is acidic pH-responsive. This approach resulted in 33-fold greater amount of TLR7/8 agonists encapsulated within the NPs. More importantly, the PLGA NP immunization elicited a stronger CD8 T cell response compared to conventional PLGA NPs, which in turn, enhanced therapeutic efficacy.

As tumor microenvironment is immune suppressive, we examined whether modulation of tumor microenvironment can enhance the therapeutic efficacy of cancer vaccine. We reduced the immune suppressive cells including myeloid-derived suppressive

cells (MDSCs) and regulatory T cells (Tregs) by daily oral dosing of a tyrosine kinase inhibitor (TKI), sunitinib. Additionally, we adapted an anti-PD-L1 antibody to block programmed death ligand 1 (PD-L1) expressed on tumor-associated (M2) macrophages and MDSCs that exhaust CD8 T cells, to augment the CD8 T cell activation at the tumor. In our study, combination of sunitinib and PD-L1 blockade significantly decreased the immune suppressive cell population and reduced PD-L1 expression on these cells. We also examined if nanoparticulate delivery of TLR7/8 agonist can potentiate NK cell-mediated cancer immunotherapy through its known effect on TH1 immunity. Antibody-dependent cellular cytotoxicity (ADCC) of monoclonal antibodies was found to be augmented in response to TLR7/8 agonist encapsulating NPs as a vaccine adjuvant.

Overall, our studies demonstrate that PLGA NPs broaden the application of TLR7/8 agonists for improved cancer treatment. Moreover, this platform holds promise to enhance the efficacy of cancer vaccines composed of tumor associated antigens (TAAs) and vaccine adjuvant

TABLE OF CONTENTS

LIST OF TABLES

LIST OF FIGURES

LIST OF ABBREVIATIONS

522GGNP	Acidic-pH responsive, gas generating 522NP
522NP	PLGA NP encapsulating 522
ACT	Adoptive cell transfer
ADCC	Antibody-dependent cellular cytotoxicity
APC	Antigen presenting cell
BMDC	Bone marrow derived dendritic cell
CAR	Chimeric antigen receptor
CFSE	Carboxyfluorescein succinimidyl ester
CpG ODN	CpG Oligodeoxynucleotide
CTL	Cytotoxic T lymphocytes
CTLA	Cytotoxic T lymphocyte antigen 4
DC	Dendritic cell
DMSO	Dimethyl sulfoxide
DLS	Dynamic light scattering
DMEM	Dulbecco`s Modified Eagle Media
EGFR	Epidermal growth factor receptor
EPR	Enhanced permeability and retention
Free522	Soluble form of 522 in DMSO
GAG	Glycosaminoglycans
GM-CSF	Granulocyte-macrophage colony stimulating factor
HER2	Human epidermal growth factor receptor 2

HPLC	High-performance liquid chromatography
IFN	Interferon
IM	Intramusculuar
IL	Interleukin
IP	Intraperitoneal
IRF	Interferon-regulatory factor
IV	Intravenous
LPS	Lipopolysaccharide
MAPK	Mitogen-activated protein kinases
mDC	Myeloid DC
MDSC	Myeloid derived suppressor cells
MHC	Major histocompatibility complex
MW	Molecular weight
MyD88	Myeloid differentiation primary-response gene 88
NF-κB	Nuclear factor-kappa B
NK cells	Natural killer cells
NP	Nanoparticle
OVA	Ovalbumin
PAMP	Pathogen associated molecular pattern
PBMC	Peripheral blood mononuclear cells
PBS	Phosphate buffered saline
pDC	Plasmacytoid DC

PLGA	Poly(lactide-co-glycolide)
Poly:IC	Polyinosinic:polycytidylic acid
PD-1	Programmed death-1
PD-L1	Programmed death-ligand 1
PFA	Paraformaldehyde
PRR	Pattern recognition receptor
PSK	Polysaccharide krestin
PVA	Polyvinyl alcohol
RPMI	Roswell Park Memorial Institute
SC	Subcutaneous
SEM	Scanning electron microscope
TAA	Tumor associated antigen
TAM	Tumor associated macrophage
TCR	T cell receptor
TEM	Transmission electron microscope
TIR	Toll/IL-1R
TKI	Tyrosine kinase inhibitor
TLR	Toll like receptor
TNF	Tumor necrosis factor
Treg	Regulatory T cell
TRIF	TIR domain-containing adaptor protein inducing IFNβ
VEGF	Vascular endothelial growth factor

Chapter 1.

Introduction

1.1. Introduction to cancer immunotherapy

Cancer immunotherapy involving the use of host immune cells to attack the tumor cells has shown promising results in both pre-clinical and clinical studies[1]. Cancer immunotherapeutic strategies, including monoclonal antibodies, adoptive cell transfer, checkpoint inhibitors, and cancer vaccines, rely on mobilizing cytotoxic CD8 T cells and natural killer (NK) cells[2]. However, anti-tumor efficacy of immunotherapeutics is often hampered by insufficient potency to stimulate desired effector cells and the immune-suppressive tumor microenvironment[3]. Thus, improvement of the therapeutic outcome requires both potentiating the anti-tumor immune response as well as modulating the tumor microenvironment. To achieve these goals, potent immune stimulant and combination therapy with reagent(s) to downregulate immune-suppressive mechanisms were investigated. In this chapter, the background information that led to our specific approaches is provided. The remaining chapters describe the experimental details, results and discussion. The concluding chapter provides a summary and the significance of this work and possible directions for future research.

1.2. Cancer immunotherapeutics

Monoclonal antibodies play multiple roles in cancer immunotherapy with their ability to block tumor-promoting receptors, activating or inhibiting other immune cells and inducing antibody-dependent cellular cytotoxicity (ADCC) responses[4]. Monoclonal antibodies that target the tumor-specific receptors include cetuximab, which targets epidermal growth factor receptor (EGFR) and trastzumab, which targets human epidermal

growth factor receptor 2 (HER2)[5,6]. These antibodies block the tumor progression signaling and elicit ADCC responses to kill tumor cells. Tumor-angiogenic growth factors, including vascular endothelial growth factors (VEGF) and platelet-derived growth factor (PDGF), can be inhibited by bevacizumab[7]. Monoclonal antibodies that target leukemia/lymphoma related molecules including CD20, CD30, CD33 and CD52 are also approved therapeutics [8].

Checkpoint inhibitors are therapeutics that promote an anti-tumor response by neutralizing the inhibitory signals, which deactivate T cells and NK cells[9]. Cytotoxic T lymphocyte antigen 4 (CTLA4) is a homologue of CD8 T cell activating molecule CD28[10]. CTLA4 is expressed on CD8 T cells and can be activated by co-stimulatory molecules CD80 and CD86 of dendritic cells (DCs) and macrophages. Therefore, anti-CTLA4 antibodies can block the inhibitory CTLA4 and enhance CD8 T cell stimulatory CD28-CD80/86 signaling, which leads to activation of effector CD8 T cells.

Programmed death-1 (PD-1)/programmed death ligand-1 (PD-L1) signaling is also a major tumor escape mechanism. PD-L1 is expressed on tumor cells, monocytes, macrophages and myeloid-derived suppressive cells (MDSCs). PD-L1 ligates PD-1 expressed on CD8 T cells and NK cells and cause exhaustion of these cells [11]. It has been reported that upregulation of PD-L1 on solid tumors reduces the tumor-infiltration of T cells. With these aspects, PD-L1 is reported to be associated with poor prognosis of solid tumors and thereby is used as a biomarker for cancer immunotherapy[12,13].

Adoptive cell transfer (ACT) therapies that infuse effector cells to donor cells are also clinically used. ACT strategies include infusion of *ex vivo* stimulated T cells that were

isolated from patient tumors[14]. Engineered T cells that possess chimeric antigen receptor (CAR) or T cell receptor (TCR) are also a potent source for ACT-based cancer immunotherapy [15].

1.3. Cancer vaccine strategies and challenges

Cancer vaccines are developed to mobilize cytotoxic CD8 T cells and NK cells. To elicit a tumor-specific immune response, sufficient tumor-associated antigens (TAAs) must be provided to antigen presenting cells (APCs) including DCs, macrophages and B cells [16]. Immunostimulatory adjuvants are often required to enhance the activity of APCs to produce a sufficient immune response.

The first cancer vaccine was comprised of autologous tumor cells collected from patients. The benefit of autologous tumor cells is the large repertoire of antigens that covers TAAs of the patient's tumor [17]. Allogeneic tumor cell vaccines, which are mixtures of established immunogenic tumor cell lines, are also used for the treatment of melanoma and non-small cell lung cancer [18]. However, due to the limited availability of patients' samples and intricate procedures to prepare tumor cell vaccines, TAA associated peptide/proteins were investigated. As opposed to tumor cell vaccines, TAA peptide/proteins are cost-effective and can elicit TAA-specific T cell response and as such represent an advanced antigen source for cancer immunotherapy [19].

There are several types of TAAs. Antigens that are normally muted in the normal tissue but can be reactivated in tumor cells include MAGE-1, NY-ESO-1, BAGE, and SSX-2, which are cancer-testis antigens [20]. Antigens that are highly expressed compared

to normal tissues include melanoma antigens (gp100, MART-1) [21], prostate cancer antigens (PSA, PSP) [22], MUC-1 and HER-2 [23]. Mutated oncogenes, including RAS and BRAF, are reported to be uniquely expressed on the tumor cells [24] and therefore may be potent TAA peptide vaccines.

To elicit a TAA-specific T cell response, DCs need to be provided with sufficient amount of TAAs and be in mature state to present TAA to T cells and upregulate stimulatory signals. However, tumor cells and peptide/protein TAAs are often not sufficiently immunogenic to trigger a T cell response. This then requires a immunostimulant for promoting DC activation to elicit a strong T cell response[25]. For this purpose, irradiated tumor cells and co-incubation with stimulatory cytokines including IL-12 [26] and granulocyte-macrophage colony-stimulating factor (GM-CSF) [27] were investigated to enhance the immunogenicity of tumor cells. Toll-like receptor (TLR) agonists [28] are also actively being examined in clinical trials as a vaccine adjuvant for peptide/protein vaccines.

1.4. TLR signaling promotes activation of APCs

Host immune system detect the pathogens via several mechanisms. TLRs are part of pattern recognition receptors (PRRs) that recognize pathogen-associated molecular patterns (PAMPs) which include flagellin, bacteria, virus, nucleic acids and toxins[29]. TLRs are mainly expressed on the APCs including DCs, macrophages, and B cells and also on mast cells, monocytes and epithelium cells. Expression of TLRs varies among species, and TLR 1~10 are reported in human[29]. In humans, TLRs 1, 2, 4, 6 and 10 are located at the

cellular membrane, while TLRs 3, 7, 8, and 9 are located in the intracellular endo/lysosomes. Ligands for TLRs can be divided to three categories; TLRs 1, 2, 4, 6 recognize lipids, TLR5 recognizes proteins and intracellular TLRs 3, 7, 8, and 9 recognize nucleic acids.

Upon ligation, TLRs 1, 2, 5, 6, 7, 8, and 9 activate myeloid differentiation primary-response gene 88 (MyD88) and TLR3 and 4 as well as toll/IL-1R (TIR) domain-containing adaptor protein inducing IFNβ (TRIF) signaling pathways[30]. MyD88 signaling activates interferon-regulatory factor (IRF)7, nuclear factor-kappa B (NF-κB) and mitogen-activated protein kinases (MAPKs) that results in production of multiple IFN type I, including IFNα, IFNβ, IFNλ and IFNω. Furthermore, MyD88 signaling upregulates co-stimulatory molecules CD40, CD80 and CD86 and triggers secretion of pro-inflammatory cytokines, such as IL-1β, IL-12, IL-18, tumor necrosis factor alpha (TNF-α), and interferon gamma (IFN-ɣ). In addition to NF-κB and MAPKs, TRIF signaling activates IRF 3 to trigger IFN and co-stimulatory responses.

With these aspects, TLR agonists were examined as immunostimulatory adjuvants of cancer vaccines to enhance the immunogenicity of TAAs. TLR2 agonist (polysaccharide krestin; PSK), TLR 3 agonist (polyriboinosinic-polyribocytidylic acid-polylysine carboxymethylcellulose; poly ICLC), TLR 4 agonist (lipopolysaccharide; LPS) and TLR9 agonist (CpG Oligodeoxynucleotide; CpG ODN) combined with TAAs including NY-SEO-1, MUC-1 and MART1 showed promising anticancer efficacy in pre-clinical studies and clinical trials [31–34].

1.5. TLR7/8 agonists for cancer immunotherapy

Synthetic imidazoquinoline derivatives are potent TLR7 or 8 specific or 7/8 bi-specific agonists[35]. TLR7 selective agonist, named imiquimod, was first introduced in 1997. Imiquimod was approved by US Food and Drug Administration (FDA) for treatment of basal and squamous cell carcinoma and genital warts as a single agent[36]. Imiquimod activates plasmacytoid DCs (pDCs) and macrophages via TLR7 ligation to promote the pro-inflmmatory cytokine induction including type I IFN, TNF-α and IL-12[37]. These cytokines induce activation of CD4 T cells, CD8 T cells and NK cells that can kill malignant tumor cells[38,39]. Previous studies also report that imiquimod can induce apoptosis of TLR expressing tumors[40]. These findings suggest that imidazoquinoline-based small molecules can foster a potent adaptive immune response, which is important for cancer treatment.

Professor David M. Ferguson (Department of Medicinal Chemistry, University of Minnesota) and coworkers have reported a series of imidazoquinoline derivatives that are TLR7 or 8-specific or 7/8 mixed agonists[41–43]. Based on the cytokine induction, TLR7/8 activities are associated with the C2-alyl chain length of imidazoquinoline structure, where butyl and pentyl derivatives potentiate TLR 7 and 8, respectively.

TLR7 and 8 are both intracellular receptors and recognize single-stranded RNA (ssRNA) and ligate NF-κB signaling pathways. However, recent studies report that, although TLR7 and TLR8 recognize similar molecular patterns, they are functionally different[44]. While TLR7 is mainly expressed on pDCs, an induced type I IFN secretion, TLR8 is expressed mainly on myeloid DCs (mDCs) and potentiates TNF-α and IFN-ɣ

response. This suggests that TLR7/8 mixed agonists can help foster stronger TH1 immunity than TLR7 or 8 specific agonists. Previous studies reported that stimulating both plasmacytoid and CD8α DCs is required to elicit strong CD8 T cell response[45], which implies that using TLR7/8 agonist would be more advantageous as immunostimulatory adjuvant for cancer immunotherapy. The chemical structure of the available TLR7/8 agonist, termed 522, is shown at **Figure 1.1**.

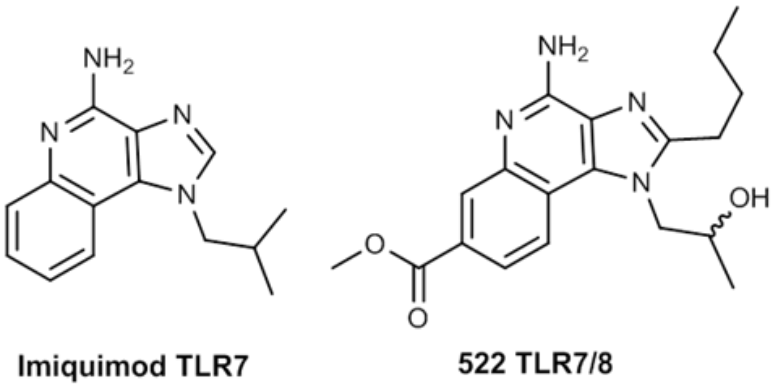

Figure 1.1. Structures of prototypical TLR7 selective compound imiquimod and dual TLR7/8 agonist 522.

1.6. Nanoparticulate drug delivery

Nanoparticles (NPs) are an efficient platform for delivery of conventional drugs in overcoming the limitations of their inherent pharmacokinetics, both bioavailability and elimination. In addition to small molecular weight drugs, polymeric NPs and liposomes have been used to proteins, vectors and nucleic acids[46]. Discovery of the enhanced permeability and retention (EPR) effect[47], which explains enhanced accumulation of macromolecules via extravasation through leaky blood vessels in the tumor, has led to the application of nanoparticles as a carrier for chemotherapy against solid tumors. Two

notable examples of FDA-approved nanomedicines are liposomal doxorubicin (Doxil) and albumin-bound paclitaxel (Abraxane) [48,49].

With the successful use of NPs, recent studies have focused on the use of NPs to enhance therapeutic efficacy of cancer immunotherapy involving antigens and/or vaccine adjuvants[50,51]. For successful cancer immunotherapy, efficient delivery of immunostimulatory molecules to targeted immune cells is critical. In this study, we sought to potentiate CD8 T cells by stimulating DCs, which suggest the importance of TLR7/8 agonist delivery to DCs. Therefore, we compared efficacy of nanoparticulate delivery of TLR7/8 agonist relative to a soluble form as immunostimulatory adjuvant for cancer immunotherapy.

1.7. PLGA NPs as drug delivery platform of TLR7/8 agonists

Poly(lactide-co-glycolide) (PLGA) is a FDA-approved polymer, and the biocompatibility and potential cytotoxicity is well-established[52]. In vivo PLGA undergoes decomposition into lactide and glycolide by hydrolysis; hence, it is by definition biodegradable[53]. Size and drug release kinetics of PLGA NPs can be fine-tuned by modulating the composition of PLGA including the molar ratio of lactide to glycolide, molecular weight, and terminal groups[54]. Additionally, targeting moieties can be readily attached to the surface of PLGA NPs by covalent modification of the terminal groupsor by adsorption due to its hydrophobicity.

In addition to these chemical and physical properties, several features further suggest PLGA NP as suitable vaccine delivery platform. DC uptake of antigens and/or

immunostimulatory adjuvant is critical to elicit T cell immunity. Previous studies report that size, surface charge, hydrophobicity, and shape significantly influence the DC uptake of macromolecules[55]. Among the factors, size plays a critical role as nanoparticles have shown superior DC internalization compared to microparticles[56]. It has also been reported that sub-micron sized macromolecules with a size range of 20-200 nm can be efficiently internalized into DCs via clathrin-dependent and caveolae-dependent endocytosis pathways[57]. However, endocytosis of micro-sized macromolecules is mainly facilitated through pinocytosis and phagocytosis, which is favorable for uptake by macrophages and Langerhans cells.

Previous studies report that PLGA NPs can internalize to *in vitro* generated DCs including human peripheral blood-monocytes-derived DCs, human cord-blood CD34+ DCs, and murine bone marrow-derived DCs (BMDCs) within 24 hr of incubation[58]. Efficient DC uptake of PLGA NPs is particularly advantageous for delivery of endosomal TLR agonists. TLR3, 7, 8 and 9 are located at the luminal side of endo/lysosome, and thus TLR agonists must cross the cellular membrane and internalize into endo/lysosome to ligate the TLR signaling. Following endocytosis, PLGA NPs enter endo/lysosomes, which is the target site for TLR3, 7, 8 and 9 ligation [59]. Therefore, these features suggest that PLGA NPs can provide efficient delivery of TLR agonists for DC uptake.

Several studies report that *in vivo* efficacy of cancer vaccines is often hampered by rapid clearance from the injection site[60,61]. This leads to insufficient vaccine delivery to lymphoid organs and results in sub-optimal therapeutic efficacy. Biodegradation

mechanisms facilitate the rapid clearance following injection. Subcutaneous (SC) injection is the conventional vaccine administration route, as vaccine components need to migrate to draining lymph nodes to stimulate APCs and cytotoxic cells[61]. SC administration delivers the vaccine components to interstitial space of hypodermis composed of adipocytes, fibroblast, collagen and glycosaminoglycans (GAGs) [62]. PLGA NPs can protect encapsulated payloads from biodegradation at the injection site, which is particularly important for peptide/protein-based vaccines. PLGA NPs are sufficiently robust to protect encapsulated payload, because their glass transition temperature is higher than physiological temperature of 37°C and therefore reside in the glassy state. Peptide/proteins encapsulated in the polymeric NPs also maintain their activities longer than soluble form[46,63], when incubated in the mouse/human serum, further supporting the rationale of their use.

Upon SC injection, vaccine components can enter blood circulation or lymphatic systems. While blood capillaries are tightly structured, lymphatic vessels are relatively more permeable as they lack inter-endothelial tight junctions[57]. Due to this permeability difference, large molecules have limited entry to blood circulation and preferably enter the lymphatic system. It was shown that molecules with a molecular weight (MW) of 16 kDa or less and/or a size of 10 nm or smaller preferentially enter systemic circulation via blood capillaries following the SC injection[60,62].

Blood capillary absorption mediated clearance is problematic for vaccine delivery as vaccine components need to migrate to draining lymph nodes to stimulate APCs and cytotoxic T cells. Previous studies report that SC injected macromolecules can directly

migrate to the lymph node via paracellular uptake or DC-meditated mechanism[64,65]. It is reported that macromolecules with size of 100 ~ 200 nm can directly enter lymphatic system via lymphatic capillaries within hours after injection[64]. On the other hand, macromolecules with size of 200 ~ 500 nm can be transported within DCs to the lymphatic system. These findings suggest that rapid clearance following SC injection can be reduced by nanoparticulate delivery of vaccine components.

Simultaneous co-stimulatory molecule signaling and antigen-presentation by DCs is required to elicit antigen-specific CD8 T cell response. The rationale is that without co-stimulatory signaling T cell activation fails, and without antigen-presentation non-specific T cell expansion occurs[66]. Therefore, co-delivery of antigen and vaccine adjuvant is critical to elicit antigen-specific T cell response [67]. However, co-delivery of TAA and synthetic TLR7/8 agonist is challenged by formulation limitations. While most of TLR agonists including ICLC, LPS, and CpG ODN are soluble in normal saline and aqueous buffers, synthetic TLR7/8 agonists are soluble in organic buffers and have limited solubility in normal saline and aqueous buffers. As such, formulations have been limited to creams and gels[68,69], and current application of synthetic TLR7/8 agonists are limited to topical treatments (ClinicalTrials.gov; NCT01676831, NCT01808950,) and intratumoral injection (NCT02556463). In clinical studies where topical treatment of TLR7/8 agonists were utilized as vaccine adjuvants (NCT01748747, NCT00960752), peptide/protein-based TAAs were administered separately by SC injection. Thus, there is a need for an approach that can deliver TLR7/8 agonists by SC or IM injection together with TAA-peptides.

Encapsulation of TLR7/8 agonists in PLGA NPs can fulfill this need. Previous studies reported that PLGA NPs can encapsulate both hydrophilic and hydrophobic compounds[53]. Imidazoquinoline-based synthetic TLR7/8 agonists, which are slightly hydrophobic small molecules, can be loaded to PLGA NPs using emulsification solvent evaporation methods[54]. As PLGA NPs can be dispersed in the aqueous buffers, encapsulated TLR7/8 agonists can be delivered via conventional vaccine administration routes including SC and IM injection, which allows co-delivery of peptide/protein-based TAA and TLR7/8 agonists. These aspects suggest PLGA NPs will be not only suitable for delivery of TLR7/8 agonist for *in vivo* immunization but also superior to current commercialized formulations.

1.8. Specific aims

Specific aim 1. Development of drug carrier for TLR7/8 agonist using PLGA NPs

We fabricated PLGA NPs as drug carrier for 522 (522NP). The size of PLGA NPs was fine-tuned to ~ 200 nm, to facilitate efficient DC uptake and *in vivo* lymph node drainage. Cancer vaccine composed of peptide/tumor cell lysate-based antigen and 522NP elicited robust antigen-specific CD8 T cell response, which resulted in enhanced prophylactic and therapeutic efficacy in murine tumor models. Result of studies on Specific aim 1 is reported at Chapter 2.

Specific aim 2. Adapting pH-responsive drug delivery system to enhance TLR7/8 agonist-based vaccine

We fabricated acidic-pH responsive, gas-generating PLGA NPs by incorporating sodium bicarbonate in the NPs (522GGNP). New formulation generated carbon dioxide gas in acidic pH, which resulted in rapid release of encapsulated drug. Additionally, new formulation showed significantly increased encapsulation efficiency compared to conventional PLGA NPs. CD8 T cells and NK cells significantly expanded in mice immunized with acidic-pH responsive NPs and showed enhanced therapeutic efficacy compared to conventional PLGA NPs. Result of studies on Specific aim 2 is reported at Chapter 3.

Specific aim 3. Modulation of tumor microenvironment to enhance therapeutic efficacy of nanoparticle-based vaccine

To enhance the therapeutic efficacy of nanoparticle-based vaccine, we modulated immune-suppressive tumor microenvironment. Co-treatment of sunitinib with nanovaccine resulted in reduction of MDSCs and Tregs. We further combined anti-PD-L1 antibody to inhibit PD-L1/PD-1 signaling. Triple combination therapy with nanovaccine+sunitinib+PD-L1 blockade significantly increased the CD8 T cell activation at the tumor, and induced antigen-specific memory response. Result of studies on Specific aim 3 is reported at Chapter 4.

Specific aim 4. Application of TLR7/8 agonist-encapsulating NPs for antibody-based cancer immunotherapy

We examined the application of 522GGNP as vaccine adjuvant to augment therapeutic efficacy of antibody-based cancer immunotherapy. In our study, 522 triggered secretion of IL-12, IL-1β, TNF-α and IFN-ɣ from human peripheral blood mononuclear cells (PMBCs), and upregulated co-stimulatory molecules CD70, 80 and 86 on murine DCs, all of which are potent modulators of NK cell activation. 522GGNP treatment potentiated strong *in vivo* NK cell cytotoxicity and elongated NK cell activation. When combined with cetuximab, 522GGNP treatment significantly enhanced the NK cell degranulation and augmented ADCC. Result of studies on Specific aim 4 is reported at Chapter 5.

Chapter 2.

Polymeric nanoparticles encapsulating novel TLR7/8 agonists as immunostimulatory adjuvants for enhanced cancer immunotherapy

*This chapter was published elsewhere[70]. Reproduced with permission.

2.1. Summary

Cytotoxic T lymphocytes (CTLs) play a major role in cancer immunotherapy because of their ability to directly kill tumor cells and secrete tumor suppressive cytokines. Anticancer vaccines aim to provoke tumor-specific CTL responses, which require activation of antigen presenting cells (APCs) including dendritic cells (DCs) and macrophages. Therefore, a potent immunostimulatory adjuvant capable of activating APCs is an essential component of anticancer vaccines. In this study, we introduce novel TLR 7/8 bi-specific agonists that significantly enhance cytokine secretion compared to TLR7 mono-selective compounds. Encapsulation of these TLR 7/8 agonists in poly(lactide-co-glycolide) (PLGA) nanoparticles increased the co-stimulatory molecule expression and antigen presentation via MHC I by DCs compared to the soluble agonist. When administered subcutaneously, these nanoparticles migrated to draining lymph node and triggered DC activation and expansion. This lead to expansion of antigen-specific CD8 T cells and enhanced CTL response, which resulted in significant prophylactic and therapeutic efficacy in melanoma, bladder and renal cell carcinoma tumor models. Importantly, our studies demonstrate significant reductions in systemic metastasis with the nanoparticle vaccine. Our results suggest novel TLR 7/8 agonist-encapsulated nanoparticles are potent immunostimulatory adjuvants for cancer immunotherapy.

2.2. Introduction

Anticancer vaccines aim to stimulate the host immune system by providing tumor-associated antigens (TAAs) in the presence of an immune adjuvant to activate dendritic cells (DCs) and trigger tumor-specific immunity [71], and Toll-like receptor (TLR) agonists have proven valuable as vaccine adjuvants [72]. Activation of TLRs induces NF-κB-mediated expression of proinflammatory cytokines and chemokines necessary to generate a robust immune response. Of the known human TLRs, the endosomally located TLR7 and TLR8 are particularly interesting because they can be activated by either single-stranded nucleic acids or synthetic small molecules [73,74]. We have recently reported a series of highly substituted imidazoquinoline-based esters that potently stimulate both TLR7 and 8, resulting in higher levels of cytokine production compared to the TLR7-specific agonist imiquimod, the only TLR agonist approved for clinical use [42,75]. Despite their high *in vitro* TLR agonist activity, small molecules often fail to demonstrate satisfactory *in vivo* immune response [76]. Soluble drugs are rapidly cleared from the site of injection, limiting the amount of agonist available for activating DCs, a critical early step in the induction of anti-tumor immunity. In fact, co-localization of the adjuvant and tumor antigen within DCs could be a decisive determinant for the success of adjuvant based cancer immunotherapy [77].

Nanoparticles formulated from the biodegradable polymer, poly(D,L-lactide-co-glycolide) (PLGA), enable greater and sustained cellular delivery of the encapsulated payload [78,79]. Further, DCs preferentially internalize particles <500 nm in diameter, and nanoparticles in this size range stimulate greater CD8 T cell response than micron-size particles [58,80]. Slow release of TLR agonist from polymeric matrix can facilitate sustained

TLR signaling in DCs, which can reduce the need for high and/or repeated dosing. Based on these observations, we hypothesized the encapsulation of our new imidazoquinoline-based TLR7/8 agonists in PLGA nanoparticles would enable significantly improved delivery of the agonists to DCs and further enhance their immunomodulatory activity. This hypothesis is supported by previous studies showing significant enhancements in immune response with the TLR3 agonist polyinosinic:polycytidylic acid and TLR9 agonist unmethylated CpG oligodeoxylnucleotide when delivered in polymeric nanoparticles [67,81].

In the present study, we selected two of our most promising TLR7/8 bi-specific imidazoquinoline-based esters (racemic mixture '522' and its S-configured steroisomer '528') for encapsulation in PLGA nanoparticles. These two molecules induce high levels of pro-inflammatory cytokines, pointing to their strong potential as immunostimulatory adjuvants for cancer immunotherapy. The effectiveness of these nanoparticle formulations was investigated in multiple tumor models (melanoma, bladder and renal cell carcinoma), different vaccine designs (peptide-based, whole tumor cell lysate-based and *in situ* vaccines), and vaccine modalities (prophylactic and therapeutic). These studies show our novel TLR7/8 agonists encapsulated in PLGA nanoparticles trigger a robust antigen-specific immune response and are highly effective as vaccine adjuvants for cancer immunotherapy.

2.3. Materials and Methods

2.3.1. Materials

The polymer poly(lactide-*co*-glycolide) (PLGA; 50:50 lactide-glycolide ratio; 0.55-0.75 dl/g inherent viscosity) was purchased from Lactel (Birmingham, AL). TLR 7/8 agonists (522 and 528) were synthesized and characterized as reported previously [42,75]. Polyvinyl alcohol (PVA), 6-coumarin, ammonium acetate and albumin from chicken egg white (ovalbumin, OVA) were purchased from Sigma-Aldrich (St Louis, MO). Chloroform and acetonitrile were purchased from Fisher Scientific (Rockford, IL). Carboxyfluorescein succinimidyl ester (CFSE) Cell Division Tracker Kit was purchased from Biolegend (San Diego, CA).

Fluorophore-labeled monoclonal antibodies were purchased from Biolegend (San Diego, CA) (CD3, CD8, CD11c, CD80, IFN-γ), eBioscience (San Diego, CA) (CD4, CD44, CD11a, CD40, CD86) and Tonbo Biosciences (San Diego, CA) (I-A/I-E(MHC II)). Fluorophore labeled H-2K^{b} OVA$_{257-264}$ (SIINFEKL) tetramer was provided by Dr. Dave Masopust (University of Minnesota).

2.3.2. Methods

Animals and cell lines

C57BL/6 mice (6-8 weeks, female) and Balb/c mice (7-8 weeks, female) were purchased from Charles River (Wilmington, MA) and National Cancer Institute (Frederick, MD), respectively. Mice were housed under specific pathogen free (SPF) facilities in Research Animal Resources at the University of Minnesota. All animal experiments were performed according to the protocols approved by Institutional Animal Care and Use Committee (IACUC) of the University of Minnesota.

Ovalbumin expressing murine melanoma cell line B16F10-OVA was provided by Dr. Brandon Burbach (University of Minnesota). Murine bladder cancer cell line MB49 was purchased from ATCC. B16F10-OVA and MB49 cells were cultured in RPMI 1640 medium supplemented with 10% fetal bovine serum, 100 μg/mL streptomycin and 100 U/mL penicillin. G-418 Disulfate (Research products international, Mt Prospect, IL) was added to the medium when culturing B16F10-OVA (5 μg/mL). Murine kidney adenocarcinoma Renca cell line that stably expresses firefly luciferase and green fluorescent protein (GFP) (Renca-GL) was obtained from Dr. Andrew Wilber (Southern Illinois University School of Medicine, Springfield, IL). Renca-GL cells were maintained in RPMI 1640 supplemented with 10% FBS, penicillin, streptomycin, sodium pyruvate, nonessential amino acids, and HEPES (hereafter referred to as complete RPMI) medium supplemented with 0.3 μg/ml puromycin and 300 μg/ml zeosin.

Fabrication and characterization of TLR agonist-loaded PLGA nanoparticles

The TLR7/8 agonist 522 (or 528) loaded PLGA nanoparticles (522NPs or 528NPs) were fabricated using the oil-in-water emulsion solvent evaporation method [78,79]. Briefly, 2.5% w/v PVA was prepared in endotoxin-free distilled water (D.I. water) and used as the aqueous phase. The oil phase was prepared by dissolving 1.5 mg of 522 and 50 mg of PLGA in 2 ml of chloroform. This solution was added to 8 ml of 2.5% PVA, and the mix was sonicated for 5 min using probe-sonicator (Sonicator XL, Misonix, Melville, NY) to form an emulsion. This emulsion was stirred for ~18 h under ambient conditions, followed by an additional 1 h in a desiccator under vacuum. Nanoparticles were separated by

centrifugation (Optima XPN-80 Ultracentrifuge, Beckman Coulter Inc., Fullerton, CA) (35,000 RPM, 35 min) and then resuspended in D.I. water. The procedure was repeated two additional times to remove unencapsulated agonist and residual PVA. Nanoparticles were then lyophilized (Labconco FreeZone 4.5, Kansas City, MO), and stored at -20°C until further use.

Size and zeta potential of nanoparticles were measured by dynamic light scattering (DLS) (Delsa^{TM} Nano C, Beckman Coulter Inc.). One milligram of nanoparticles was dispersed in D.I. water and sonicated before measurements. Morphology of nanoparticles was imaged using transmission electron microscope (TEM) (FEI Tecnai G2 F30) and scanning electron microscope (SEM) (Hitachi SU8230, Hitachi).

Agonist encapsulation and *in vitro* release

To determine the amount of agonist loaded in the nanoparticles, methanol was added to 1 mg of nanoparticles to extract the agonist from the PLGA matrix. Extracted 522 or 528 was quantified using high-performance liquid chromatography (HPLC; Beckman Coulter). Separation was achieved using a 50:50 mixture of ammonium acetate buffer (pH 4) and acetonitrile as the mobile phase, run at an isocratic flow rate of 1 ml/min through Eclipse C-18 reverse-phase HPLC column (Agilent, 4.6 x 150 mm, particle size 4 µm). The agonists were detected and quantified using a fluorescence detector (Jasco Inc, Easton, MD; λ_{ex}: 260 nm, λ_{em}: 340 nm).

In vitro release of 522 from NPs was determined using a previously reported dialysis technique [82]. Nanoparticles (2 mg/ml) were dispersed in release buffer (PBS, pH

7.4) and transferred to Float-A-Lyzer® dialysis tubes (molecular weight cut-off 20 kDa, Pierce). Dialysis tubes were immersed in release buffer (6 ml) contained in a 15-ml plastic tube. Sample tubes were incubated in a water bath shaker (Thermo scientific) at 37°C at 100 RPM. At pre-determined time points, release buffer was collected and sample tubes were refilled with fresh release buffer. Collected samples were lyophilized, 522 was extracted with methanol and quantified by using HPLC as described above.

PBMC isolation and stimulation

Human PBMCs were isolated from heparinized blood obtained by venipuncture from healthy donors using standard density-gradient centrifugation over Ficoll-Plaque Plus (Pharmacia, Uppsala, Sweden). PBMCs (5×10^5 cells/1 ml/well in a 24-well plate) were cultured in complete RPMI medium. Soluble 522 was prepared in DMSO (hereafter referred to as Free522) and 522NP was prepared in complete RPMI. Free522 and 522NPs were added to the wells (in triplicate) so that the final concentration was between 50 μM and 0.39 μM. Some wells received only DMSO. After 24 h, culture supernatants were collected and frozen at -80°C until analysis. The concentration of cytokines in the supernatants was determined by using ELISA (BioLegend).

For cytotoxicity assay, PBMCs (2×10^4 cells/well in a 96-well plate) were incubated with 522NPs (15.6 ~250 μg/ml, equal to 0.47 ~ 7.5 μM of 522), Free522 (0.47 ~ 7.5 μM) for 48 h. After 48 h, culture supernatants were collected. Cytotoxicity of the treatments was measured according to the manufacturer's protocol (LDH Cytotoxicity Assay Kit, Thermo).

TLR7 and 8 reporter cell assay

Human TLR-specific reporter cell assays were carried out as previously reported [75]. Briefly, reporter cells (HEK-Blue^{TM}-hTLR7 and 8, InvivoGen, San Diego, CA) were seeded at 40,000 cells per well in 96-well cell culture plate. After 24 h, imiquimod, Free522 and 522NPs were prepared in DMEM media (25 μM) and added to the reporter cells. The supernatants were collected the following day for colorimetric assay.

Culture of bone marrow-derived dendritic cells (BMDCs)

BMDCs were produced using established protocols with modifications [83]. Briefly, tibias and femurs from C57BL/6 mice were harvested, disinfected with 70% ethanol, and rinsed twice with cold PBS (pH 7.4). Both ends of the bones were cut, and bone marrow precursor cells were flushed with PBS using a 27-gauge needle (Medtronic, Minneapolis, MN). The flushed bone marrow was filtered using a 70-micron nylon mesh, and erythrocytes were removed using lysis buffer (Pharm Lyse, BD Bioscience, San Jose, CA). Single cell suspension of bone marrow precursor cells was added to a petri dish and incubated with complete RPMI 1640 media supplemented with 20 ng/mL granulocyte-macrophage colony-stimulating factor (GM-CSF) (PeproTech, Rocky Hill, NJ) and 50 μM 2-mercaptoethanol (Sigma) for 6 d to generate immature BMDCs. Media was changed once on day 3.

Cellular uptake and intracellular trafficking of nanoparticles in BMDCs

6-coumarin, a hydrophobic fluorescent dye, was co-encapsulated with 522 to label nanoparticles (C6NPs). The fabrication of C6NP was identical to that of 522NPs, except for the addition of 700 µg of 6-Coumarin to the organic phase. For *in vitro* cellular uptake study, BMDCs (10^6/well) were seeded in a 24-well cell culture plate. The following day, C6NPs (0.2 mg/ml) were added to BMDCs and incubated for 2 h. Cells were detached using non-enzymatic cell dissociation solution (Sigma-Aldrich) and rinsed twice with PBS, followed by staining with anti-CD11c mAb. Cellular uptake of C6NPs by BMDCs was determined by monitoring the 6-coumarin-associated fluorescence signal in the $CD11c^+$ cells by flow cytometry (BD LSR II, BD Biosciences, San Diego, CA).

Intracellular distribution of C6NPs was determined by confocal laser scanning microscopy (Olympus FluoView FV1000 BX2 Upright Confocal, Olympus, Center Valley, PA). BMDCs (5000/chamber) were seeded into a Lab-Tek® Chamber Slide™ system (Sigma). The next day, the BMDCs were incubated with C6NPs (0.1 mg/ml) for 2 h, and then rinsed with PBS twice. Cells were stained with LysoTracker® Red DND-99 (Thermo scientific) and fixed with 3% paraformaldehyde (PFA), followed by staining with 4',6-diamidino-2-phenylindole (DAPI; Thermo scientific). Confocal images were further analyzed by Olympus Fluoview viewer 2.0 software.

In vitro BMDC activation and antigen presentation

BMDCs (10^6/well) were seeded in a 24-well cell culture plate. Following attachment, Blank NPs (PLGA nanoparticles without any TLR agonist, 50 µg/ml), 522NPs (50 µg /ml, equivalent to 50 ng/ml of Free522) or Free522 (50 ng/ml) were added to each

well. After 24 h, BMDCs were collected and analyzed for co-stimulatory molecule (CD40, CD86, and CD80) expression by flow cytometry. To assess antigen presentation, OVA (30 µg) was co-incubated with treatment groups. After 24 h, BMDCs were collected and stained with anti-$OVA_{257-264}$ (SIINFEKL) peptide bound to H-$2K^b$-APC (eBioscience) antibody and analyzed by flow cytometry to detect DCs presenting OVA-specific peptides via MHC I.

In vivo distribution of nanoparticles

C6NPs (2.6 mg/mouse) were injected subcutaneously in the flank of C57BL/6 mice. Mice were sacrificed at 1 h and 6 h, and inguinal lymph nodes, liver, kidney, spleen, heart and lung were collected. Harvested organs were homogenized in D.I. water using the Omni Tissue Homogenizer (OMNI, Kennesaw.GA) and lyophilized. 6-coumarin was extracted from lyophilized samples with diethyl ether and methanol, and quantified using HPLC [84]. To measure extraction efficiency, organs were harvested from untreated mice and homogenized with a known amount of 6-coumarin and processed identical to the samples. Extraction efficiencies for each of the organs is presented in Table 2.2

For lymph node imaging, mice were sacrificed 6 h after injection, and inguinal lymph nodes were collected, embedded in Tissue-Tek® OCT compound (Sakura Finetek USA, Inc.) and frozen at -80°C. Frozen lymph node sections (5 µm thick) were mounted on glass slides, stained with anti-CD11c-AF700 antibody to label DCs, and imaged by confocal microscopy.

Immunization protocol

C57BL/6 mice were immunized daily for 5 d with OVA (100 µg) admixed with Free522 (2 µg) or 522NPs (2 mg; equivalent to 2 µg of Free522) dispersed in 200 µl of sterile PBS. For TRP immunization, 100 µg of TRP-2 peptide (180-188) was used. Each dose was divided into two 100 µl subcutaneous injections, administered to the left and right thighs.

For tumor cell lysate vaccine formulation, MB49 cell lysate was prepared by five cycles of freeze (liquid nitrogen)-thaw (56°C water bath). Cell debris was pelleted down and the protein concentration of the supernatants was measured using Pierce™ BCA Protein Assay Kit (Thermo). Cell debris pellets were reconstituted with supernatants. Free522 (2 µg) or 522NPs (2 mg) and 100 µg of the cell lysate were mixed with 200 µl of sterile PBS to create the vaccine. Vaccination schedule and injection sites were identical to those used for OVA immunization.

***In vivo* DC and T cell proliferation assay**

C57BL/6 mice were immunized as described above. For DC analysis, four groups were used: untreated, OVA alone, OVA+Free522 and OVA+522NP. For T cell proliferation assays, a group of mice receiving 522NP without OVA (522NP only) group replaced the OVA+Free522 group. Mice were euthanized 2 d after the final dose (d 8). For T cell proliferation assay, 100 µg of $OVA_{257-264}$ peptide was injected intravenously to each mouse on the day of harvest. Mice were euthanized and organs were harvested 4 h after the peptide injection.

A single cell suspension of lymph nodes and spleen was prepared following an established protocol [45]. Briefly, lymph nodes and spleens were mechanically homogenized using gentleMACS Dissociator (Miltenyi BioTeck Inc., Auburn, CA). Homogenized cell suspension was then digested in Hanks' Balanced Salt solution (HBSS) supplemented with 0.15 mg/ml DNAse I (Sigma) and 0.56 Wuensch units/ml Liberase Blendzyme 3 (Roche, Branford, CT). After 30 min, erythrocytes were removed using lysis buffer, and cells were blocked with anti-CD16/32 (Tonbo) and normal mouse serum. Cells were stained to identify DCs and T cells, and analyzed using flow cytometry. For DCs, the following antibodies were used: anti-CD11c-APC Cy7, I-A/I-E (MHC II) -vF450, CD40-PE, CD86-FITC, and CD80-PE Cy5. For T cells, the following antibodies were used: CD3-PerCP Cy5.5, CD4-PE Cy7, CD8-BV650, CD44-AF700, $OVA_{257-264}$:H-$2K^b$ Tetramer-APC, and IFN-γ-BV605. Intracellular staining of IFN-γ was performed according to the manufacturer's protocol (Foxp3/Transcription Factor Staining Buffer Set, eBioscience). Counting beads (eBioscience) were used to calculate cell numbers. Acquired data was analyzed using FlowJo software (TreeStar Inc., Ashland, OR).

In vivo cytotoxic T lymphocyte (CTL) assay

C57BL/6 mice were immunized as described above and an *in vivo* CTL assay was conducted two days after the final vaccination (d 8). Splenocytes from naïve C57BL/6 mice were pulsed with either 2 µg/ml of $OVA_{257-264}$ peptide or PBS for 1 h in 37°C. $OVA_{257-264}$ pulsed cells and PBS incubated cells were stained with 7 µM and 0.7 µM CFSE, respectively, for 20 min. Equal numbers ($5x10^6$ each, total 10^7) of $CFSE^{high}$ ($OVA_{257-264}$

pulsed, “Target”) and $CFSE^{low}$ (unpulsed, “Control”) cells were mixed in 100 µl PBS and injected intravenously in the immunized mice. On d 9, splenocytes of the immunized mice were analyzed by flow cytometry for $CFSE^{+}$ population. $CFSE^{low}$:$CFSE^{high}$ cell ratio was calculated to determine the percentage of *in vivo* OVA-specific lysis.

In vivo tumor models

In prophylactic studies, C57BL/6 mice were immunized as described above. For metastatic lung tumor model, B16F10-OVA cells (1×10^5 in 100 µl PBS) were injected intravenously through the tail vein on d 8. Lungs were collected on d 26 and number of tumor foci on each lung was counted under SMZ-2T trinocular stereoscope (Nikon). On a different set of similarly treated animals, spleens were harvested on d 13 and T cells were analyzed by flow cytometry. For subcutaneous tumor model, B16F10-OVA cells (5×10^5 in 100 µl PBS) or MB49 cells (1.5×10^5 in 100 µl PBS) were inoculated subcutaneously near the abdominal region on d 8.

In therapeutic studies, B16F10-OVA cells (2×10^5 in 100 µl PBS) or MB49 cells (1.5×10^5 in 100 µl PBS) were inoculated subcutaneously near the abdominal region of C57BL/6 mice. Once tumors were palpable, mice were immunized as described above. Subcutaneous tumor size was measured using digital calipers (Thermo Fisher Scientific). Tumor volume was calculated as $V = 0.5 \times (L \times W^2)$ (L: longest diameter, W: shortest diameter). Mice with tumor volume greater than 2000 mm^3 or those that developed tumor ulceration were removed from the study and euthanized.

In situ vaccination in an orthotopic kidney tumor model

For intrarenal (IR) tumor challenge, Balb/C mice were anesthetized, a skin incision was made on the left flank, and 2×10^5 Renca-GL cells were injected through the intact peritoneum into the left kidney in a 100 µl volume of HBSS [45,85]. On d 7, mice were re-injected in the same kidney with sterile PBS, Ad5-TRAIL (10^9 pfu), and/or Free528 (1 µg) or 528NPs (1mg, equivalent to 1 µg of Free528) in a 100 µl volume. Renal tumor growth and lung metastasis burden were measured via bioluminescence imaging using a Xenogen IVIS Spectrum (PerkinElmer, Waltham, MA). Mice were intraperitoneally (I.P.) injected with 100 µl of D-Luciferin (Goldbio, St. Louis, MO) (15 µg/ml) 10 min before imaging. Renca-GL generated radiance (photons/s/cm2) was quantified within a region of interest using Living Image software (Version 2.5). For end time-point experiments, lungs were harvested on d 21 and renal tumor burden was measured via BLI.

Statistical analyses

Results were reported as mean ± standard deviation (SD) or mean ± standard error of the mean (SEM). One-way analysis of variance (ANOVA), with a *post hoc* Tukey test was used to examine the statistical difference between the groups, unless otherwise stated. Data was analyzed with Prism4 GraphPad software (GraphPad Software, La Jolla, CA). A *p*-value <0.05 was considered statistically significant.

2.4. Result

2.4.1. 522 activates TLR7 and 8 pathways

In our initial experiments, we wanted to demonstrate the specificity and potency of the canonical TLR7 agonist imiquimod and our new imidazoquinoline-based agonist 522 **(Figure 2.1A)**. To assess specificity, reporter cell assays were used to examine ability of imiquimod and 522 to stimulate TLR7 or TLR8 relative to that of imiquimod. Using identical concentrations of each agonist, we saw both imiquimod and 522 could stimulate TLR7 signaling, but 522 showed significantly enhanced TLR7 activity compared to imiquimod **(Figure 2.1B)**. Moreover, only 522 was able to stimulate TLR8.

One characteristic outcome of TLR engagement is the production of cytokines [73]. We next examined the ability of imiquimod and 522 to stimulate cytokine production from human PBMCs *in vitro*. Consistent with previous data [75], human PBMCs stimulated with 522 produced significantly greater concentrations of IL-1β, IL-12p70, IFN-γ, and TNF-α over imiquimod (**Figure 2.1C**). These data show the dual specificity of 522 results in a much stronger pro-inflammatory cytokine production by PBMC compared to the TLR7-specific agonist imiquimod.

(A)

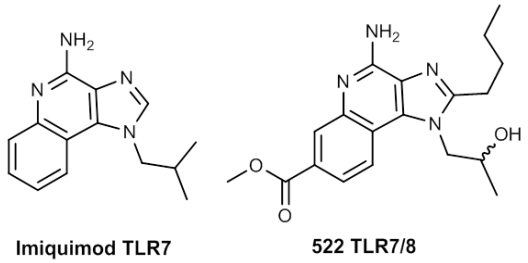

(B)

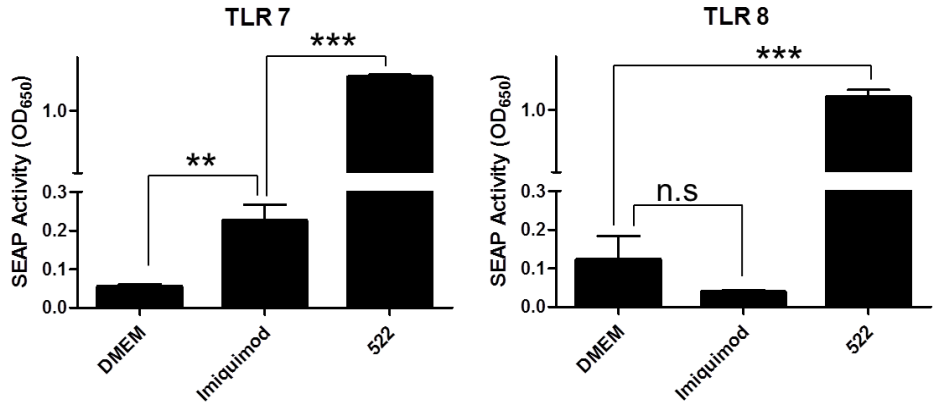

(C)

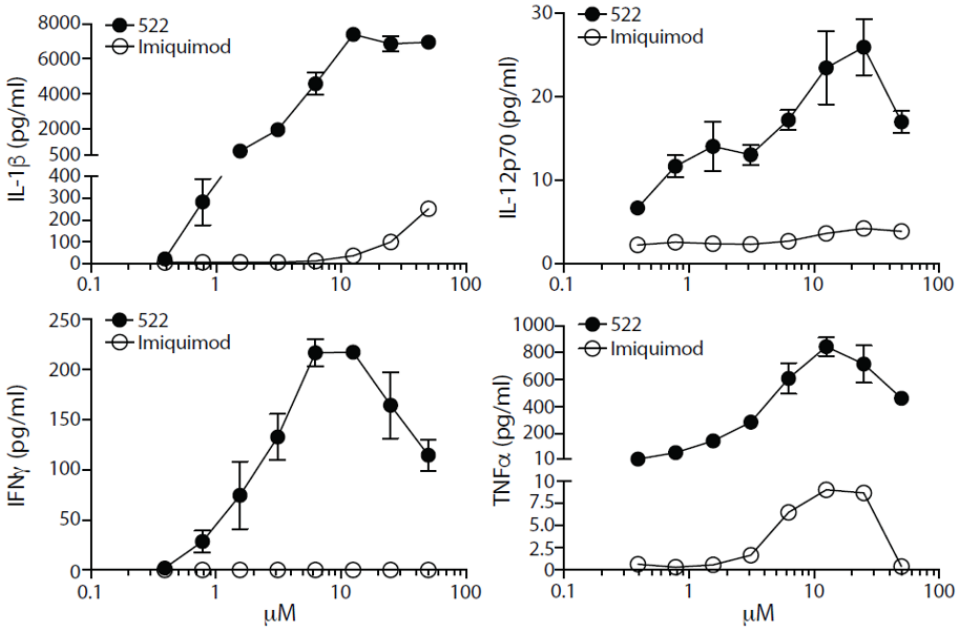

Figure 2.1. 522 is a dual TLR 7/8 agonist

(A) Structures of prototypical TLR7 selective compound imiquimod and dual TLR7/8 agonist 522. **(B)** Human TLR7 or TLR8 specific reporter cells were incubated with imiquimod or 522 for 24 h. TLR specific activity is measured by SEAP activity at OD_{650}. Results are reported as mean ± SD, n=4, $^{**}p<0.01$, $^{***}p<0.001$, n.s.=not significant, One-

way ANOVA. **(C)** Human PBMCs were incubated with imiquimod or 522 for 24 h and IL-1β, IL-12p70, IFN-γ, and TNF-α were measured by ELISA. Results are reported as mean ± SD, n=3.

2.4.2. Physicochemical characterization and in vitro release profile of 522NPs

Nanoparticle characteristics are highly dependent on the materials and parameters used during fabrication [54]. The 522NPs were spherical in shape (**Figure 2.2A**) and had an average diameter of 156 ± 26 nm as determined by scanning electron microscopy (**Figure 2.2B**). This size range was consistent with the hydrodynamic size measured by DLS (**Table 2.1**). Nanoparticles were negatively charged, with an average zeta potential of –16.4 ± 1.2 mV. 528NPs had similar particle size, surface charge and drug loading characteristics as the 522NPs (**Table 2.1**). *In vitro* release studies revealed the nanoparticles released ~40% of their payload within the first 24 h, followed by a slower release over the next 200 h in pH 7.4 buffer (**Figure 2.2C**). LDH assay using human PBMC confirmed both 522NPs and Free522 have negligible cytotoxicity against primary cells **(Figure 2.2D)**. To determine the extent to which 522 maintains its activity after encapsulation in PLGA nanoparticles, TLR reporter cell and PBMC stimulation assays were conducted. 522NPs maintained TLR7 and 8 activity and were able to induce IFN-γ secretion from PBMCs to a similar extent as Free522 **(Figure 2.2E,F)**.

(A)

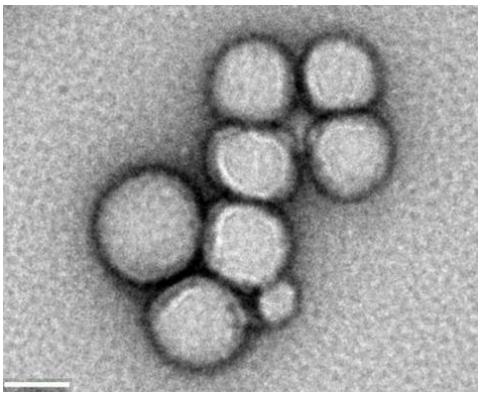

(B)

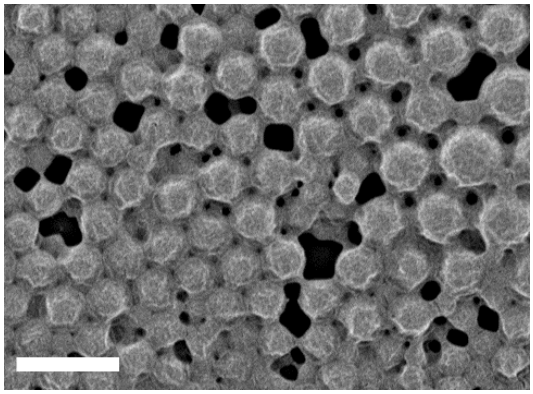

(C)

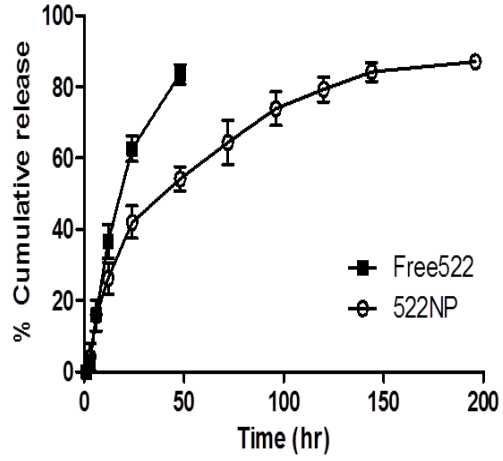
% Cumulative release
Time (hr)
Free522
522NP

(D)

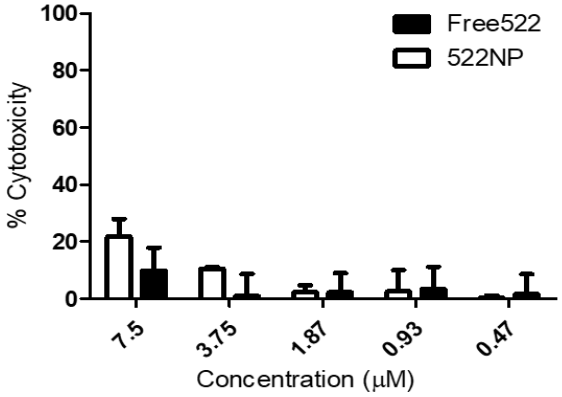
% Cytotoxicity
Free522
522NP
Concentration (μM)

(E)

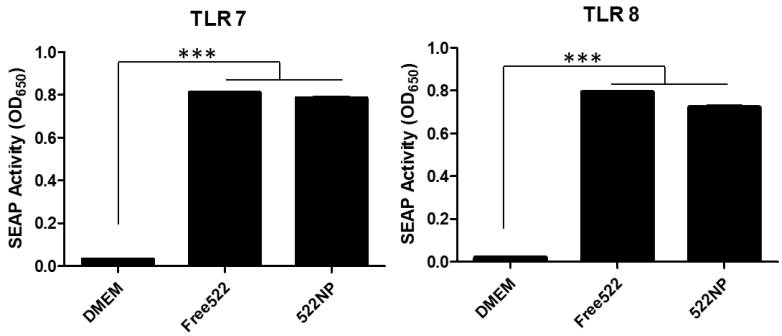
TLR 7
TLR 8
SEAP Activity (OD650)
***
DMEM
Free522
522NP

(F)

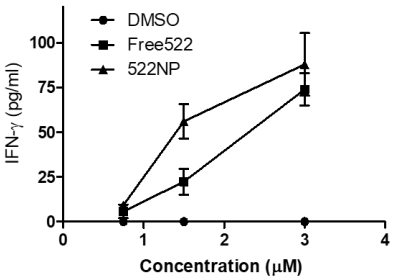
DMSO
Free522
522NP
IFN-γ (pg/ml)
Concentration (μM)

Figure 2.2. 522NP in vitro release profile and *in vitro* efficacy

(A) A representative TEM image of 522NPs. Scale bar, 50 nm. **(B)** A representative SEM image of 522NPs. Scale bar, 200 nm. **(C)** Cumulative release of 522 from PLGA nanoparticles in pH 7.4 PBS. Results are reported as mean ± SD, n=3. **(D)** Cytotoxicity of 522NPs and Free522 against PBMCs. Treatments were incubated with PBMC for 48 h and LDH assay was conducted to measure cytotoxicity. Results are reported as mean ± SD, n=4. **(E)** Human TLR7 or TLR8 specific reporter cells were incubated with DMEM, Free522 and 522NP for 24 h. TLR specific activity was measured by SEAP activity at OD_{650}. Results are reported as mean ± SD, n=3, ***p<0.001, One-way ANOVA. **(F)** Human PBMCs were incubated with DMSO, Free522 and 522NP for 24 h and IFN-γ was measured by ELISA. Results are reported as mean ± SD, n=3.

	522NP	528NP
Particle size (nm)	210 ± 12	218 ± 24
Zeta-potential (mV)	-16.4 ± 1.2	-9.1 ± 0.9
Polydispersity index	0.12 ± 0.01	0.16 ± 0.04
Loading amount of drug (μg/mg NP)	0.94 ± 0.04	1.15 ± 0.16
Loading efficiency (%)	3.1 ± 0.1	3.8 ± 0.5

Table 2.1. Physiochemical characterization of 522NPs and 528 NPs

Particle size, zeta-potential and polydispersity index of 522NPs and 528NPs were measured by DLS. Amount of 522 or 528 loaded in nanoparticles was quantified using HPLC. Results are reported as mean ± SD, n=3.

2.4.3. Uptake of nanoparticles by BMDCs and the effects of nanoparticle delivered 522

Unencapsulated TLR agonists are well known for their ability to stimulate their cognate TLR, while encapsulation into nanoparticles (such as the PLGA-based nanoparticles using herein) can delay/prevent degradation, improve cellular uptake, and/or serve as a depot for prolonged release. Thus, we next examined the interaction between BMDCs with nanoparticles and the consequences of NP-mediated delivery of 522 compared to Free522. Following incubation with fluorescently labeled 522NPs, the entire population of $CD11c^+$ BMDCs increased in fluorescence **(Figure 2.3A)**, suggesting BMDCs efficiently internalize 522NPs. To further confirm the nanoparticles were indeed internalized by BMDCs and investigate the intracellular localization of nanoparticles, BMDCs incubated with nanoparticles were fixed and imaged using confocal microscopy after staining with DAPI (blue) and lysotracker (red) to visualize the nucleus and acidic endo/lysosomes, respectively. The majority of nanoparticles were localized in the endo/lysosomes (shown by the presence of yellow fluorescence in the merged picture) and a small fraction of the internalized nanoparticles was found in the cytosol **(Figure 2.3B)**. These data show 522NPs can be internalized efficiently by BMDCs and reach the endo/lysosomes where TLR7 and 8 are located [86].

We next examined the extent to which 522, soluble or encapsulated within NPs, can activate BMDCs. BMDCs were incubated alone or with Blank NP, Free522, or 522NP for 48 h, and then evaluated for CD40, CD80, and CD86 expression. While BlankNP did

not alter co-stimulatory molecule expression on BMDCs compared to unstimulated cells, there was a significant increase in the frequency of cells expressing CD40, CD80, or CD86 after exposure to either Free522 or 522NPs **(Figure 2.3C)**. Just as co-stimulatory molecule expression ("signal 2") by antigen-presenting cells is needed for proper T cell activation [87], adequate expression of antigenic peptides within the context of MHC is required for antigen-specific T cell activation [88]. Thus, we examined the expression of the well-known OVA-derived MHC I-restricted epitope SIINFEKL on BMDCs incubated with whole OVA alone, or in combination with Free522 or 522NPs [89]. In contrast to the nearly identical increase in co-stimulatory molecule expression after exposure to either Free522 or 522NPs, the frequency of BMDCs expressing the SIINFEKL:MHC I complex was significantly increased after stimulation with 522NPs (**Figure 2.3D**). These results suggest the greatest potential for T cell activation occurs with the combination of antigen and agonist loaded NPs.

(A)

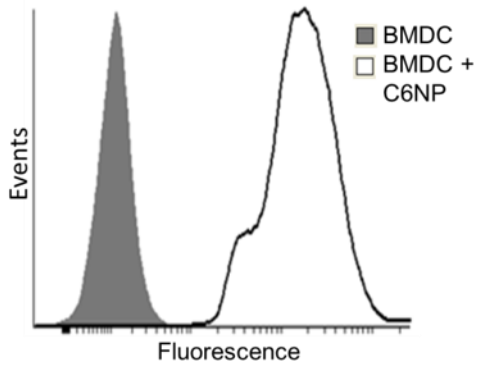

(B)

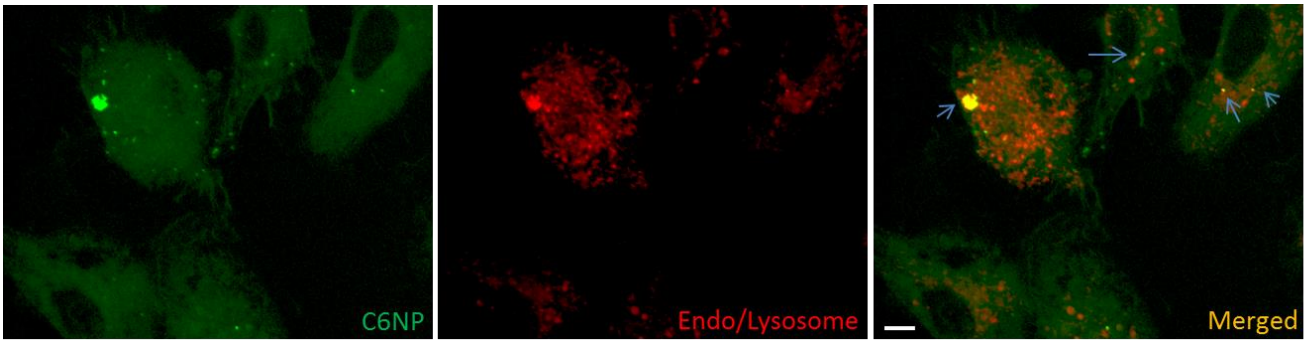
C6NP
Endo/Lysosome
Merged

(C)

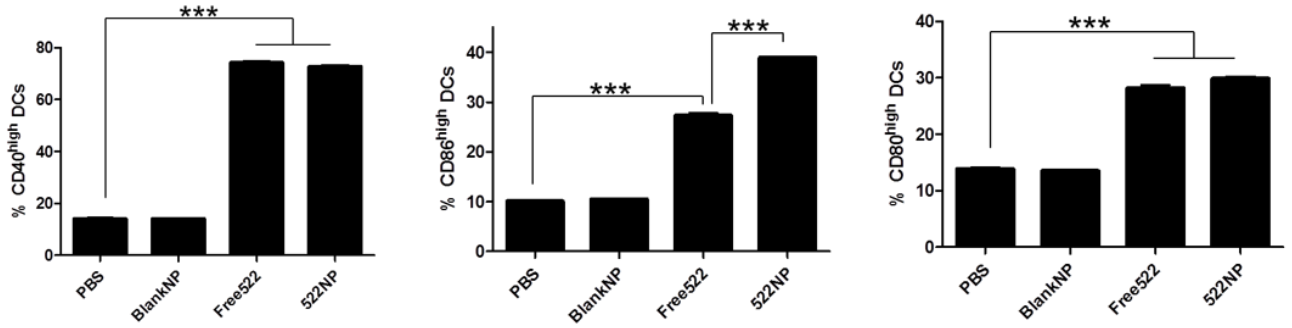
% CD40high DCs
% CD86high DCs
% CD80high DCs
***
PBS
BlankNP
Free522
522NP

(D)

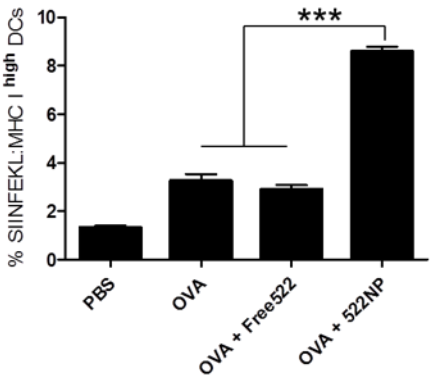
% SIINFEKL:MHC I high DCs
***
PBS
OVA
OVA + Free522
OVA + 522NP

Figure 2.3. BMDC internalization and activation

(A) BMDCs were incubated with C6NPs for 2 h and fluorescence intensity of BMDCs was then measured by flow cytometry. A representative histogram for each of the groups (n=3) is shown. **(B)** A representative confocal image of BMDCs treated with C6NPs (Green: Nanoparticles, Red: Endo/lysosome). Merged signals are shown in yellow and highlighted with arrows. Scale bar, 5 μm. **(C)** Flow cytometry analysis of CD40, CD80 and CD86 expression on BMDCs after 48 h incubation with 522 treatments. Results are reported as mean ± SEM, n=3, ***p<0.001, One-way ANOVA. **(D)** BMDCs were incubated with OVA and/or 522 treatments for 48 h. Flow cytometry analysis of BMDCs expressing $OVA_{257-264}$ (SIINFEKL) peptide bound to H-$2K^b$ are shown. Results are reported as mean ± SEM, n=3, ***p<0.001, One-way ANOVA.

2.4.4. Nanoparticle migration to lymph node

To efficiently activate DCs *in vivo*, it is crucial for 522NPs reach the lymphoid organs including lymph nodes and spleen where a majority of DCs are located [65]. Following S.C. injection, nanoparticles were detected in all organs 1 h later and showed a slight increase at 6 h (**Figure 2.4A**). Inguinal lymph nodes, which drain the subcutaneous injection site, showed the highest distribution of nanoparticles. These results suggest S.C. injected nanoparticles enter both the lymphatic and systemic circulation efficiently. Accumulation of 522NPs in the draining lymph node was further examined by

immunofluorescence imaging. Nanoparticles were tracked using their green fluorescence and DCs were labeled with an anti-CD11c antibody. Nanoparticles were evenly distributed in the lymph node (**Figure 2.4B**), and merged signals indicate co-localization of nanoparticles and DCs. Although we could not distinguish DCs that internalized nanoparticles at the injection site and migrated to lymph nodes from lymph node resident DCs, our data demonstrate 522NPs can access the DCs in the lymph node.

Initiation of an immune response can be determined by DC expansion and activation in lymph nodes [90]. As our results showed 522NPs drain to lymph nodes and co-localize with DCs, we next examined the extent to which 522NP vaccination triggered DC expansion and activation *in vivo*. Mice were vaccinated with a model antigen OVA, and inguinal lymph nodes were collected to measure the number of total DCs and co-stimulatory molecule expressing DCs. We found the total number of DCs in lymph node of mice vaccinated with OVA+522NP increased 3- and 1.5-fold compared to those in the untreated and OVA only treated groups, respectively **(Figure 2.4C)**. DCs expressing co-stimulatory molecules CD40, CD86 and CD80 were significantly higher in the OVA+522NP vaccinated mice compared to those in the untreated and OVA-only treated groups. These data demonstrate the inclusion of 522NP in the vaccine enhances DC maturation in lymph nodes, a key step in priming T cells.

(A)

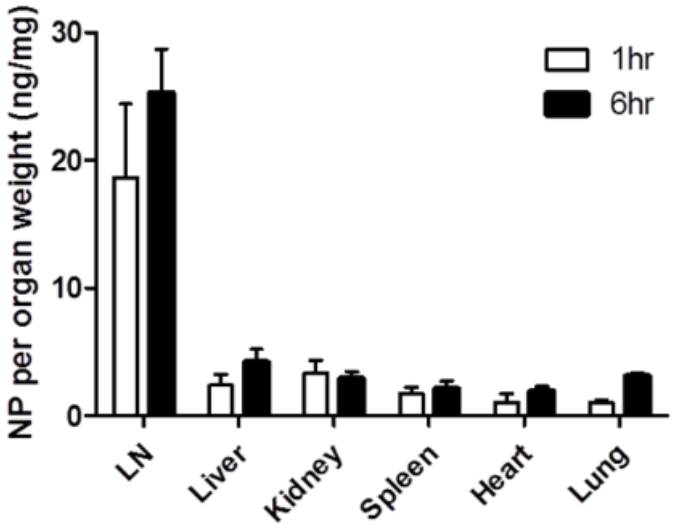
NP per organ weight (ng/mg)
30
20
10
0
1hr
6hr
LN
Liver
Kidney
Spleen
Heart
Lung

(B)

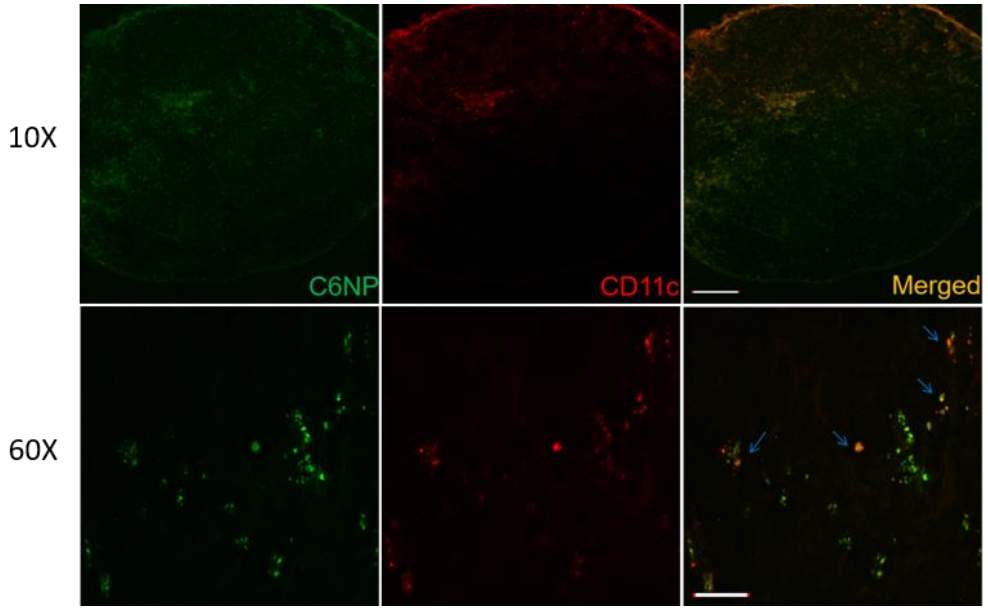
10X
60X
C6NP
CD11c
Merged

(C)

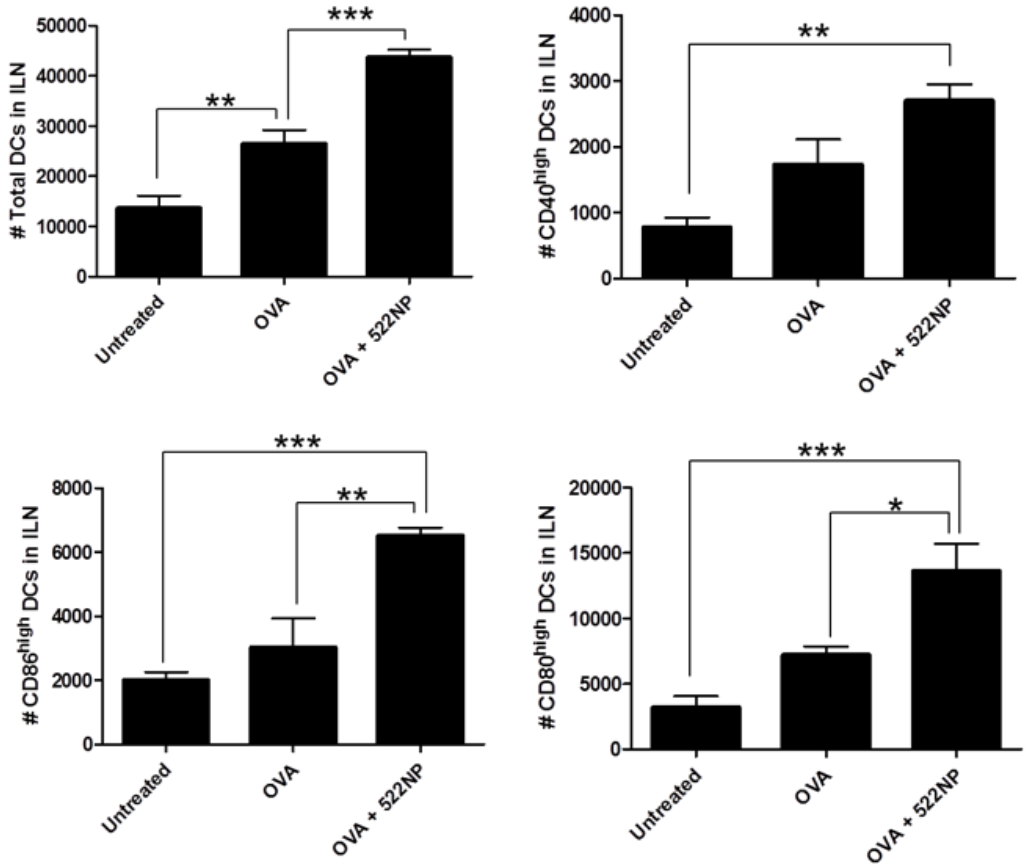

Figure 2.4. 522NPs migrate to draining lymph node and mature DCs

(A) C6NPs were injected S.C. and organs were harvested 1 and 6 h later. The amount of 6-coumarin in different organs was quantified by HPLC. **(B)** Inguinal lymph nodes were collected 6 h after S.C. injection of C6NPs and processed for immunofluorescence. A representative confocal image of the inguinal lymph node is shown. Green signal indicates location of C6NPs and red signal indicates $CD11c^+$ cells. Orange signals from merged image indicate co-localization of C6NPs and $CD11c^+$ cells. Images were taken at 10X and 60X magnification. Scale bar, 200 µm (10X), 20 µm (60X). **(C)** Inguinal lymph nodes were

harvested on d 7 after 5 doses of OVA vaccination. $CD11c^{+}$/MHC II^{+} cells were gated as DCs and numbers of total DCs, $CD40^{high}$, $CD86^{high}$ and $CD80^{high}$ cells were counted. Results are reported as mean ± SEM, *p<0.05, **p<0.01, ***p<0.001, n=3~4, one-way ANOVA.

Organ	Extraction Efficiency (%)
LN	46.3 ± 6.9
Liver	85.8 ± 8.5
Kidney	94.1 ± 5.9
Spleen	67.4 ± 9.1
Heart	57.4 ± 2.1
Lung	86.4 ± 3.8

Table 2.2. Extraction efficiency of C6NPs

Mouse organs were harvested and processed with 1 µg of 6-coumarin. Amount of 6-coumarin per organ was measured by HPLC. Extraction efficiency was calculated by (amount extracted (µg) / 1 µg) x 100. Results are reported as mean ± SD, n=3~4.

2.4.5. 522NP vaccination generates antigen-specific effector CD8 T cells

We next investigated the extent to which vaccination with 522NPs activated T cells. Since we were using OVA as the model antigen, we were in the position to examine the priming of OVA-specific CD8 T cells using the $OVA_{257-264}$:H-$2K^{b}$ tetramer [91]. We first measured the overall expansion of $OVA_{257-264}$-specific CD8 T cells, and found 4.5-fold and 3-fold more in OVA+522NP vaccinated mice than in untreated and OVA only treated

groups, respectively **(Figure 2.5A)**. One of the key functions of effector CD8 T cells is the production of IFN-γ [92]. We measured IFN-γ secretion by OVA-specific CD8 T cells after stimulating the vaccinated mice with $OVA_{257-264}$ peptides, and found OVA+522NP vaccinated mice showed the highest number of $OVA_{257-264}$-specific IFN-γ^+ CD8 T cells **(Figure 2.5B)**. Expansion of overall and effector OVA-specific CD8 T cells in OVA+522NP vaccinated mice demonstrates the DCs matured by 522NPs are able to efficiently process and present the antigens to generate Ag-specific effector CD8 T cells.

Effector CD8 T cells have the ability to directly kill target cells with granule exocytosis and death ligand expression [93]. To assess the efficacy of 522NP vaccination in inducing antigen-specific, CTL-mediated cell lysis, an *in vivo* CTL assay was conducted. The ratio of control cells (unpulsed, $CFSE^{low}$) to target cells ($OVA_{257-264}$ pulsed, $CFSE^{high}$) (C:T ratio) in the untreated group was 1.1, which indicates negligible target cell specific lysis **(Figure 2.5C)**. The C:T ratio of OVA+522NP vaccinated mice was 9.01. OVA- and 522NP-only groups had C:T ratios of 2.5 and 1.3, respectively **(Figure 2.5D)**. We then calculated the percent specific lysis using the C:T ratios. Mice immunized with OVA+522NP showed 87% Ag-specific lysis, suggesting OVA+522NP generated CD8 T cells can selectively find and kill the target cells **(Figure 2.5E)**. In contrast, OVA only treated group and 522NP only treated group each showed 52% and 12% specific lysis, respectively. The lower percent specific lysis in the OVA only and 522NP only groups suggest either the antigen or adjuvant alone is insufficient to induce a strong antigen-specific CTL response.

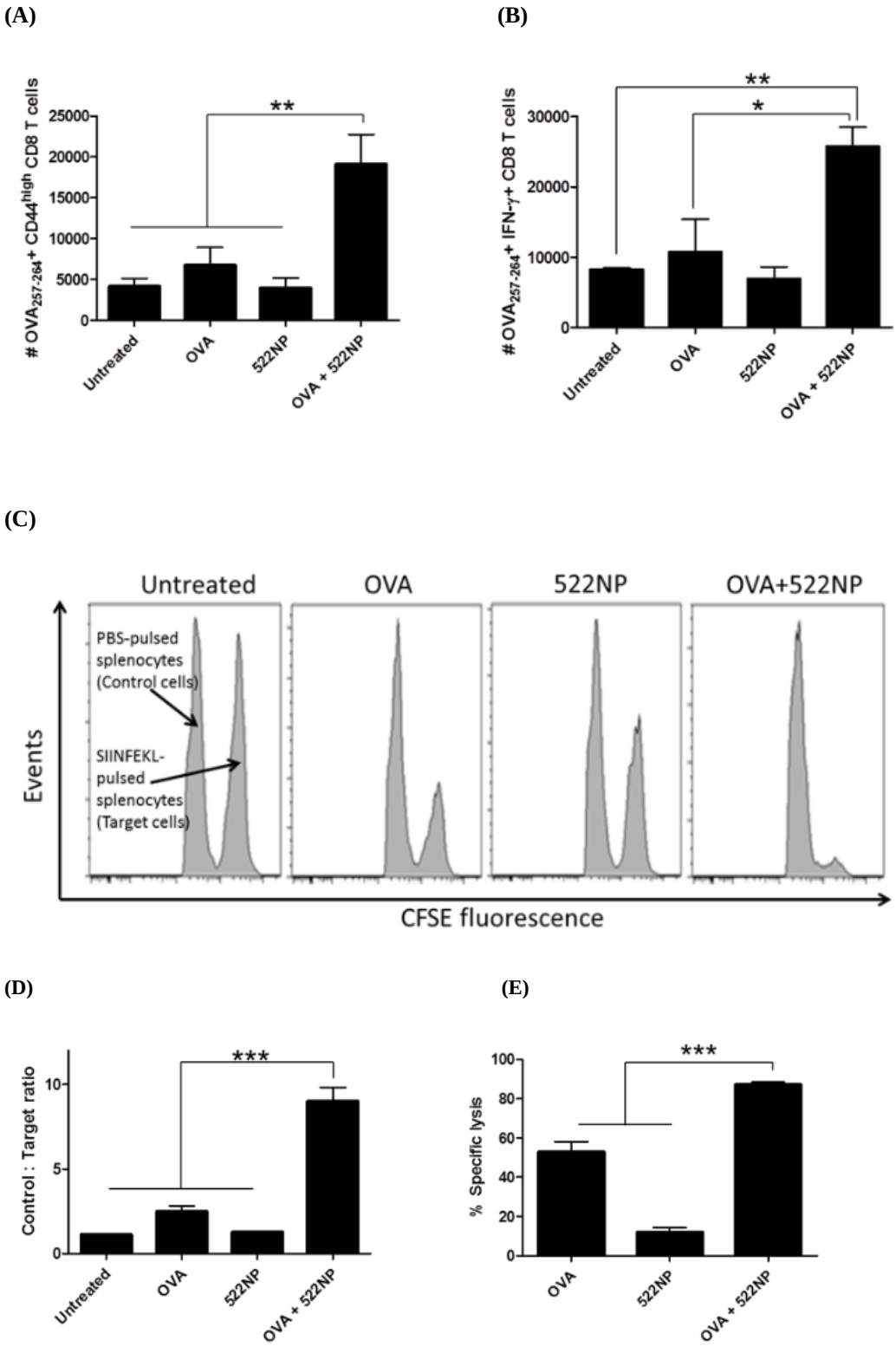

Figure 2.5. T cell expansion and CTL activity

(A,B) T cell expansion - Spleens of immunized mice were collected and analyzed using flow cytometry. The number of $CD8^+$ T cells were calculated using counting beads. **(A)** Number of $OVA_{257-264}$-specific $CD44^{high}$ CD8 T cells **(B)** Number of $OVA_{257-264}$-specific IFN-γ^+ CD8 T cells. Results are reported as mean ± SEM, *p<0.05, **p<0.01, n=3~4, one-way ANOVA. **(C-E) CTL assay** - Splenocytes labeled with CFSE were injected into immunized C57BL/6 mice. After 24 h, spleens were harvested for flow cytometry analysis. Only $CFSE^+$ cells are shown. **(C)** Representative flow cytometry plots for $OVA_{257-264}$-pulsed ($CFSE^{high}$, target cells) and unpulsed splenocytes ($CFSE^{low}$, control cells)**. (D)** Ratio of number of $CFSE^{low}$ splenocytes (*C*) to $CFSE^{high}$ splenocytes (*T*) in the spleen of the immunized mice. **(E)** Percent specific lysis of $OVA_{257-264}$-pulsed splenocytes is shown. Results are reported as mean ± SEM, ***p<0.001, n=4, one-way ANOVA.

2.4.6. B16F10-OVA lung metastasis and subcutaneous model

All of the data obtained thus far showing potent priming of CD8 T cells using 522NPs led us to examine the therapeutic efficacy of 522NPs using a variety of immunization protocols in different tumor models. We first investigated the prophylactic and therapeutic efficacy of OVA+522NP vaccination in mice bearing B16F10-OVA tumors [94]. Prophylactic efficacy of OVA+522NP was initially investigated in a lung metastasis model. Untreated and OVA+Free522 vaccinated mice had numerous lesions in the lung, while OVA+522NP immunized mice had relatively clear lungs **(Figure 2.6A)** with significantly fewer tumor modules **(Figure 2.6B)**. Further, OVA+522NP immunized mice had 7- and 2.5-fold higher number of Ag-specific CD8 T cells compared to the

untreated and OVA+Free522 treated mice, respectively **(Figure 2.6C)**. These results suggest the significantly increased number of Ag-specific CD8 T cells in OVA+522NP immunized mice protected them against the massive lung metastasis seen in the control groups.

Prophylactic efficacy of OVA+522NP immunization was also investigated in a S.C. tumor model where the tumor growth mimics human primary melanoma [95]. Palpable tumors were detected in all groups except OVA+522NP treated mice on d 10. In untreated group, tumors grew rapidly and reached a volume of 1000 mm^3 by d 21. OVA only, OVA+Free522 and 522NP only groups also demonstrated similar tumor growth trends **(Figure 2.6D)**. On the contrary, OVA+522NP vaccinated mice developed palpable tumors on d 14 and only two mice in the group (n = 6) had established tumors on d 21. At the end of the study, OVA+522NP vaccinated mice had significantly slower tumor growth and 100% survival. Data from both the lung metastasis and S.C. melanoma models suggest OVA+522NP prophylactic vaccination induces strong protective immune response against the B16F10-OVA cells and can delay the tumor growth significantly. We next examined the efficacy of OVA+522NP immunization against established tumors. The B16F10-OVA tumors were palpable by d 13 and mice were immunized for five days (d 13-17). Up to d 25, all the groups showed similar tumor growth trends. However, OVA+522NP immunized started to show reduced tumor growth on d 28 compared to the other treatment groups **(Figure 2.6E)**. It takes 7-10 days to generate antigen-specific T cells after immunization [96], which is identical to the time point where OVA+522NP therapy became effective.

OVA is a foreign antigen and highly immunogenic [97], prompting us to investigate the extent to which immunization with 522NP will generate anti-cancer immune response with endogenous tumor antigens, which can be less immunogenic and more challenging to elicit a protective T cell response. As we are using B16F10 cells in these experiments, we took advantage of the immunizing with the tyrosine related protein 2 (TRP-2), an endogenous antigen expressed on B16F10 cells [77,97]. In this study, B16F10 tumors were palpable on d 15 and mice received 5 vaccination doses (d 15-19). TRP-2 + Free522 immunized mice showed slight tumor inhibition by d 28, but aggressive growth was observed on d 31 **(Figure 2.6F)**. On the other hand, TRP-2 + 522NP immunized mice showed delayed tumor growth up to d 31. Consistent with OVA immunization, TRP-2 + 522NP immunization became effective ~10 days after the final dose. These results suggest 522NP immunization can induce both prophylactic and therapeutic immunity when co-administered with tumor-specific antigen.

(A)

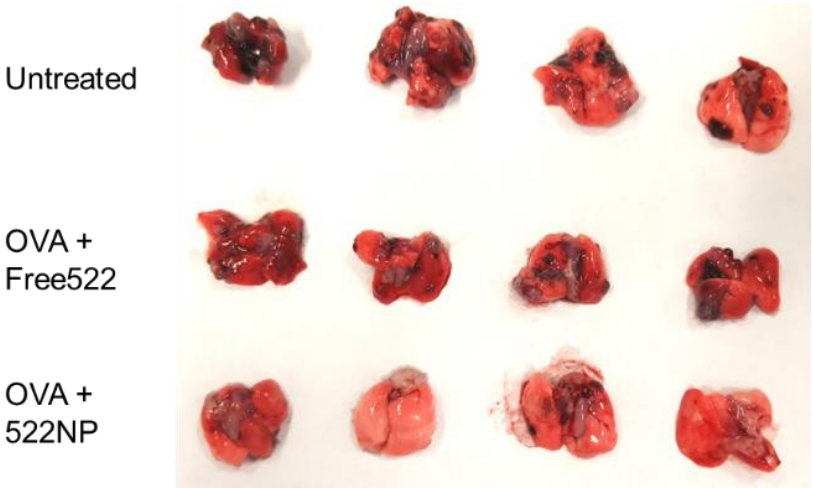

(B)

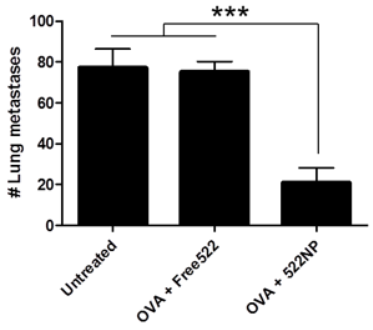
#Lung metastases
100
80
60
40
20
0
***
Untreated
OVA + Free522
OVA + 522NP

(C)

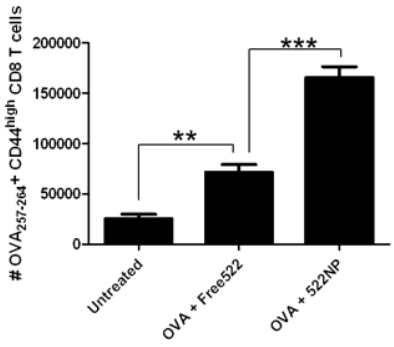
OVA257-264+ CD44high CD8 T cells
200000
150000
100000
50000
0
**
***
Untreated
OVA + Free522
OVA + 522NP

(D)

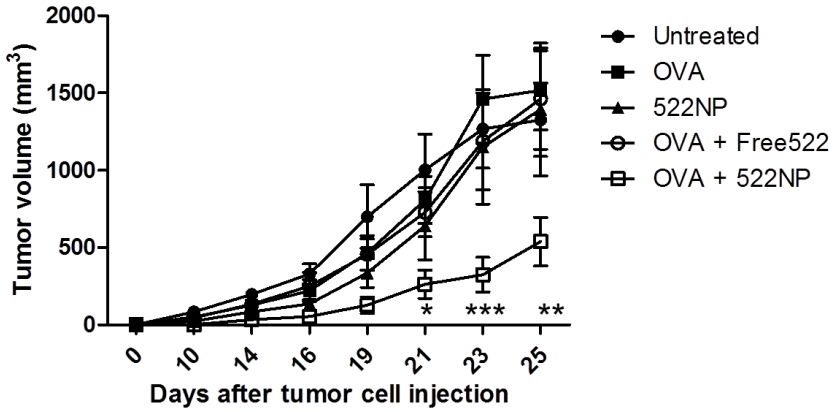
Tumor volume (mm3)
2000
1500
1000
500
0
0
10
14
16
19
21
23
25
Days after tumor cell injection
*
***
**
Untreated
OVA
522NP
OVA + Free522
OVA + 522NP

(E)

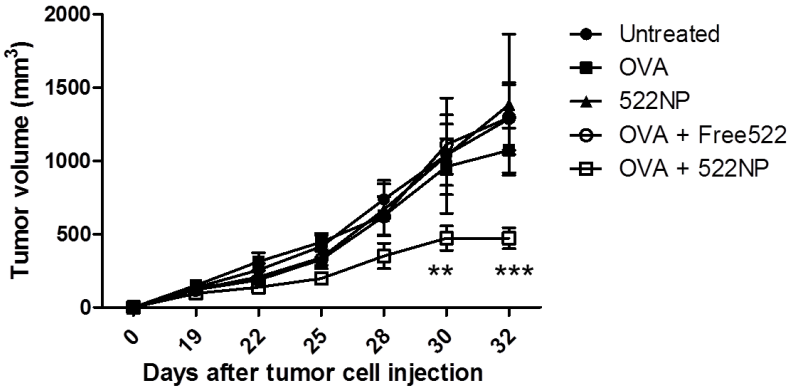
Tumor volume (mm3)
2000
1500
1000
500
0
0
19
22
25
28
30
32
Days after tumor cell injection
**
***
Untreated
OVA
522NP
OVA + Free522
OVA + 522NP

(F)

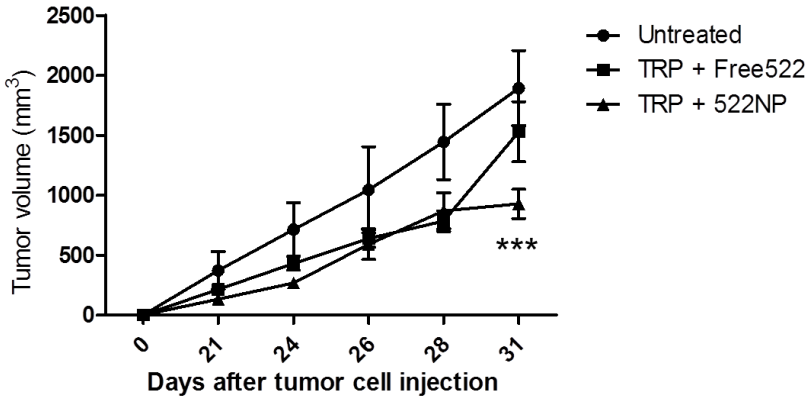

Figure 2.6. Tumor challenge using B16F10-OVA melanoma tumor models

(A-C) Lung metastasis model - C57BL/6 mice were immunized and B16F10-OVA cells were injected intravenously to establish lung tumors. **(A)** Images of lungs harvested on d 28 after cell injection **(B)** Number of lung tumor metastases were counted using a trinocular stereoscope. Results are reported as mean ± SEM, ***p<0.001, n=4, one-way ANOVA. **(C)** A different cohort of animals were treated as in **(A)** and spleens were harvested on d 13 and $OVA_{257-264}$ -specific $CD44^{high}$ CD8 T cells were counted. Results are reported as mean ± SEM, **p<0.01, ***p<0.001, n=4~5, one-way ANOVA. **(D-F) S.C. tumor model - (D)** C57BL/6 mice were immunized (d 1-5) and B16F10-OVA cells were injected subcutaneously to establish the tumor on d 8. Average volumes of tumors are shown. Results are reported as mean ± SEM; statistical analysis indicates Untreated Vs OVA+522NP groups, *p<0.05, **p<0.01, ***p<0.001, n=6, Repeated-measures ANOVA with posthoc Bonferroni test. **(E)** B16F10-OVA cells were inoculated on d 0 and treatments were given for five days (d 13-17). Results are reported as mean ± SEM; statistical analysis

indicates Untreated Vs OVA+522NP groups, $^{**}p<0.01$, $^{***}p<0.001$, n=7~9, Repeated-measures ANOVA with posthoc Bonferroni test. **(F)** B16F10-OVA cells were inoculated on d 0 and treatments were given for five days (d 15-19). Results are reported as mean ± SEM; statistical analysis indicates Untreated Vs TRP-2+522NP groups, $^{***}p<0.001$, n=5~6, Repeated-measures ANOVA with posthoc Bonferroni test.

2.4.7. Whole tumor vaccine against MB49 tumors

The above results suggest vaccination with 522NP induces antigen-specific CTL responses that effectively kill antigen-expressing tumor cells. However, tumor-specific antigens (e.g., RAS, BRAF, EGFR) are not available for all tumor types [98,99]. Whole tumor cell lysate-based vaccines are a promising alternate modality that seeks to overcome some of the limitations associated with peptide-based vaccines [100]. Therefore, we used a whole tumor cell lysate (CL) as the antigen source and investigated the effectiveness of 522NP to prime antitumor immunity when a non-peptide antigen source was used. For this purpose, we selected the immunogenic murine bladder cancer MB49 cell line as the antigen source [101,102]. We first examined the CD8 T cell response by determining the frequency of "Ag-experienced" $CD11a^{hi}CD8\alpha^{lo}$ CD8 T cells in the spleen [103]. We found the frequency of $CD11a^{hi}CD8\alpha^{lo}$ CD8 T cells increased when mice were vaccinated with CL+522NP, suggesting 522NP is able to enhance the immunogenicity of a tumor cell lysate and elicit a tumor-specific CD8 T cell response **(Figure 2.7A)**. Prophylactic efficacy of CL+522NP was investigated against S.C. MB49 tumors. CL+522NP significantly delayed tumor growth compared to control groups **(Figure 2.7B)**. On d 30, average tumor volumes

reached ~1000 mm^3 in untreated mice and ~500 mm^3 in CL alone and CL+Free522 treated groups. However, CL+522NP vaccinated mice showed remarkably very little tumor growth (~120 mm^3) over the same time period. Moderately delayed tumor growth in CL alone and CL+Free522 mice indicates the MB49 CL with or without Free522 can provide sufficient antigens to trigger an immune response, but the maximal response was achieved only when 522NP was used as the adjuvant. In the therapeutic study, only CL+522NP treatment was effective in delaying tumor growth **(Figure 2.7C)**. Unlike in the prophylactic study, where CL alone had a moderate effect, therapeutic effects were not observed from CL alone or CL+Free522 groups. We propose sustained release of 522 from nanoparticles allows for long-term generation of Ag-experienced ($CD11a^{hi}CD8\alpha^{lo}$) CD8 T cells, which leads to the observed efficacy of the CL+522NP treatment.

(A)

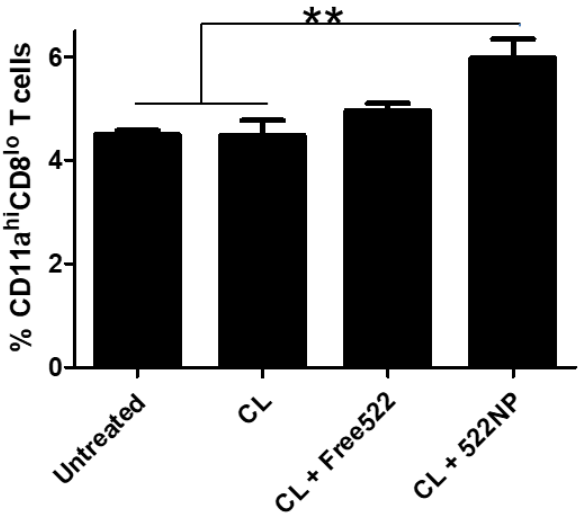

(B)

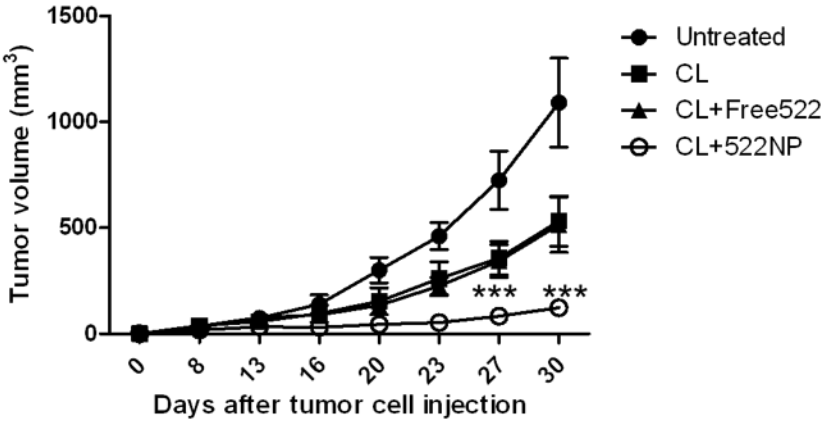

(C)

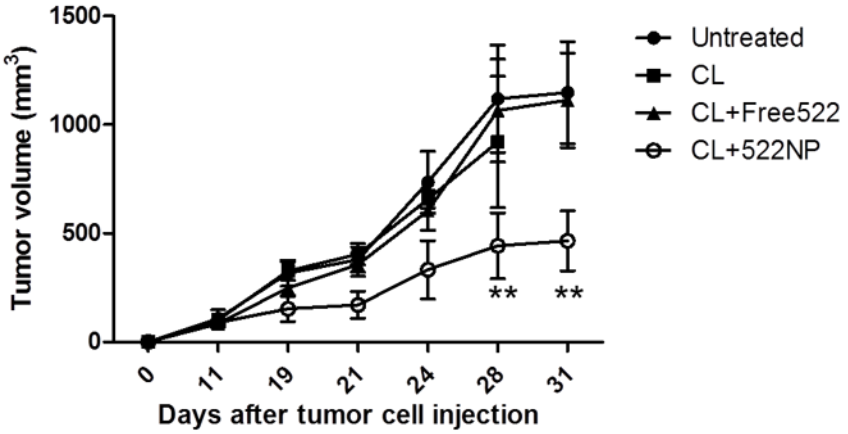

Figure 2.7. Cell lysate vaccine efficacy against murine bladder cancer MB49 tumor models.

(A) Number of $CD11a^{hi}/CD8^{lo}$ CD8 T cells from spleens of MB49 cell lysate vaccine immunized mice. Results are reported as mean ± SEM, $*p<0.05$, n=4, one-way ANOVA. **(B)** C57BL/6 mice were immunized (d 1-5) and MB49 cells were injected subcutaneously to establish the tumor on d 8. Results are reported as mean ± SEM, Statistical analysis

indicates Untreated Vs CL+522NP groups,***p<0.001, n=5, Repeated-measures ANOVA with posthoc Bonferroni test. **(C)** MB49 cells were inoculated on d 0 and treatments were given for five days (d 8-12). Results are reported as mean ± SEM, Statistical analysis indicates Untreated Vs CL+522NP groups,**p<0.01, n=5, Repeated-measures ANOVA with posthoc Bonferroni test.

2.4.8. *In situ* vaccination in an orthotopic renal cell carcinoma (RCC) model

In situ generated tumor cell lysates can be a rich source of tumor antigens to elicit anti-tumor immunity [104,105]. Previously, our group reported *in situ* vaccine composed of adenovirus-encoded murine TNF-related apoptosis-inducing ligand (Ad5mTRAIL) and TLR9 agonist CpG, which induced a robust CD8 T cell response, that resulted in eradication of both primary and metastatic RCCs [45,106]. Therefore, we used Ad5mTRAIL to induce tumor ablation and investigated the extent to which nanoparticles encapsulating 528 (528NPs) could augment systemic T cell immunity in this physiologically relevant orthotopic Renca tumor model. After a single intrarenal (IR) administration of treatments, whole body tumor burden was monitored by BLI. Consistent with previous studies, Ad5mTRAIL without immune stimulant treatment (Ad5mTRAIL + BlankNP) was not effective in reducing tumor growth. The tumor burden was significantly lower in mice immunized with Ad5mTRAIL + Free528 and Ad5mTRAIL + 528NP compared to other control groups, which demonstrates strong adjuvant capacity of 528 **(Figure 2.8A)**. As tumor burdens from the primary tumor (kidney) and metastases could not be differentiated

based on whole body imaging, we excised the lungs and measured tumor-associated bioluminescence at the end of the study. *Ex vivo* imaging showed only Ad5mTRAIL + 528NP was effective in reducing lung metastasis compared to the other control groups **(Figure 2.8B)**. As CD8 T cells are known to play a key role in eradicating secondary lesions [107,108], these results suggest 528NP immunization can invoke persistent CTL response capable of reducing the growth of both primary and metastatic tumors. This is also consistent with our B16F10-OVA lung tumor model study where 522NPs induced protective immunity by expanding Ag-specific CD8 T cells.

(A)

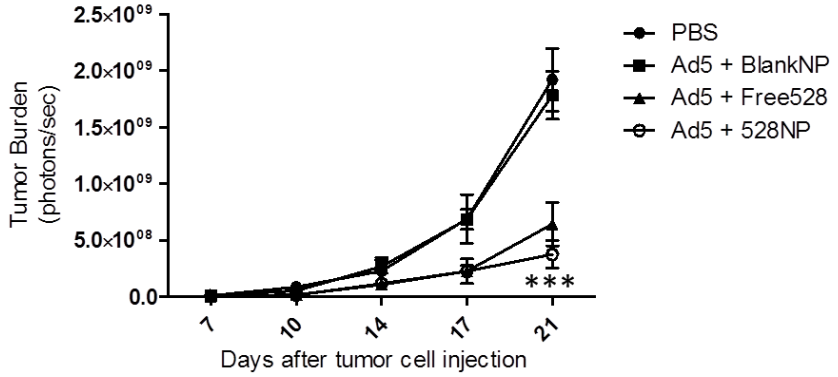

(B)

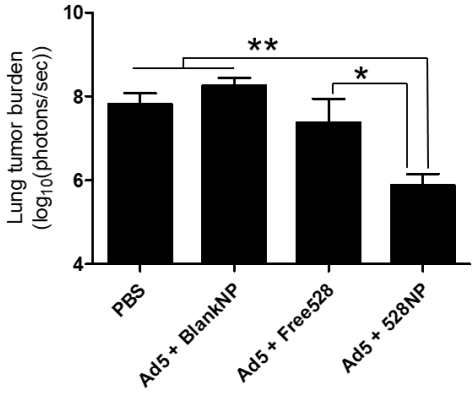

Figure 2.8. *In situ* vaccine against renal cell carcinoma

Balb/c mice bearing IR Renca-GL tumors were treated with PBS alone or Ad5-TRAIL combined with BlankNP, Free528 or 528NP IR on d 7. **(A)** Whole body tumor burden was tracked with bioluminescent imaging. Results are reported as mean ± SEM, Statistical analysis indicates Untreated Vs Ad5-TRAIL +528NP groups, ***p<0.001, n=5, Repeated-measures ANOVA with *post hoc* Bonferroni test. **(B)** On d 21, lungs were excised and imaged separately. Results are reported as mean ± SEM, Statistical analysis indicates Untreated Vs Ad5-TRAIL +528NP groups, *p<0.05, **p<0.01, n=5, one-way ANOVA.

Discussion

Immune-based therapies for solid tumors have the potential to improve long-term survival against cancers of various stages, including metastatic cancers [14,71,109,110]. The goal of cancer immunotherapy is to activate T cells to recognize and eliminate tumor cells in an antigen -specific manner, which can be achieved by activation of APCs, mainly DCs and macrophages [111]. TLR agonists stimulate DCs, resulting in increased expression of co-stimulatory molecules and pro-inflammatory cytokine secretion, which in turn leads to T cell expansion [26,37]. Unlike other TLRs present on the cell membrane, TLR 3, 7, 8 and 9 are located on the luminal side of the endo/lysosome [86]. Therefore, localization of the agonist molecule to endo/lysosomes is critical for triggering TLR 7/8 signaling and DC activation. In our study, 522NPs are efficiently internalized by APCs, which is consistent with previous reports that sub-micron size particles are suitable for DC uptake [58,80]. Intracellular trafficking study showed 522NPs are located in endo/lysosomes after

internalization, suggesting 522NPs can deliver 522 to the target intracellular compartment in DCs.

While both Free522 and 522NPs significantly increased the overall co-stimulatory molecule expression in BMDCs, 522NPs resulted in higher CD86 expression than Free522. CD86:CD28 engagement results in stronger DC:T-cell interactions than CD80 engagement, thereby initiating a more potent T cell response [112]. BMDCs treated with 522NPs also showed remarkable antigen (OVA)-presentation compared to those treated with Free522. One possible explanation for this finding is that positively charged OVA aggregated on the negatively charged 522NP surface and was internalized into DCs more efficiently to be processed by proteasome, as aggregation of proteins on nanoparticles increase uptake by APCs [76,113,114]. Furthermore, a previous study suggested MyD88-dependent TLR signaling can augment antigen cross-presentation by inducing phagosomal MHC I delivery from endosomes [115]. In our case, this could have been achieved by persistent TLR 7 and 8 signaling enabled by sustained release of 522 from 522NPs. These results are consistent with other studies demonstrating improved immune response with nanoparticles over the soluble form of TLR ligand [67,116,117].

An additional advantage of using nanoparticles as vaccine adjuvants is their tendency to accumulate in draining lymph nodes following S.C. or I.M. administration [65]. Recent studies report nanoparticle drainage to the lymph node is dependent on the size of the particles [57,118]. Small particles (20-200 nm) efficiently migrate directly into the lymphatic system while larger particles (>500 nm) are carried by DCs. In our studies, 522NPs were detected in the inguinal lymph nodes 1 h after S.C. injection. This relatively rapid

distribution is likely the result of their small size that allows direct drainage to the lymph node as well as DC-associated migration, which is supported by co-localization of 522NPs and $CD11c^+$ cells in inguinal lymph node.

OVA+522NP immunization dramatically increased the number of $CD11c^+$ MHC II^+ DCs in the draining lymph nodes relative to those in untreated and OVA alone group, suggesting 522NPs facilitate increased DC migration to the lymph nodes. Furthermore, co-stimulatory molecule expression on these DCs was also higher following the immunization with OVA+522NPs. These data are consistent with the above studies showing nanoparticle encapsulated TLR7/8 agonist can potentiate DC migration and activation in draining lymph nodes by co-delivering antigens and persistent TLR 7/8 activation [76,113].

CD8 T cells selectively recognize and eliminate target cells in an MHC I-restricted manner. Therefore, priming antigen-specific CD8 T cells is critical for achieving selective killing of target cells. We observed a 4.5-fold increase in the number of splenic OVA-specific $CD44^{hi}$ CD8 T cells and a 2.5-fold increase in the number of OVA-specific IFN-γ^+ CD8 T cells when mice were immunized with OVA+522NP compared to untreated mice. Expression of CD44 implies these CD8 T cells can become memory T cells and respond to a secondary antigen encounter, which can provide protective immunity against cancer recurrence [119]. IFN-γ plays a key role in cancer immunotherapy as it can enhance the survival and activation of DCs and T cells and increase the susceptibility tumors to T cells [92]. Thus, the expansion of antigen-specific $CD44^{hi}$ and IFN-γ^+ CD8 T cells strongly suggests 522NP immunization can prime antigen-specific effector CD8 T cells. Additionally, OVA+522NP immunized mice showed dramatically higher specific lysis

efficacy against $OVA_{257-264}$-pulsed target cells compared to unpulsed control cells, further suggesting the combination of antigen and 522NP is highly effective in priming antigen-specific CD8 T cells.

To examine the extent to which this antigen-specific CD8 T cell response was effective against tumor cells, protective T cell immunity was investigated in primary and lung metastatic models induced by B16F10-OVA melanoma cells. Mice immunized with a combination of OVA and 522NP showed reduced lung tumor foci and significantly delayed tumor growth in these aggressive tumor models, demonstrating antigen+522NP immunization can potentiate protective immunity in an antigen-specific manner. Furthermore, OVA+522NP immunization was effective against established B16F10-OVA tumor model, where the overall immune response can be hampered by tumor evasion and immune-editing [120,121]. These data demonstrate OVA+522NP immunization can elicit a T cell response even in immune-suppressive environments. Endogenous antigens often induce self-tolerance, which inhibits expansion of effector T cells [25]. In our study, TRP-2+522NP immunization was also effective in inhibiting the growth of established B16F10 tumors. Although tumor inhibition was moderate when compared with OVA-based vaccine, this is expected given the relatively low expression of the TRP-2 epitope (compared to the antigenic epitopes within OVA) and its low binding affinity to K^b [97].

Clinical trials with tumor vaccines using synthetic peptides derived from tumor antigens have met with limited success [98,99], with one limitation being MHC restriction, diminishing its utility in diverse populations [122]. The sub-optimal efficacy could also result from poor immunogenicity of tumor antigens, tumor heterogeneity, emergence of tumor

cells that lose the targeted antigen, and immunological changes that decrease the initiation of a productive antitumor immune response [3,123]. Autologous whole tumor cells contain all the antigens that a patient's own immune system could potentially react with, representing a more exhaustive repertoire of tumor antigens [100]. Therefore, we tested the adjuvant capacity of 522NPs with tumor cell lysate, a poorly immunogenic antigen source without immune stimulants [100,124]. T cell responses were examined after immunizing the mice with MB49 cell lysates in which no tumor specific antigens have been identified to this point [125]. Although there were limitations to measuring MB49 tumor cell-specificity of T cells, our data demonstrate an increase in 'Ag-experienced' ($CD11a^{hi}CD8^{lo}$) $CD8^{+}$ T cells when mice were immunized with 522NPs. Furthermore, cell lysate+522NP immunization was effective in delaying tumor growth in both prophylactic and therapeutic settings, suggesting 522NP can potentiate tumor-specific CD8 T cell response even with an undefined, poorly immunogenic antigen source. The therapeutic efficacy of Ad5mTRAIL-mediated *in situ* vaccine against the metastatic RCC model further demonstrates the potency and versatility of these novel TLR 7/8 agonist loaded nanoparticles. We have previously reported both plasmacytoid and CD8α DCs are required for successful TRAIL-based immunotherapy, which suggests 528NPs can efficiently activate both DC subsets [45]. Additionally, the RCC study suggests nanoparticle-based vaccination is not limited to S.C. or I.M. routes but can also be utilized for intratumoral (I.T.) administration, where local delivery can enhance the immunogenicity of the vaccine [126,127].

We have focused our efforts to investigate the ability of 522NPs to elicit an anticancer T cell response. Recent studies show TLR 7/8 agonists can also augment

antibody-dependent cell cytotoxicity (ADCC) of therapeutic antibodies by activating NK cells [128,129]. Combination of TLR7 agonist and chemotherapy induces synergistic tumoricidal effects in breast cancer and vulval intraepithelial neoplasia [130,131]. Radiation-induced *in situ* vaccine using TLR7 agonist generates anti-tumor effects against lymphoma and melanoma [132,133]. Combination of TLR7 agonist with PD-1 blockade suppressed tumor growth and prevented metastasis in head and neck squamous cell carcinoma (HNSCC) models [134]. These reports strongly suggest TLR7/8 agonists can be used as versatile immune adjuvants in a variety of cancer immunotherapy settings. Furthermore, the well-established use of biocompatible PLGA polymer for human applications and the recent approval of polymeric nanoparticles [135,136] suggests 522NP-based vaccines have the potential to achieve regulatory approvals.

In this study, PLGA nanoparticles were utilized as the carrier for TLR 7/8 agonist with because of the biocompatibility of the polymer [137]and the facile fabrication techniques that result in nanoparticle physiochemical properties for optimal DC internalization and LN drainage [51,56]. Other studies have utilized PLGA nano and microparticles as anticancer vaccine adjuvants [67,77,138]. Nanoparticle carriers including N-(2-hydroxypropyl)methacrylamide (HPMA), chitosan and liposomes which have been utilized for vaccine delivery are also promising candidates for TLR 7/8 delivery carrier [76,139,140].

For successful clinical translation of 522NPs, further studies on safety of 522NPs and optimization of the vaccine formulation are required. Currently, the TLR7-specific agonist imiquimod is approved only for topical use. Therefore, potential adverse effects of

our novel TLR7/8-specific agonists including possible systemic cytokine and autoimmune reactions following S.C or I.M. delivery [126,141] need to be investigated. We also need to optimize the fabrication of 522NPs. The loading efficiency of 522 in the PLGA matrix was relatively low, which was similar to that reported in previous studies investigating the loading of imidazoqunolines in PLGA nanoparticles [142,143]. Higher loading of 522 in nanoparticles could allow for fewer doses of the vaccine. With these issues addressed, we expect 522NPs can be a highly valuable and potent adjuvant for cancer immunotherapy.

Chapter 3.

Acidic pH-responsive PLGA nanoparticles as TLR7/8 agonist delivery platform for cancer immunotherapy

3.1 Summary

Synthetic imidazoquinoline-based toll-like receptor (TLR) 7/8 bi-specific agonists are promising vaccine adjuvants that can induce maturation and activation of dendritic cells (DCs) and activate them to secrete pro-inflammatory cytokines. However, *in vivo* efficacy of these small molecule agonists is often hampered by their fast clearance from the injection site, limiting their use to topical treatments. In this study, we investigated the use of acidic pH-responsive poly(lactide-co-glycolide) (PLGA) nanoparticles for endo-lysosome specific release of 522, a novel TLR7/8 agonist. Bicarbonate salt was incorporated in the new formulation to generate carbon dioxide ($CO_{2)}$ gas in acidic pH, which can disrupt the polymer shell to rapidly release the payload. Compared to conventional PLGA nanoparticles, the pH responsive formulation resulted in 33-fold higher loading of 522. The new formulation demonstrated acid-responsive CO_2 gas generation and drug release. The acid-responsive formulation increased the *in vitro* expression of co-stimulatory molecules on DCs and improved antigen-presentation via MHC I, both of which are essential for CD8 T cell priming. *In vivo* studies showed that pH-responsive formulation elicited stronger antigen-specific CD8 T cell and natural killer (NK) cell responses than conventional PLGA nanoparticles, resulting in enhanced anticancer efficacy in a murine melanoma tumor model. Our results suggest that acidic-pH responsive, gas-generating nanoparticles is an efficient TLR7/8 agonist delivery platform for cancer immunotherapy.

3.2. Introduction

Imidazoquinoline-based synthetic toll-like receptor (TLR) 7/8 agonists are promising vaccine adjuvants for cancer immunotherapy [144]. TLR7/8 ligation triggers MyD88-dependent signaling in dendritic cells (DC), resulting in the production of pro-inflammatory cytokines and co-stimulatory molecule expression [145]. DC activation leads to expansion of activated natural killer (NK) cells and antigen (Ag)-specific CD8 T cells, both of which can kill malignant tumor cells [146]. Current vaccine designs seek to deliver TLR agonists to DCs present in the skin and/or draining lymph nodes [57]. However, small molecules are not retained in the skin for an extended duration because of rapid clearance from the well-vascularized dermal layers. This can result in undesirable systemic immune response [76]. Further, following uptake by DCs, the agonist molecules have to distribute into endo-lysosomes to activate TLR 7/8 [147]. Thus, endo-lysosomal specific delivery of the agonists to DCs present in the dermal layers and lymph nodes can result in efficient TLR7/8 ligation and superior anticancer immune response.

We previously reported the use of poly(D,L-lactide-co-glycolide) (PLGA) nanoparticles for the delivery of a novel TLR7/8 agonist (termed '522') [70]. These nanoparticles (referred to as '522NP') traffic to draining lymph nodes after subcutaneous (S.C.) injection and potently activate DCs. When combined with a peptide or whole tumor cell lysate-based Ag, 522NP immunization significantly increased the number of Ag-specific effector CD8 T cells. Moreover, this vaccination modality enhanced the prophylactic and therapeutic anticancer efficacy in murine tumor models. Yet, these

nanoparticles were limited by low encapsulation efficiency (which limited the dose of 522 that could be used) and non-specific agonist release.

In this study, we investigated the use of acidic pH responsive PLGA nanoparticles to both increase agonist encapsulation and improve endo-lysosome (pH 4-6)-specific agonist release. We hypothesized the higher dose and acidic-pH responsive release of 522 would result in stronger activation of DCs and elicit robust CD8 T cell response for enhanced cancer immunotherapy. We adapted the use of bicarbonate salt, which generates carbon dioxide (CO_2) gas in acidic pH, to incorporate pH responsiveness. Thus, NPs encapsulating both 522 and sodium bicarbonate were expected to generate CO_2 gas in the acidic pH of the endo-lysosomes and mechanically disrupt the polymer matrix, resulting in a burst release of the encapsulated 522 in endo/lysosomes. In our study, co-incorporation of sodium bicarbonate resulted in significantly increased encapsulation of 522 and acidic pH responsive 522 release. Our data further suggest this new formulation elicits a much stronger anti-cancer immune response than conventional PLGA NPs.

3.3. Materials and Methods

3.3.1. Materials

Poly(lactide-*co*-glycolide) (PLGA) (50:50 lactide-glycolide ratio; 0.55-0.75 dl/g inherent viscosity) was purchased from Lactel (Birmingham, AL). TLR 7/8 agonist (termed '522') was synthesized and characterized as previously reported [42,75]. Albumin from chicken egg white (ovalbumin, OVA), polyvinyl alcohol (PVA), 6-coumarin, ammonium acetate and dimethyl sulfoxide (DMSO) were purchased from Sigma-Aldrich (St Louis,

MO). Sodium bicarbonate, chloroform, acetonitrile, fluorescein conjugated ovalbumin, Foxp3 transcription factor staining buffer kit were purchased from Fisher Scientific (Rockford, IL). Fluorophore-labeled monoclonal antibodies for flow cytometry were purchased from Biolegend (San Diego, CA) (CD3, CD8, CD11c, CD80, CD49b, CD69, IFN-γ), eBioscience (San Diego, CA) (CD4, CD44, CD40, CD86) and Tonbo Biosciences (San Diego, CA) [I-A/I-E(MHC II)].

Animals and cell line

All animal experiment protocols were reviewed and approved by Institutional Animal Care and Use Committee (IACUC) of the University of Minnesota. Immunocompetent C57BL/6 mice (7-8 weeks, female) were purchased from Charles River (Wilmington, MA) and housed under specific pathogen free (SPF) units in Research Animal Resources at the University of Minnesota.

B16F10-OVA, a murine melanoma cell line which expresses ovalbumin, was provided by Dr. Brandon Burbach (University of Minnesota). B16F10-OVA was cultured in RPMI 1640 medium supplemented with 10% fetal bovine serum, 100 μg/mL streptomycin, 100 U/mL penicillin (hereafter referred to as complete RPMI) and 5 μg/mL G-418 Disulfate (Research products international, Mt Prospect, IL).

3.3.2. Methods

Fabrication of nanoparticles

522NP formulation was prepared as previously reported [70], using 3 mg 522 and 44 mg PLGA. Acidic pH-responsive nanoparticle formulation of 522 (hereafter referred to as '522GGNP') were formulated using a variation of the water-in-oil-in-water (w/o/w) double-emulsion solvent evaporation technique. For the primary w/o emulsion, the aqueous phase was prepared by dissolving 2.5 mg of sodium bicarbonate in 500 µl of 1% w/v PVA in endotoxin-free distilled water (D.I. water). This aqueous phase was transferred to the oil phase, which consisted of 44 mg PLGA and 3 mg 522 dissolved in 2 ml chloroform. This mixture was sonicated using probe sonicator (Sonicator XL, Misonix, Melville, NY) for 1 min to form w/o emulsion. This primary emulsion was then added to 8 ml of 2% PVA and sonicated for 5 min to form secondary w/o/w emulsion. The final emulsion was stirred for ~18 h, followed by 1 h in a desiccator under vacuum to evaporate chloroform. Nanoparticle dispersion formed was washed by centrifugation (Optima XPN-80 Ultracentrifuge, Beckman Coulter Inc., Fullerton, CA) (35,000 RPM, 35 min) and reconstitution with D.I. water three times. After final wash, nanoparticles were resuspended in D.I. water and lyophilized (Labconco FreeZone 4.5, Kansas City, MO). Nanoparticles were stored at -20°C until use.

Characterization of nanoparticles

To determine size and zeta potential of the nanoparticles, ~1 mg of nanoparticles were dispersed in D.I. water and sonicated for 30 sec and subjected to dynamic light scattering (DLS) analysis (Delsa^{TM} Nano C, Beckman Coulter Inc.). Nanoparticles were

also imaged using a cryo-transmission electron microscope (TEM) (FEI Tecnai G2 F30) as described previously [148].

The amount of 522 encapsulated into the nanoparticles was quantified using high-performance liquid chromatography (HPLC; Beckman Coulter) as previously reported [70]. The amount of sodium bicarbonate encapsulated into the nanoparticles was measured by quantifying sodium ion using inductively coupled plasma optical emission spectrometry (ICP-OES) (Thermo Scientific iCAP 6000 Series). Briefly, a mixture of nitric acid and hydrochloric acid (3:1 molar ratio) was added to 1 mg of nanoparticles in a glass vial. Glass vial was heated to 90°C in an oil bath for 5 h to fully dissolve nanoparticles. Mixture was then cooled and diluted with D.I. water for ICP-EOS analysis.

Cytotoxicity of nanoparticles

Splenocytes from C57BL/6 mice were used to measure cytotoxicity of nanoparticles. A single cell suspension of splenocytes was prepared using an established protocol [45]. Briefly, spleens were mechanically homogenized using gentleMACS Dissociator (Miltenyi BioTeck Inc., Auburn, CA). The cell suspension was washed with HBSS and digested in HBSS supplemented with 0.15 mg/ml DNAse I (Sigma) and 0.56 Wuensch units/ml Liberase Blendzyme 3 (Roche, Branford, CT). After 30 min, red blood cells (RBCs) were removed by incubating the cell suspension with lysis buffer (Pharm Lyse, BD Bioscience, San Jose, CA) with for 5 min. Cells were then washed with PBS and suspended in HBSS until further use. To evaluate cytotoxicity of nanoparticles, mouse splenocytes (2×10^4 cells/well) were incubated with 522GGNP (15.6~250 μg/ml) in a 96-

well plate. After 48 h incubation period, supernatants were collected and cytotoxicity was determined according to the manufacturer's protocol (LDH Cytotoxicity Assay Kit, Thermo).

TLR7 and 8 reporter cell assay

Human TLR-specific reporter cell assays were performed as previously reported [75]. Reporter cells (HEK-Blue^{TM}-hTLR7 and 8, InvivoGen, San Diego, CA) (40,000 cells per well) were seeded in 96-well cell culture plate, and soluble form of 522 in DMSO (referred to as 'Free522') (30 μM) or 522GGNP (522 equivalent to 30 μM) were added to the wells. After 24 h, supernatants were collected for measuring TLR-specific activity according to manufacturer's protocol.

***In vitro* release kinetics**

Release of 522 from 522GGNPs was determined in acidic (5.5, 6.5) and neutral pH (7.4) buffers. Release buffer was added to 1 mg of nanoparticles in 2 ml plastic tubes. Sample tubes were incubated in a water bath shaker at 37°C (100 RPM). At pre-determined time points, samples were centrifuged and 0.5 ml of the supernatant was collected. Sample tubes were refilled with fresh 0.5 ml buffer to maintain a constant volume. Collected samples were lyophilized and agonist was extracted with methanol. Amount of agonist released at each time point was analyzed using HPLC.

Generation of CO_2 bubbles was tested as previously described [149]. Briefly, 10 ml of buffer solution (pH 5.5 or 7.4) was added to ~6 mg of nanoparticles in a 15-ml plastic tube.

The CO_2 bubbles generated were visualized using an ultrasound imaging system (Vevo2100, Visualsonics) equipped with a 21 MHz transducer. Intensity of bubbles were measured by quantifying white values in ultrasound images using ImageJ software. Sodium bicarbonate (50 mg) and 522NPs (6 mg) were used as positive and negative controls, respectively.

Culture of bone marrow-derived dendritic cells (BMDCs)

BMDCs were prepared as described previously [70]. Briefly, bone marrow precursor cells were collected from tibias and femurs from C57BL/6 mice. Cells were filtered with a 70 micron nylon mesh and red blood cells were removed using lysis buffer to obtain single cell suspension. Cells were seeded in petri dish and incubated with complete RPMI media, supplemented with 20 ng/mL granulocyte-macrophage colony-stimulating factor (GM-CSF) (PeproTech, Rocky Hill, NJ), 10 ng/mL IL-4 and 50 μM 2-mercaptoethanol (Sigma) for 6 d to generate immature BMDCs.

Uptake of nanoparticles in BMDCs

To label and track nanoparticles, 6-coumarin, a hydrophobic fluorescent dye, was co-encapsulated in 522GGNPs by adding 300 μg of 6-coumarin to the organic phase during 522GGNP fabrication [150]. For *in vitro* cell uptake study, BMDCs were seeded in a 24-well culture plate (10^6/well), and then incubated with NPs (0.2 mg/ml) for 2 h. Cells were collected, washed with PBS, and stained with anti-CD11c mAb. Uptake of NPs by BMDCs was examined by monitoring 6-coumarin-associated fluorescence intensity by flow

cytometry (BD LSR II). Flow cytometry data were analyzed using FlowJo software (TreeStar Inc., Ashland, OR).

Intracellular distribution of NPs was imaged by confocal laser scanning microscopy (Olympus FluoView FV1000 BX2 Upright Confocal). Glass-bottomed petri dishes (35 mm, MatTek) were coated with poly-L-lysine solution (Sigma) for 30 min. After 30 min, the poly-L-lysine solution was removed and petri dishes were rinsed with D.I. water twice. Dishes were dried in a laminar flow hood for 2 h, and BMDCs ($3x10^5$/dish) were added. After 24 h, BMDCs were incubated with NPs (0.2 mg/ml) for 4 h, and rinsed with PBS. Cells were counterstained with LysoTracker® Red DND-99 (Thermo Scientific) and imaged without fixation.

In vitro BMDC activation

BMDCs (10^6/well) were added to a 24-well cell culture plate. Following attachment, BMDCs were treated with OVA (20 µg) alone or OVA combined with 522NPs (100 µg/ml, equivalent to 120 ng/ml of 522) or 522GGNPs (100 µg /ml, equivalent to 4 µg/ml of 522) for 24 h. Expression of co-stimulatory molecules (CD40, CD80 and CD86) and MHC II on BMDCs was measured by flow cytometry.

In vitro BMDC antigen uptake and presentation

Antigen uptake by BMDCs was measured by flow cytometry. A solution of fluorescein conjugated OVA (OVA-FITC, Thermo) in PBS (10 µg/ml) was added to BMDCs ($1x10^6$/well). Subsequently, cells were incubated with 0.1 mg of 522NP or

522GGNP for 6 h. Cells were then washed with PBS and stained with anti-CD11c mAb. FITC associated fluorescence intensity was measured in $CD11c^+$ cells by flow cytometry. To examine antigen presentation by BMDCs, the above experiment was repeated by incubating unlabeled OVA (20 μg) with BMDCs for 24 h. After 24 h, BMDCs were harvested and stained with anti-$OVA_{257-264}$ (SIINFEKL) peptide bound to H-$2K^b$ (clone 25-D1.16; eBioscience) antibody and analyzed by flow cytometry.

Immunization protocol

Vaccine doses were prepared by combining OVA (100 μg) with 1.5 mg of 522NPs (equivalent to 1.8 μg of 522) or 522GGNPs (equivalent to 60 μg of 522) in 200 μl of sterile PBS. Each dose was injected s.c. to the left and right thighs (100 μl each). Mice were dosed once every day for five consecutive days.

***In vivo* T cell and NK cell activation assays**

Immunocompetent C57BL/6 mice were immunized daily as described above for 5 d (d 1~5). On d 10, mice received 100 μg of $OVA_{257-264}$ peptide via tail vein injection and euthanized after 4 h. Spleen was collected and a single cell suspension of splenocytes was prepared as described above and stained with anti-CD3, anti-CD4, anti-CD8, anti-CD44, anti-CD49b and anti- IFN-γ antibodies as well as with $OVA_{257-264}$:H-$2K^b$ Tetramer-APC. Intracellular staining of IFN-γ was conducted according to the manufacturer's protocol (Foxp3/Transcription Factor Staining Buffer Set, eBioscience). Number of cells per spleen was calculated by using counting beads (eBioscience) in flow cytometry analysis.

Tumor challenge

B16F10-OVA cells (5 x 10^5) were suspended in 100 µl PBS and inoculated s.c. in the abdominal region near the right thigh of C57BL/6 mice. Tumor volume was measured as previously described [70]. Once the tumor volume reached 100 mm^3, mice were immunized as described above. Mice that grew tumors >1500 mm^3 and/or developed ulcerations in the tumor were euthanized.

Statistical analyses

Results were shown as either mean ± standard deviation (SD) or mean ± standard error of the mean (SEM). One-way analysis of variance (ANOVA) with *post hoc* Tukey test was used to determine the statistical significance of the observed differences between the treatment groups, unless otherwise noted. A *p*-value ≤ 0.05 was considered statistically significant; *p*-values were indicated using the following scheme: *$p \leq 0.05$, **$p \leq 0.01$, ***$p \leq 0.001$, n.s = not significant ($p > 0.05$). Data was analyzed using GraphPad Prism 7 software.

3.4. Results

3.4.1. Physicochemical characterization and TLR 7/8 specific activity by NPs

522GGNPs were similar to 522NPs in physicochemical characteristics. 522GGNPs appeared as discrete spheres and without apparent aggregation when imaged by cryo-TEM **(Figure 3.1A)**. Average diameter of 522GGNP measured by DLS was 202 ± 3 nm, which was similar to that of 522NPs (210 ± 2 nm) **(Table 3.1)**. 522GGNPs were negatively charged, with an average zeta-potential of -16.5 ± 2 mV, which was comparable to that of 522NPs (-22.6 ± 1.9 mV). However, 522 encapsulation was 33-fold higher in 522GGNPs (40 µg/mg of NP) than in 522NP (1.2 µg/mg of NP). Loading of sodium bicarbonate in 522GGNP was confirmed using ICP-EOS and was 8.8 µg/mg of NP.

522GGNPs caused negligible cytotoxicity against mouse splenocytes **(Figure 3.1B)**, which is consistent to the previous studies reporting minimal cytotoxicity of PLGA nanoparticles [151,152]. We then investigated whether 522GGNPs can specifically activate TLR7 and TLR8 in TLR reporter cells. As shown at **Figure 3.1C**, 522 maintained its TLR7 and 8 activity after encapsulation in NPs.

(A) **(B)**

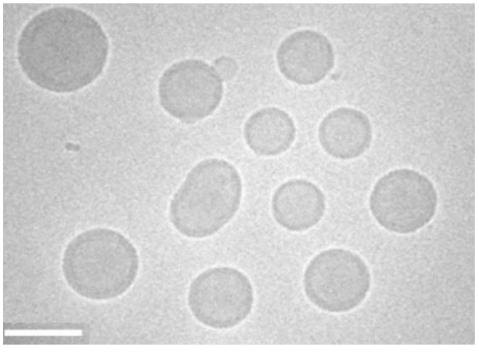

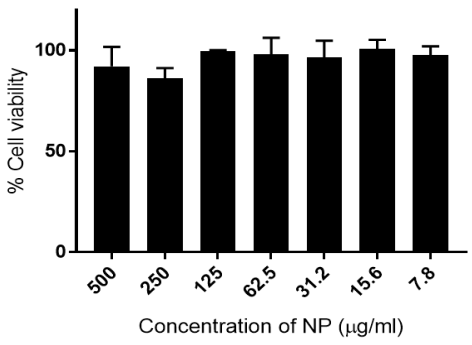

(C)

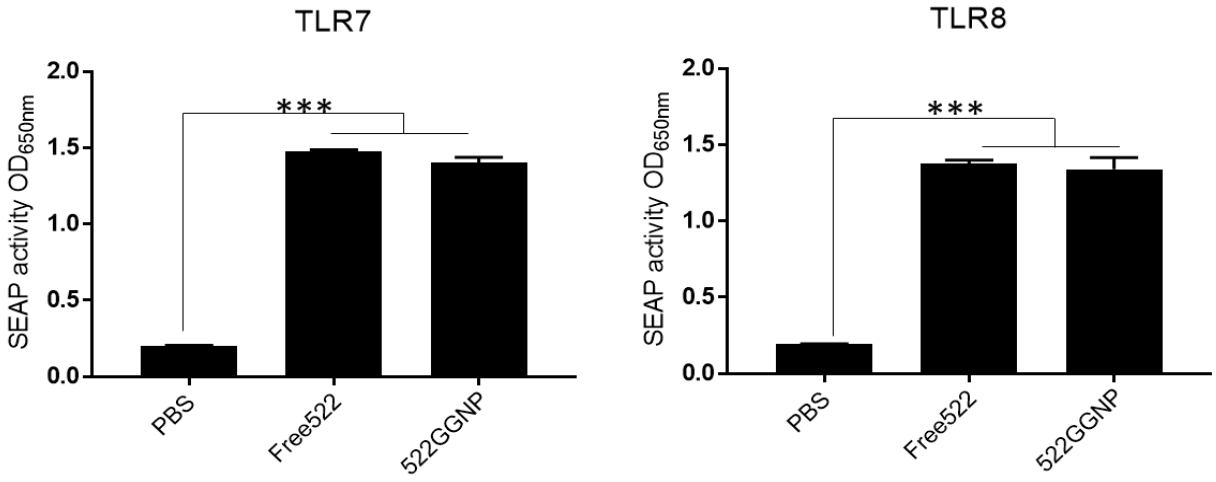

Figure 3.1. 522GGNP *in vitro* efficacy

(A) A representative cryo-TEM image of 522GGNPs. Scale bar, 100 nm. **(B)** Cytotoxicity of 522GGNP against mouse splenocytes. Treatments were incubated with mouse splenocytes for 48 h and cytotoxicity was measured by LDH assay. Results are reported as mean ± SD, n=4. **(C)** Human TLR7 or TLR8 specific reporter cells were incubated with DMEM, Free522 and 522GGNP for 24 h. TLR specific activation by treatments was measured by SEAP activity at OD_{650}. Results are reported as mean ± SD, n=4, ***p<0.001, One-way ANOVA.

	522NP	522GGNP
Particle size (nm)	210 ± 2	202 ± 3
Zeta-potential (mV)	-22.6 ± 1.9	-16.5 ± 2
Polydispersity index	0.12 ± 0.02	0.14 ± 0.01
Loading amount of 522 (μg/mg NP)	1.2 ± 0.1	40 ± 1.8
Loading efficiency (%)	1.8 ± 0.1	60 ± 2.7
Amount of $NaHCO_3$ (μg/mg NP)	-	8.8 ± 2.9

Table 3.1. Physiochemical characterization of 522NPs and 522GGNPs

Particle size, zeta-potential and polydispersity index of NPs were measured by DLS. Amount of 522 loaded in nanoparticles was quantified using HPLC. Amount of sodium bicarbonate in the 522GGNPs was measured using ICP-EOS. Results are reported as mean ± SD, n=3.

	DIW +1% PVA	Normal saline +1% PVA	PBS +1% PVA
Particle size (nm)	806 ± 74	264 ± 2	248 ± 5
Zeta-potential (mV)	-23.2 ± 6.2	-16.5 ± 2.4	-18.4 ± 0.9
Polydispersity index	0.33 ± 0.02	0.14 ± 0.01	0.09 ± 0.03
Loading amount of 522 (μg/mg NP)	3.9 ± 0.1	3.6 ± 0.1	4.9 ± 0.2
Loading efficiency (%)	5.9 ± 0.2	5.4 ± 0.2	7.3 ± 0.3

Table 3.2. Physiochemical characterization of control 522 NPs

Particle size, zeta-potential and polydispersity index of NPs were measured by DLS. Amount of 522 loaded in nanoparticles was quantified using HPLC. Results are reported as mean ± SD, n=3.

3.4.2. *In vitro* release kinetics and gas-generation by NPs

522GGNPs showed acidic pH-responsive release kinetics **(Figure 3.2A)**. In the first hour, 522GGNPs released ~90% and ~72% of encapsulated 522 in pH 5.5 and 6.5 buffers. In the neutral pH, however, 522GGNPs released only ~23% of the encapsulated 522 in the first 1 h, followed by slower release (~85%) over the next 48 h. We then monitored CO_2 generation by 522GGNPs using ultrasound imaging **(Figure 3.2B)**. In pH

5.5, sodium bicarbonate (positive control) generated large number of CO_2 bubbles. Generation of CO_2 bubbles was significantly lower but still detectable in pH 7.4. For 522NP, CO_2 generation was negligible at both pH's. 522GGNPs demonstrated significant CO_2 generation in acidic pH but not in pH 7.4 **(Figure 3.2C)**. These results provide direct evidence that 522GGNP generate CO_2 bubbles in acidic pH.

(A)

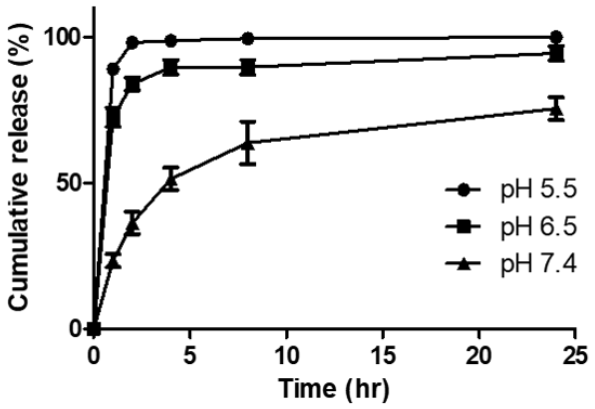

(B)

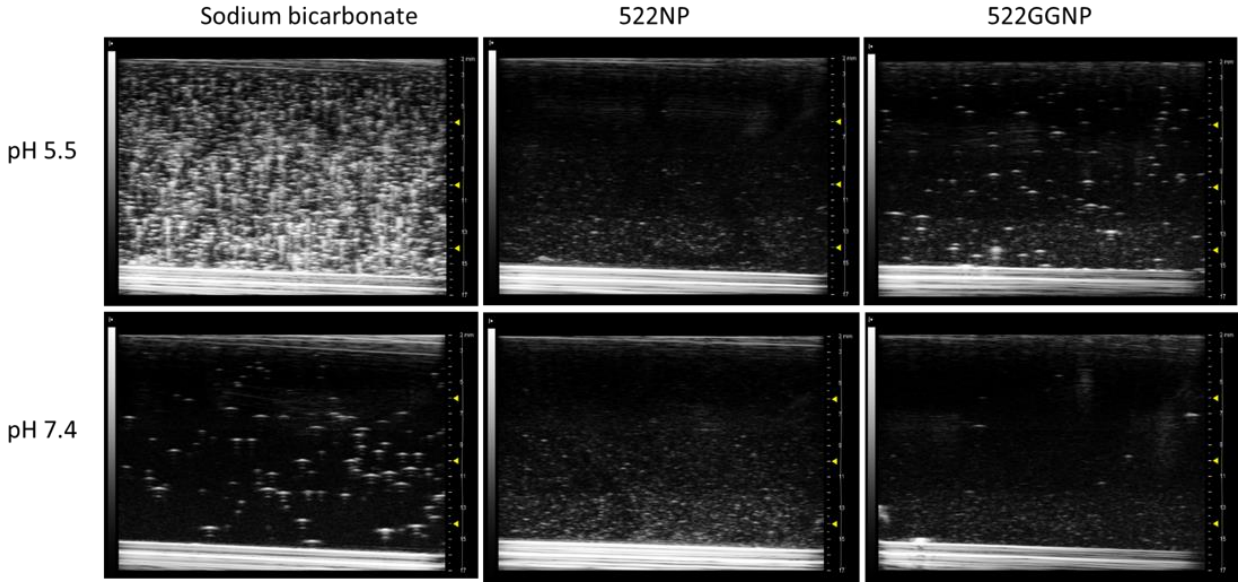

(C)

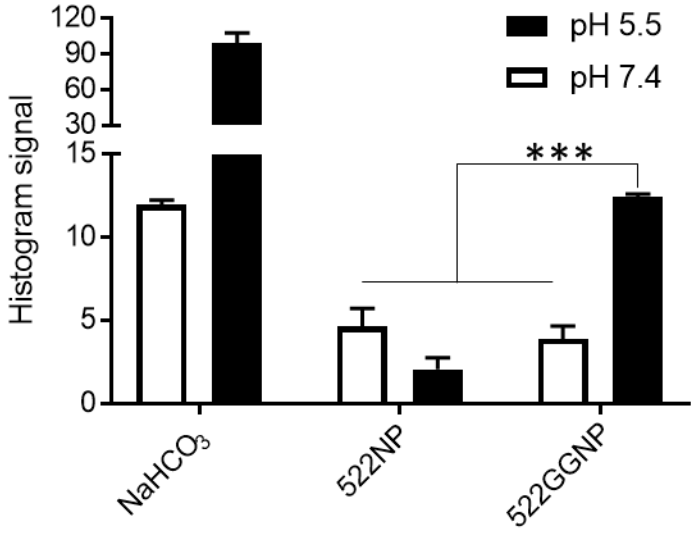

Figure 3.2. 522GGNP *in vitro* release kinetics and gas generation profiles

(A) Cumulative release of 522 from 522GGNP was measured in pH 5.5, 6.5 and 7.4. Results are reported as mean ± SD, n=3. **(B)** Gas generation from sodium bicarbonate and nanoparticles was visualized by ultrasound imaging. Representative ultrasound images at pH 5.5 and 7.4 are shown. **(C)** Generated gas was quantified by measuring histogram intensity of white signals. Results are reported as mean ± SD, n=4. ****p*<0.001, One-way ANOVA.

3.4.3. NP uptake by BMDCs

Uptake of 522GGNPs by DCs and their trafficking to the endo/lysosomal compartment is critical for efficient TLR7/8 activation [153]. As shown in **Figure 3.3A**, there was a clear shift in fluorescence intensity of BMDCs treated with NPs, which indicates that BMDCs were associated with the labeled NPs. To further investigate the internalization

and intracellular trafficking, we imaged BMDCs using confocal laser microscopy. NPs (green fluorescence) were located in both the cytosol and endo/lysosomes (stained with red fluorescence) **(Figure 3.3B)**. The presence of merged signal (yellow fluorescence) confirmed that a fraction of internalized NPs colocalized with endo/lysosomes.

(A)

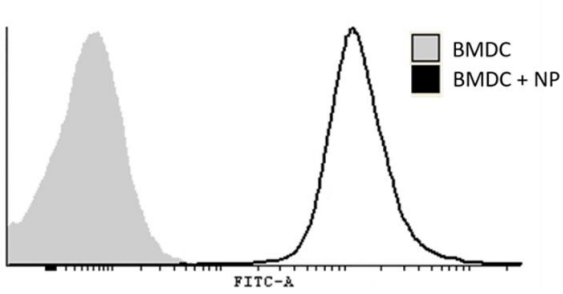

(B)

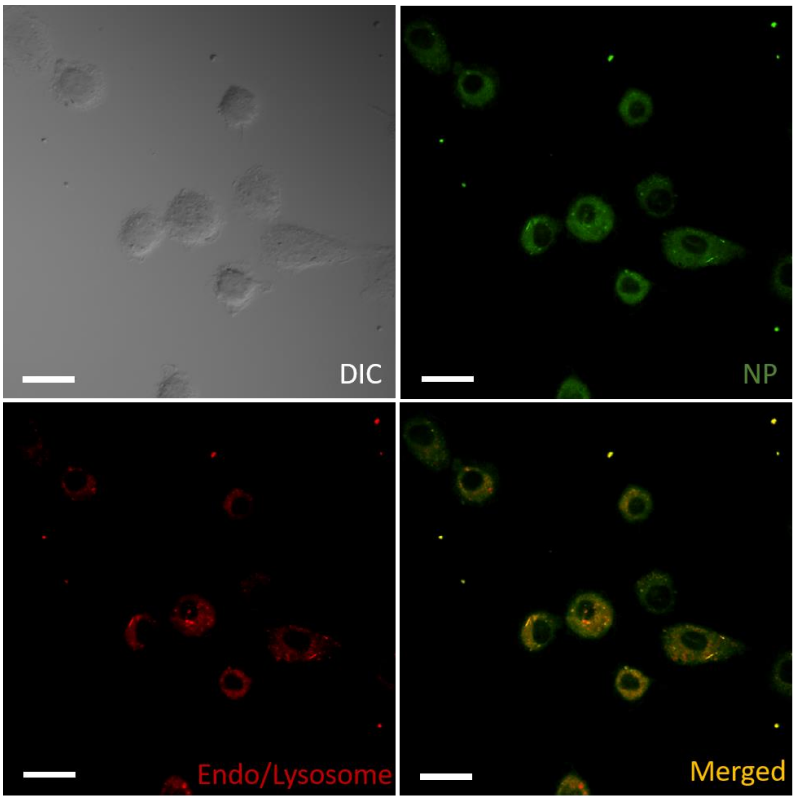

Figure 3.3. NP uptake by BMDC

(A) 6-coumarin labeled 522GGNPs were incubated with BMDCs ($CD11c^+$) for 2 h, and change in fluorescence intensity of BMDCs was measured by flow cytometry. Representative histograms of fluorescence intensity are shown. **(B)** A representative confocal image of BMDCs after incubation with 522GGNPs is shown. Green: nanoparticles, red: endo/lysosomes, yellow: merged signal of nanoparticle and endo/lysosomes. Scale bar, 20 μm.

3.4.4. BMDC activation

To elicit CD8 T cell response, DC expression of co-stimulatory molecules CD40, CD80 and CD86 is essential [154]. Therefore, we measured the extent of DC activation in the presence of 522GGNPs by measuring co-stimulatory molecule expression. OVA was used as a model antigen in these studies. As expected, OVA alone had negligible effect on DC activation. CD40 expression increased from 5% for untreated to 89% for OVA+522GGNP treatment, while 11% and 69% of the BMDC expressed CD40 when treated with OVA only and OVA+522NP, respectively **(Figure 3.4)**. OVA+522GGNP treatment also increased the frequency of BMDC expressing CD86 to 71%, while OVA only and OVA+522NP treatment resulted in 18% and 33% of the BMDC expressing CD86, respectively. CD80 also showed similar trend, where OVA+522GGNP treatment induced 66% of the cells to expression CD80, while OVA only and OVA+522NP treatments resulted in 16% and 23%, respectively. In addition to co-stimulatory molecule upregulation, OVA+522GGNP increased MHC II expression on DCs by 54%, while OVA

only and OVA+522NP treated DCs had 29% and 34% expression, respectively. These data show 522GGNPs results in enhanced DC activation compared to 522NPs.

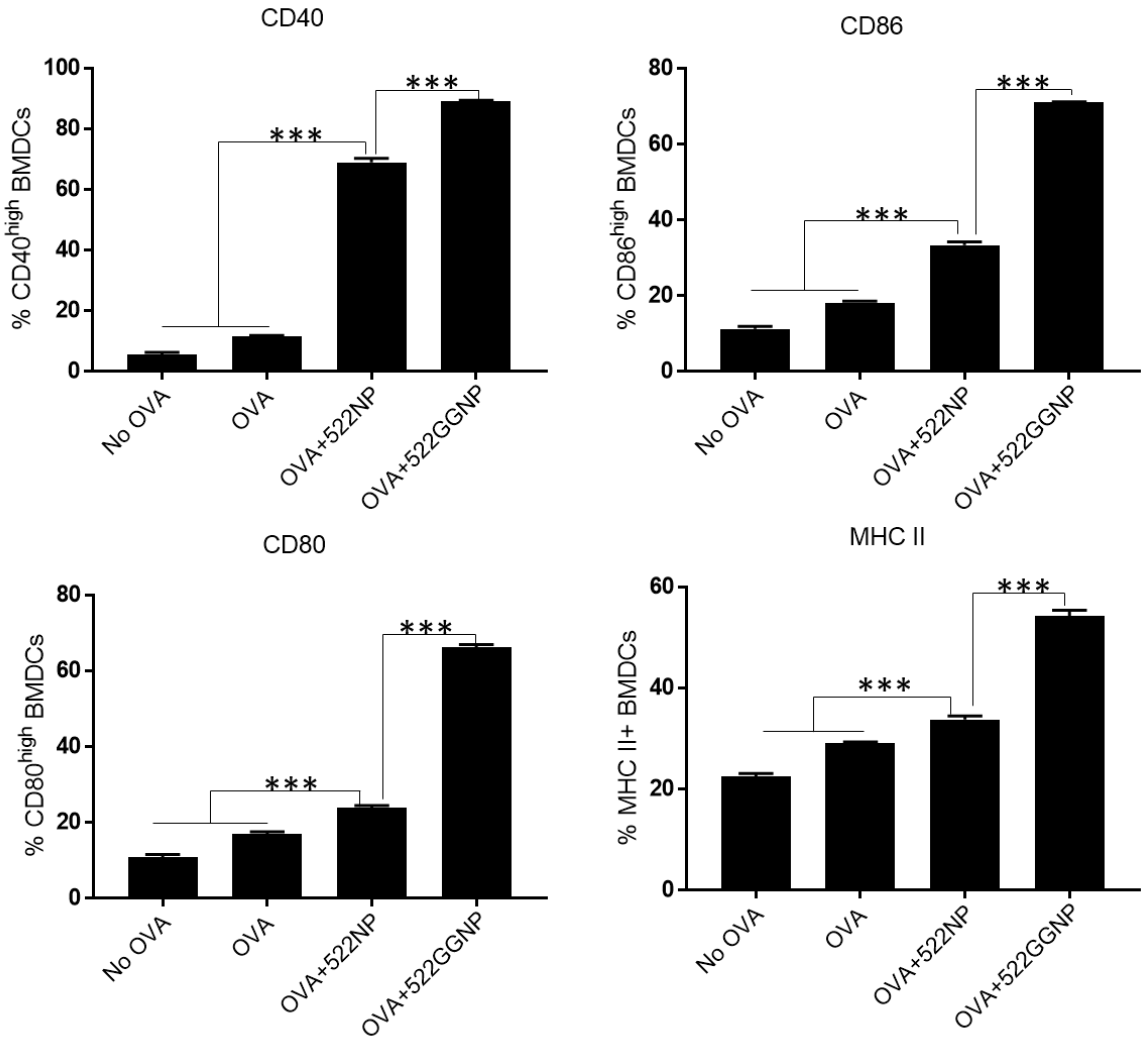

Figure 3.4. BMDC activation

Flow cytometry analysis of CD40, CD80, CD86 and MHC II expression on BMDCs after 48 h incubation with treatments. Results are reported as mean ± SD, n=4, ***p<0.001, One-way ANOVA.

3.4.5. Antigen uptake and presentation

We also investigated the other key feature of successful DC activation: Ag uptake and presentation via MHC I [155]. We determined the effect of co-incubation with 522GGNPs on Ag uptake by DCs using fluorescently-labeled OVA. After 1 h incubation, a significant increase in DC fluorescence intensity was observed **(Figure 3.5A,B),** suggesting internalization of OVA-FITC. There was a statistically significant increase in OVA uptake when DCs were co-treated with 522NP, and the highest increase was detected when DCs were co-treated with 522GGNPs. Uptake of Ag does not necessarily leads to Ag presentation by DCs [156]. Therefore, we measured $OVA_{257-264}$ (SIINFEKL) peptide:MHC I complex on DCs, [157]. Compared to Ag uptake, OVA+522GGNP treated BMDCs showed 4- and 2-fold higher expression of $OVA_{257-264}$ (SIINFEKL) peptide:MHC I complex compared to the OVA only and OVA+522NP incubated BMDCs, respectively **(Figure 3.5C)**.

(A)

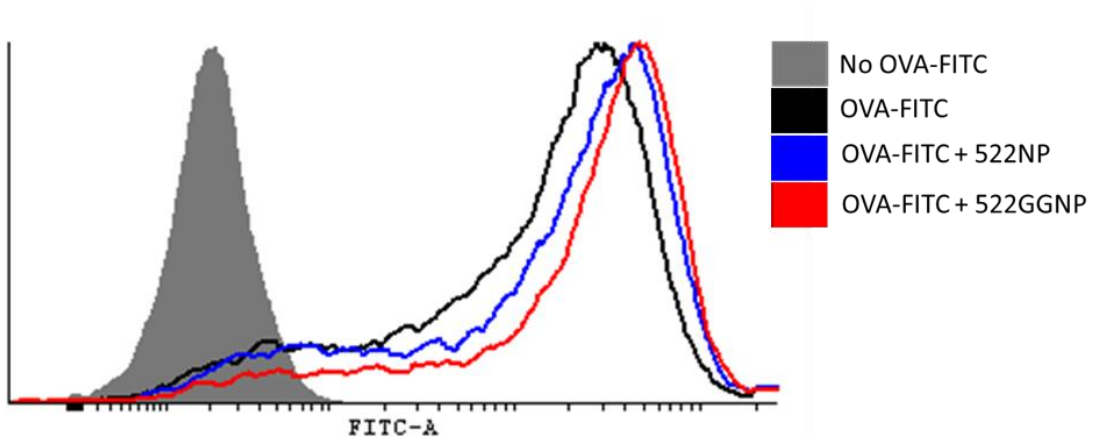

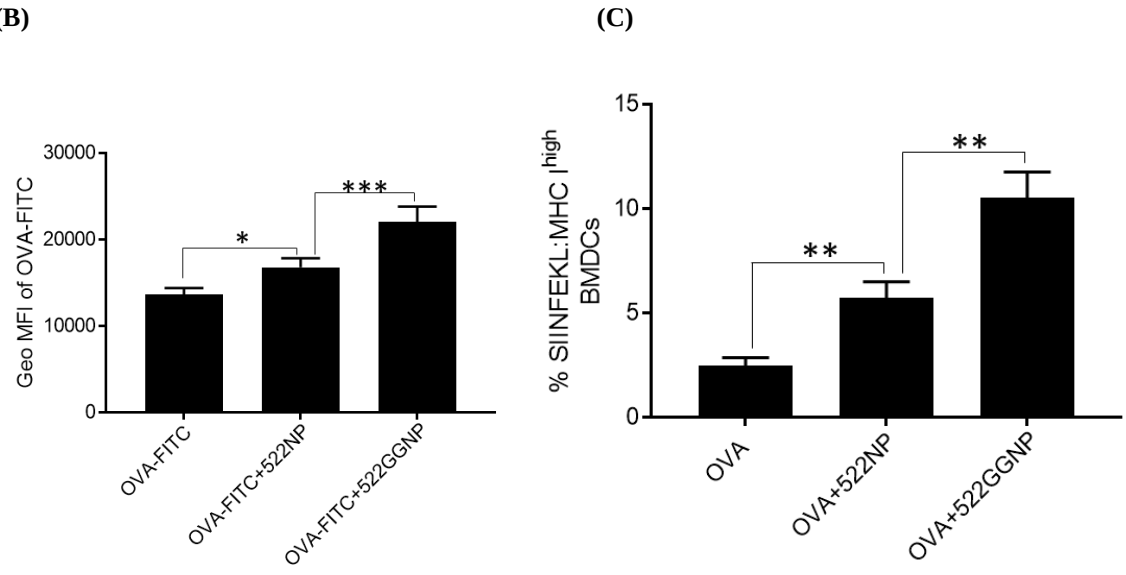

Figure 3.5. Antigen uptake and presentation via MHC I

(A,B) FITC labeled ovalbumin (OVA-FITC) and treatments were incubated with BMDCs for 6 h. **(A)** A representative histogram showing fluorescence intensity of BMDCs is shown. **(B)** FITC fluorescence was quantified as geometric mean fluorescence intensity. Results are reported as mean ± SD, n=4, *p<0.05, ***p<0.001, One-way ANOVA. (C) BMDCs were incubated with OVA and/or NPs for 48 h. BMDCs expressing $OVA_{257-264}$ (SIINFEKL) peptide bound to $H\text{-}2K^b$ (MHC I) were analyzed by flow cytometry. Results are reported as mean ± SD, n=3, **p<0.01, One-way ANOVA.

3.4.6. *In vivo* T cell assay

We next examined the extent of T cell response after immunizing immunocompetent mice. We first measured CD4 T cells, which enhance CD8 T cell

activation by secreting IFN-ɣ [158,159]. The number of IFN-ɣ$^{+}$ CD4 T cells increased 2-fold when mice were immunized with OVA+522GGNP compared to untreated and OVA only groups **(Figure 3.6A)**. OVA+522NP treated mice also showed increased IFN-ɣ$^{+}$ CD4 T cells compared to the two control groups but was less effective than OVA+522GGNP. To determine the activation of Ag-specific cytotoxic CD8 T lymphocytes that can eradicate tumor cells [160,161], we first quantitated the number of the $OVA_{257-264}$-specific $CD44^{high}$ CD8 T cells [162] to determine expansion. OVA+522GGNP immunization increased the number of $CD44^{high}$ CD8 T cells by 4- and 2.5- fold compared to untreated and OVA only-treated mice, respectively **(Figure 3.6B)**. Moreover, $OVA_{257-264}$-specific IFN-ɣ$^{+}$ CD8 T cells also increased 3- and 2.5- fold when mice were immunized with OVA+522GGNP compared to untreated and OVA only group, respectively **(Figure 3.6C)**. Consistent with our previous study [70], OVA+522NP immunization increased $OVA_{257-264}$-specific CD8 T cell responses compared to controls; however, OVA+522GGNP immunization induced stronger T cell responses than OVA+522NP immunization.

(A)

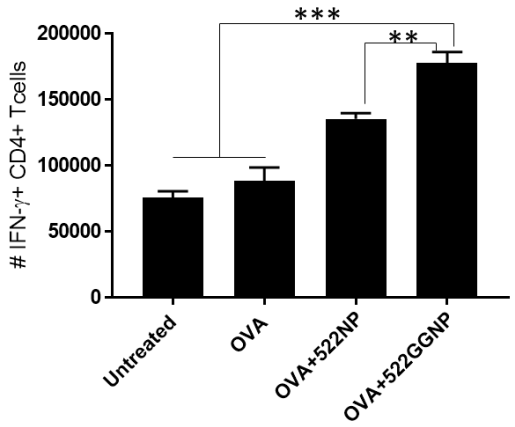

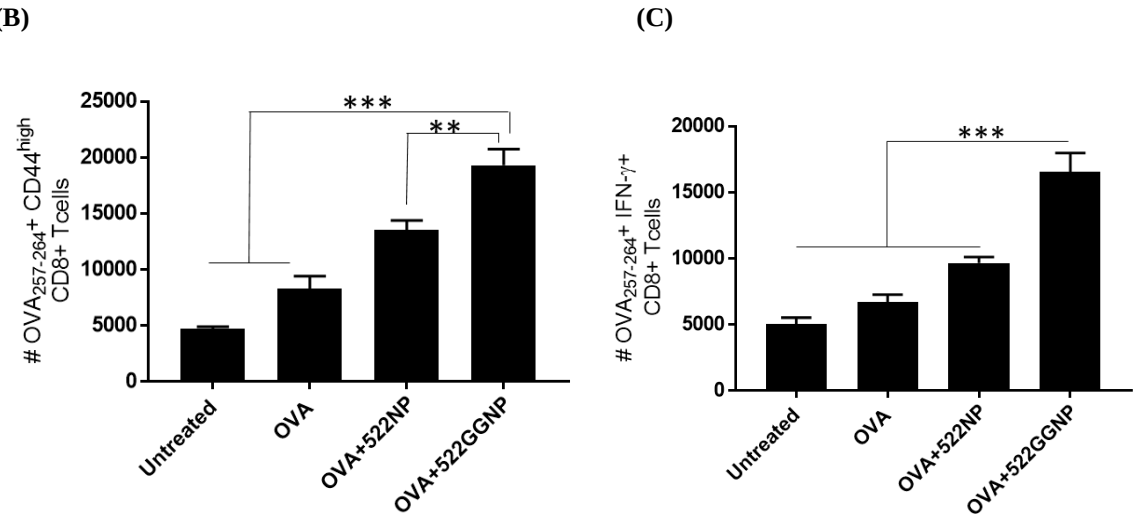

Figure 3.6. ***In vivo*** **T cell activation**

Following immunization, spleens were collected and analyzed by flow cytometry. **(A)** Number of IFN-γ^+ CD4 T ($CD3^-CD4^+$) cells; **(B)** Number of $OVA_{257-264}$-specific $CD44^{high}$ CD8 T ($CD3^-CD8^+$) cells; **(C)** Number of $OVA_{257-264}$-specific IFN-γ^+ CD8 T cells. Results are reported as mean ± SEM, $^{**}p<0.01$, $^{***}p<0.001$, n=4, one-way ANOVA.

3.4.7. *In vivo* NK cell assay

CD70 is a co-stimulatory molecule expressed on DCs that interacts with CD27 on NK cells and induces NK cell activation [163]. As seen in **Figure 3.7A**, both 522NPs and 522GGNPs induced upregulation of CD70 on DCs. We then investigated NK cell activation *in vivo*. Frequency of both $CD69^{high}$ and IFN-γ^+ NK cells increased 2.5-fold compared the untreated group **(Figure 3.7B,C)**. Consistent with the results of the T cell activation studies, 522NP immunization also induced NK cell activation, but the extent was less than that with 522GGNP immunization.

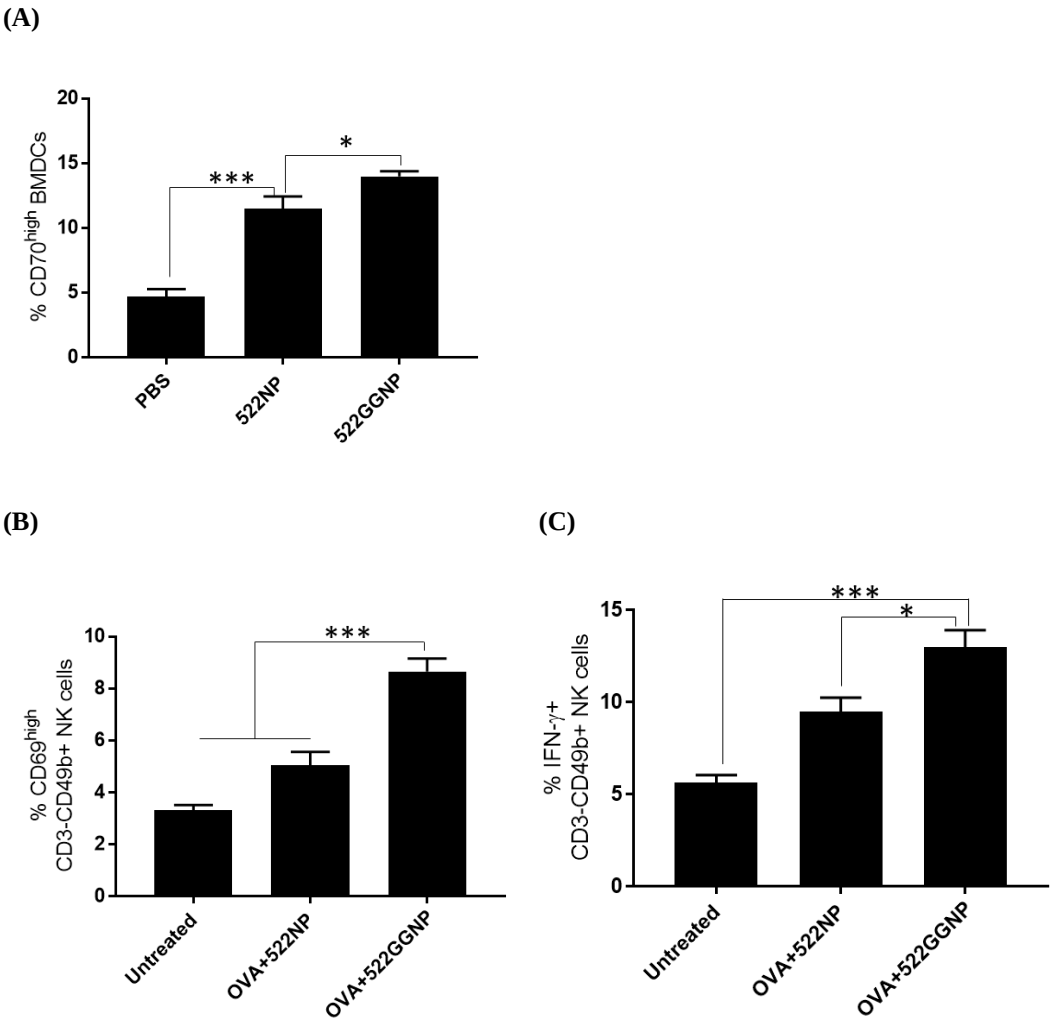

Figure 3.7. *In vivo* NK cell activation

(A) Expression of CD70 on BMDCs was measured by flow cytometry. Results are reported as mean ± SD, **p*<0.05, ****p*<0.001, n=3, one-way ANOVA. **(B,C)** Spleens of immunized mice were harvested and analyzed by flow cytometry. **(B)** Number of $CD69^{high}$ NK ($CD3^{-}$ $CD49b^{+}$) cells. **(C)** Number of IFN-γ^{+} NK cells. Results are reported as mean ± SEM, **p*<0.05, ****p*<0.001, n=4, one-way ANOVA.

3.4.8. Tumor challenge

In vivo therapeutic efficacy of OVA+522GGNP immunization was evaluated in a murine melanoma tumor model. B16F10-OVA tumors became palpable on d 11 after tumor cell injection and mice were immunized by once daily dosing of the vaccine formulation from d 11 to d 15. Both untreated and OVA alone treated groups showed rapid tumor growth, where all of the mice had tumors ≥1500 mm^3 by d 22 and d 24, respectively **(Figure 3.8)**. Consistent with our previous study [70], OVA+522NP immunization was effective in inhibiting tumor growth ($p<0.001$). However, OVA+522GGNP immunization showed enhanced therapeutic efficacy compared to OVA+522NP vaccination ($p<0.001$). Average tumor volume of OVA+522NP and OVA+522GGNP immunized animals on d 24 was 729 mm^3 and 339 mm^3, respectively.

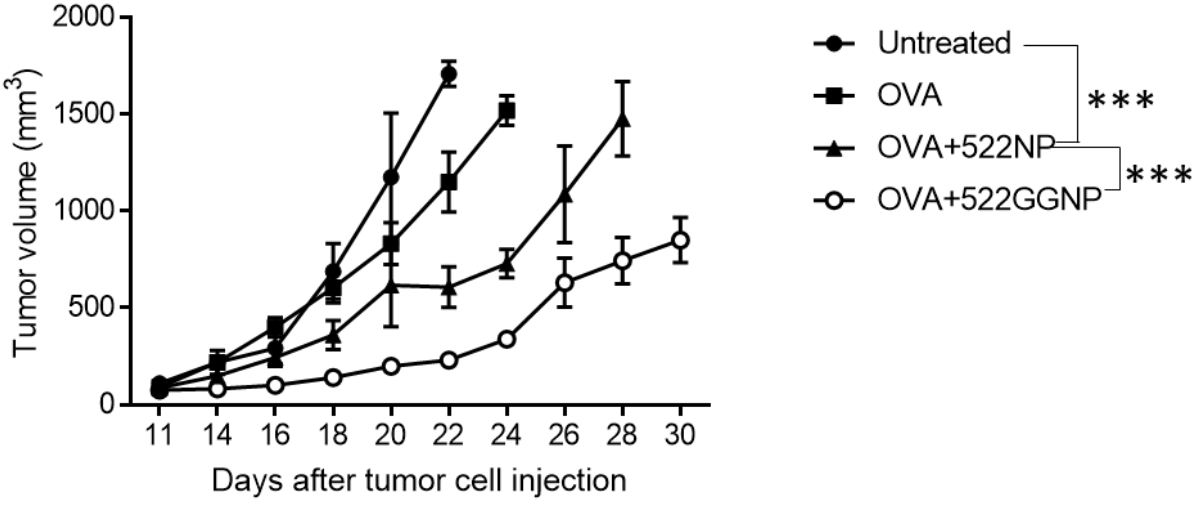

Figure 3.8. Tumor challenge using B16F10-OVA melanoma tumor model

C57BL/6 mice with established B16F10-OVA tumors were randomized and vaccine doses were administered over five days (d 11-15). Results are reported as mean ± SEM, ***p<0.001, n=4~5, Two-way ANOVA with *post hoc* Tukey's test.

3.5. Discussion

Nanoparticulate delivery of TLR7/8 agonists can broaden their application in cancer immunotherapy. Currently, TLR7/8 agonists are limited to topical administration (ClinicalTrials.gov; NCT01808950, NCT01676831) and intratumoral injection (NCT02556463). In the studies where TLR7/8 agonists have been utilized as the vaccine adjuvant, peptides derived from tumor-associated Ag (TAA) were administered S.C. (NCT01748747, NCT00960752) and the TLR7/8 agonists were applied topically on the tumor. However, co-delivery of antigen and adjuvant to the same Ag-presenting cells is critical for eliciting Ag-specific T cell response [77]. Therefore, a formulation that can deliver TLR7/8 agonists via S.C. or I.M. injection together with TAA-peptides is needed.

We investigated PLGA NPs for TLR7/8 agonist delivery because of the excellent biocompatibility and safety profile of PLGA [151]. Further, nanoparticles ≤200 nm are preferentially taken up by DCs, and can also directly drain to lymph nodes [57]. However, low drug loading was an issue in our previous study (~1 μg/mg of NPs) [70]. Low encapsulation of imidazoquinoline derivatives in PLGA nanoparticles has been reported previously [142,143]. 522 is a moderately hydrophobic compound (logP = 2.74). However, it has increased solubility in 2.5 % PVA solution (30 μg/ml). Thus, 522 can diffuse out from the oil phase to aqueous phase during the fabrication process, which appears to lead to low

encapsulation efficacy. In the present study, encapsulation efficiency increased several fold in 522GGNP compared to our previous 522NP. We presume the increased encapsulation of 522 in 522GGNP occurred because of two reasons. First, the double-emulsion evaporation method can result in higher encapsulation efficiency for both hydrophilic and hydrophobic drugs [164]. Second, the presence of the bicarbonate salt in the primary aqueous phase could also have affected the drug loading. The use of 1% PVA without sodium bicarbonate as the primary phase resulted in only 6% encapsulation efficacy. We also tested 1% PVA solutions containing sodium chloride or sodium phosphate, as the addition of salt in primary emulsion can stabilize the emulsion [165]. In our hands, these salt solutions failed to form a stable emulsion with 522 and resulted in 5% and 7% encapsulation efficiencies, respectively. In addition to their low encapsulation efficiency, these nanoparticles also had larger size.

The presence of sodium bicarbonate also contributed to the acidic pH-response release kinetics of 522GGNPs. Utilizing the bicarbonates to introduce pH-sensitive drug release has been previously reported [166,167]. In acidic pH, bicarbonates react with H^+ to form carbonic acid, which dissociates to release CO_2 gas that can mechanically disrupt the polymer shell and facilitate the rapid release of the drug payload. Ultrasound imaging confirmed acidic pH-dependent gas-generation by 522GGNPs but not 522NPs, which supports the proposed mechanism of drug release. Acidic-pH responsive release can be important for effective DC activation by TLR7/8 agonists. Both TLR7 and 8 are located on the luminal side of endo-lysosomes, which are acidic cellular compartments (pH 4~6) [153]. From flow cytometry and confocal data, we confirmed 522GGNPs localized to

endo/lysosomes in DCs. Based on these results, we expect 522GGNPs can improve the delivery of 522 to the endo-lysosomes [147,166]. Compared to the conventional 522NPs, 522GGNPs resulted in a much stronger DC activation, further substantiating improved 522 delivery to the target site. In addition to upregulation of co-stimulatory molecules, 522GGNP significantly enhanced the antigen presentation via MHC I.

T cells are key players in cancer immunotherapy because of their ability to directly kill the tumor cells and activate other immune cells [160,161]. In this study, we found 522GGNP immunization increased the number of IFN-ɣ$^{+}$ CD4 T cells, which can activate CD8 T cells and NK cells [159,168]. This data implies 522GGNP immunization can potentiate a Th1 response [169]. As CD4 T cells are primarily activated via CD40-CD40L signaling [170], it is likely 522GGNPs' ability to increase CD40 expression on DCs enables the expansion of effector CD4 T cells. In addition, increased expression of MHC II on 522GGNP treated DCs further suggests 522GGNP is effective in activating effector CD4 T cells [171]. 522GGNP immunization also increased the number of Ag-specific effector CD8 T cells. Consistent with our previous study [70], OVA+522NP increased both $OVA_{257-264}$-specific CD44^{high} CD8 T cells and $OVA_{257-264}$-specific IFN-ɣ$^{+}$ CD8 T cells compared to OVA only, which demonstrates the potent adjuvanticity of polymeric nanoparticles encapsulating TLR7/8 agonists. The greater $OVA_{257-264}$-specific CD8 T cell expansion observed with 522GGNP immunization compared to that with 522NP was likely the result of enhanced Ag-presentation and co-stimulatory molecule signaling by DCs that primed CD8 T cells and further potentiated by IFN-ɣ$^{+}$ CD4 T cells.

NK cells also play major role in cancer immunotherapy IFN-ɣ secretion upon activation and directly kill the tumor cells with cytotoxic granules [172]. As NK cells can be activated by DC-NK cell interaction and IFN-ɣ secreted by T cells [173], we investigated NK cell expansion following 522GGNP immunization. Similar to the observed increase in T cell activation, 522GGNP immunization increased both $CD69^{high}$ NK cells and IFN-$ɣ^{+}$ NK cells. CD69 expression triggers cytolytic activation of NK cells [174]. Activation of NK cells can provide several benefits in cancer immunotherapy. First, NK cells can kill the tumor cells before CD8 T cells are primed by DCs. It has been reported that 7-9 days are required to generate antigen-specific CD8 T cells after immunization, but the tumor cells continue to proliferate during that time span [175]. However, NK cells become effective as early as few hours after immunization, and kill the tumor cells before CD8 T cells are primed [176]. This leads to another benefit of activated NK cells, as NK cells can induce immunogenic tumor cell death [177,178]. As a result, more TAAs will be available to DCs. In addition, IFN-ɣ secretion by NK cells can modulate other Ag presenting cells and T cells for Th1 response [179].

To evaluate whether enhanced antigen-specific CD8 T cell and NK cell response by OVA+522GGNP immunization could lead to improved anticancer efficacy, we performed a tumor challenge study using B16F10-OVA tumor model. While OVA+522NP immunization was effective in inhibiting tumor growth compared to untreated and OVA only treatment, OVA+522GGNP immunization showed superior therapeutic efficacy. Interestingly, OVA+522GGNP showed effectiveness two days earlier (d 16) than OVA+522NP (d 18). As 7~10 days are required to prime CD8 T cells, it is possible that

activated NK cells could have contributed to the early effectiveness of OVA+522GGNP treatment. Taken together, our data thus demonstrate 522GGNP can elicit robust antigen-specific CD8 T cell and NK cell responses, resulting in enhanced therapeutic efficacy compared to that with 522NP.

In this study, we introduced the use of an acidic pH responsive NP formulation for endo/lysosomal delivery of TLR7/8 agonists. The new formulation was characterized by higher drug encapsulation and acidic-pH responsive release kinetics. 522GGNPs showed more potent NK cell and CD8 T cell responses than 522NPs. Our results suggest acidic-pH responsive, gas-generating nanoparticles is an efficient drug delivery platform for TLR7/8 agonists for cancer immunotherapy.

Chapter 4.

Combination of sunitinib and PD-L1 blockade enhances anticancer efficacy of TLR7/8 agonist-based nanovaccine

4.1. Summary

Cancer vaccines composed of tumor-associated antigens (TAAs) and toll-like receptor (TLR) agonists have shown promising antitumor efficacy in pre-clinical studies by generating antigen-specific CD8 T cells, but translation of cancer vaccines to the clinic has been limited due to response variabilities and recurrence of tumor. The tumor microenvironment has various immune escape mechanisms that neutralize CD8 T cells, which can lead to these sub-optimal therapeutic efficacies. Therefore, we hypothesized that modulation of the tumor microenvironment can augment CD8 T cell activation and enhance therapeutic efficacy of cancer vaccine. To accomplish this enhancement, we aimed to eliminate immune suppressive cells and block their inhibitory signaling. Combination of the tyrosine kinase inhibitor (TKI) sunitinib with a nanoparticle-based cancer vaccine (nanovaccine) resulted in reduction of immune-suppressive myeloid-derived suppressive cells (MDSCs) and regulatory T cells (Tregs). Blockade of programmed death-ligand 1 (PD-L1) using anti-PD-L1 antibody was adapted to reduce CD8 T cell exhaustion. Combination of nanovaccine+sunitinib+PD-L1 antibody treatment reduced PD-L1^{high} M2 macrophages and MDSCs and upregulated activation of CD8 T cells in the tumor. Nanovaccine+sunitinib+PD-L1 antibody treatment also stimulated antigen-specific CD8 T cell response, which lead to significant therapeutic efficacy in a murine tumor model. These results suggest that modulation of tumor microenvironment using sunitinib and PD-L1 blockade can significantly enhance the anti-tumor efficacy of cancer nanovaccine.

4.2. Introduction

Synthetic vaccine adjuvants have shown considerable potential in stimulating a robust cytotoxic CD8 T cell response, which is critical for eradicating established tumors [33,180]. In our previous studies, we described the development of a series of novel imidazoquinoline derivatives that activate Toll-like receptor (TLR) 7 and/or 8 and stimulate robust pro-inflammatory cytokine production [42]. Encapsulation of these agonists in polymeric nanoparticles improved their ability to activate dendritic cells (DCs) and resulted in a robust expansion of antigen-specific CD4 and CD8 T cells and enhanced cytotoxic response [70].

Nanoparticle-encapsulated agonist induced strong protective immunity in prophylactic tumor models; however, it was less effective against established tumors [70]. Sub-optimal outcomes in the therapeutic models may have resulted from tumor-induced immune suppression [181]. Tumor microenvironment is highly immune suppressive [182], as tumor growth leads to the recruitment of immunosuppressive cells including myeloid derived suppressive cells (MDSCs), regulatory T cells (Tregs) and M2 macrophages, which deactivate natural killer (NK) cells and T cells [183]. Tumors also upregulate programmed death-ligand 1 (PD-L1), which ligates PD-1 on CD8 T cells and induces T cell exhaustion [184]. Therefore, modulating the immunosuppressive tumor microenvironment can significantly improve the effectiveness of anticancer vaccines.

Previous pre-clinical and clinical studies show sunitinib, a tyrosine-kinase inhibitor (TKI) used in the treatment of renal cell carcinoma (RCC) [185], can reduce MDSC and Treg populations [186,187]. Further, several tumors express high levels of PD-L1 when exposed to

IFN-ɣ, such as that following vaccination [188,189]. Additionally, immunosuppressive macrophages (M2) and MDSCs express high levels of PD-L1 [190]. PD-L1 blockade using anti-PD-L1 antibody can reduce the T cell exhaustion in the tumor and enhance the therapeutic efficacy of the nanovaccine.

In this study, we examined the ability of sunitinib and anti-PD-L1 blockade enhance the anticancer efficacy of our TLR7/8 agonist-based nanovaccine. We determined the effect of sunitinib co-therapy on MDSC and Treg in tumor-bearing mice. We also examined the effect of PD-L1 blockade on PD-L1^{high} M2 macrophages and MDSCs, and on activation of CD8 T cells. Tumor-specific IFN-ɣ response was also measured to examine long-term memory response. Overall, our results suggest the combination of sunitinib and PD-L1 blockade can significantly improve the therapeutic efficacy of TLR7/8 agonist based nanovaccine.

4.3. Materials and Methods

Chemicals and reagents

TLR7/8 agonist 522 was synthesized and characterized as previously reported [42]. Sunitinib and 2-mercaptoethanol were purchased from Sigma-Aldrich (St Louis, MO). Murine granulocyte-macrophage colony-stimulating factor (GM-CSF), IL-4, IL-6 and IFN-ɣ were purchased from Peprotech (Rocky Hill, NJ). Enzyme-linked immunosorbent assay (ELISA) kits were purchased from Biolegend (San Diego, CA).

Fluorophore-labeled monoclonal antibodies for flow cytometry analysis were purchased from Biolegend (CD3, CD8, CD11a, CD11c, CD80, CD206, F4/80, Gr-1, PD-

L1), eBioscience (San Diego, CA) (CD11b, CD44, CD86, Foxp3) and BD Biosciences (San Jose, CA) (CD4).

Animals and cell line

All the protocols involving the use of animals were approved by the Institutional Animal Care and Use Committee (IACUC) of the University of Minnesota, and experiments were performed accordingly. Immunocompetent C57BL/6 mice (6-9 weeks, female) were purchased from Charles River (Wilmington, MA) and housed in specific pathogen free (SPF) facilities maintained by the Research Animal Resources at the University of Minnesota. The murine urothelial carcinoma cell line MB49 (ATCC) was cultured in RPMI 1640 medium supplemented with 10% fetal bovine serum, 100 μg/mL streptomycin and 100 U/mL penicillin (complete RPMI).

Cultivation of bone marrow-derived DCs (BMDCs) and bone marrow-derived MDSCs (BM-MDSCs)

Primary cells were isolated from tibias and femurs of mice as described previously [70]. Isolated cells were transferred to petri dishes and incubated with complete RPMI media. For BMDC cultivation, complete RPMI media was supplemented with 20 ng/mL GM-CSF, 10 ng/ml IL-4 and 50 μM 2-mercaptoethanol. For BM-MDSC cultivation, 40 ng/mL GM-CSF and 40 ng/mL IL-6 were added to complete RPMI media as previously reported [191]. Cells were supplemented with fresh media on d 3 and harvested on d 6 for assays.

In vitro BMDC assays

BMDCs (10^6/well) were seeded in 24-well plates and incubated with 0.1, 1, or 10 µM of 522 for 24 h, and cell culture supernatants were collected for ELISA. In a separate study, 522 (28 µM) and/or sunitinib (5 µM) were added to cells and incubated for 24 h. Cells were then stained with fluorophore-labeled antibodies to measure co-stimulatory molecule (CD80, CD86) expression on $CD11c^+$ BMDCs by flow cytometry (BD LSRFortessa H0081). Cell culture supernatants were collected for ELISA.

PD-L1 on MB49 cells

MB49 cells were incubated with murine IFN-ɣ (100 ng/ml) as previously reported [189]. After 24 h, cells were collected and stained with anti-PD-L1 antibody (BioXcell, West Lebanon, NH) followed by a AF647-labeled secondary antibody (anti-rat IgG, Abcam, Cambridge, MA). PD-L1 expression on MB49 cells was measured by flow cytometry.

Cytotoxicity assay

BMDCs and BM-MDSCs (4×10^4/well) were seeded in 96-well plates. On the same day, 0.78 ~ 100 µM of sunitinib or 522 were added to the cells. After 24 h, cell culture supernatants were collected to measure LDH release according to manufacturer's protocol (LDH Cytotoxicity Assay Kit, Thermo). MB49 cells (10^4/well) were seeded in 96-well plates. Following the attachment of cells to the plate (~18 h), cytotoxicity of sunitinib and 522 were determined as described above.

Ex vivo splenocyte cytokine assay

Spleens were harvested from MB49 tumor bearing mice. Single cell suspension of splenocytes was prepared as previously reported [45]. Briefly, spleens were mechanically homogenized with Hanks' Balanced Salt solution (HBSS) using gentleMACS Dissociator (Miltenyi BioTeck Inc., Auburn, CA). Homogenized cell suspension was washed with PBS and incubated in HBSS supplemented with 0.15 mg/ml DNAse I (Sigma) and 0.56 Wuensch units/ml Liberase Blendzyme 3 (Roche, Branford, CT) in a water bath (37°C) for 30 min. Cells were further washed with HBSS and the red blood cells were removed using ACK lysis buffer (Thermo). Cell suspension was washed with PBS, resuspended in complete RPMI and seeded in a 24-well plate (10^6/well). Splenocytes were then incubated with 522 (28 µM) and/or sunitinib (1.25, 2, 5 µM) for 24 h, and the supernatants were collected for ELISA.

In vivo tumor model and treatments

MB49 cells (2 x 10^5) suspended in 100 µl of PBS were injected subcutaneously in the abdominal area of C57BL/6 mice. Treatments began when the tumors were 100~150 mm^3. Tumor dimensions were measured using digital calipers as previously reported [70]. Mice that developed ulcerated core in the tumor or had a tumor volume greater than 1500 mm^3 were removed from the study and euthanized.

Nanoparticles loaded with 522 (522NPs) and MB49 cell lysates were prepared as previously reported [70]. 522NPs (2 mg/mouse, equivalent to 2 µg of 522) were combined with MB49 cell lysate (100 µg/mouse) in 200 µl of PBS (referred to as ‘nanovaccine’) and

injected subcutaneously once daily for five days. Sunitinib (10 mg/kg) was prepared in sterile normal saline and administered once daily by oral gavage from d 1 to the end of study [187,192]. Anti-PD-L1 antibody (BioXcell, West Lebanon, NH) was prepared in PBS and a total of 3 doses (each 200 μg) were administered intraperitoneally once every three days [193,194].

In vivo MDSC, Treg, M2 macrophage and CD8 T cell measurement

Tumor-bearing mice were administered various treatments as described above. Spleens and tumors were collected 9 days after treatment began. Single cell suspensions of spleen and tumor were prepared as described above and stained with fluorophore-labeled antibody to identify MDSC ($Gr\text{-}1^+CD11b^+$), Tregs ($CD3^+CD4^+Foxp3^+$), M2 macrophages ($CD11b^+F4/80^+CD206^+$), and CD8 T ($CD3^+CD8^+$) cells. Intracellular staining of Foxp3 was performed according to manufacturer's manual (Foxp3/Transcription Factor Staining Buffer Set, eBioscience). Cells were analyzed by flow cytometry.

ELISA for tumor specific IFN-ɣ measurement

Splenocytes from immunized mice were seeded in a 24-well plate (5×10^6/well) in complete RPMI supplemented with 50 μM 2-mercaptoethanol [195]. MB49 cell lysates (100 μg) were added to cells. After 48 h, cell culture supernatants were collected for ELISA.

Statistical analysis

Results are shown as mean ± standard deviation (SD) or mean ± standard error of the mean (SEM) as indicated. The statistical significance of the observed differences between the treatment groups were determined by one-way analysis of variance (ANOVA) with *post hoc* Tukey test, unless otherwise noted. A p-value less than 0.05 was considered statistically significant; *p<0.05, **p<0.01, ***p<0.001. Statistical analyses were performed using GraphPad Prism 7 software (GraphPad Software, La Jolla, CA).

4.4. Results

4.4.1. IL-10 secretion and PD-L1 upregulation

BMDCs cultured with 0.1 ~ 10 μM of 522 secreted 150 ~ 300 pg/ml of IL-10 while PBS treated BMDCs secreted 14 ng/ml of IL-10 **(Figure 4.1A)**. Consistent with a previous study [189], we detected increased PD-L1 expression on MB49 cells when stimulated with IFN-ɣ **(Figure 4.1B,C)**. Similar to that shown by others [193,194], even untimulated MB49 cells had a moderately high basal level of PD-L1 expression.

(A)

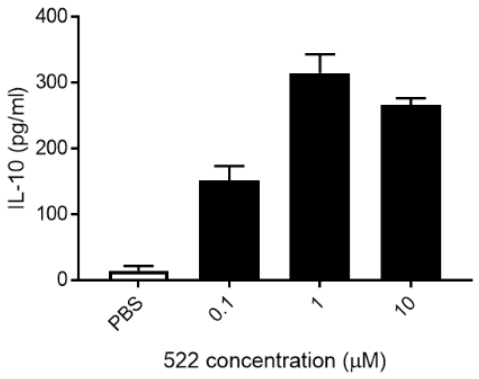

(B) **(C)**

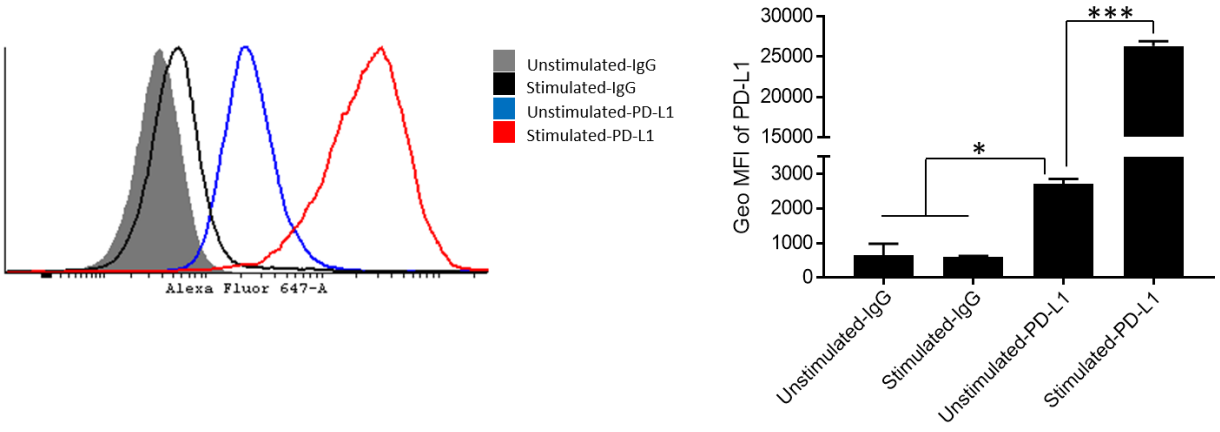

Figure 4.1. Cytokine and PD-L1 measurement

(A) Cell culture supernatant was collected from BMDCs incubated with PBS or 522. IL-10 levels were measured by ELISA. Results are reported as mean ± SD, N=3 **(B,C)** PD-L1 expression on MB49 cells was measured by flow cytometry. **(B)** Representative histogram of fluorescence intensity. **(C)** Geometric MFI of AF647 was quantified. Results are reported as mean ± SD, N=2, *p<0.05, ***p<0.001, One-way ANOVA with *post hoc* Tukey's test

4.4.2. Cytotoxicity assays

Cytotoxicity of sunitinib was examined in MB49, BM-MDSCs and BMDCs **(Figure 4.2A)**. Sunitinib induced 87% and 75% cytotoxicity against MB49 cells at 100 µM and 50 µM, respectively. However, sunitinib had negligible cytotoxicity at lower concentrations (IC_{50} of 30 µM). Sunitinib was more cytotoxic to BM-MDSCs and BMDCs

(IC_{50} of 3.7 µM and 9.2 µM, respectively). We also tested the cytotoxicity of 522 against BMDCs and BM-MDSCs. 522 had negligible cytotoxicity in the 0.78 ~ 50 µM range (23% and 22% cytotoxicity against BMDCs and BM-MDSCs, respectively, at 100 µM) **(Figure 4.2B)**.

(A)

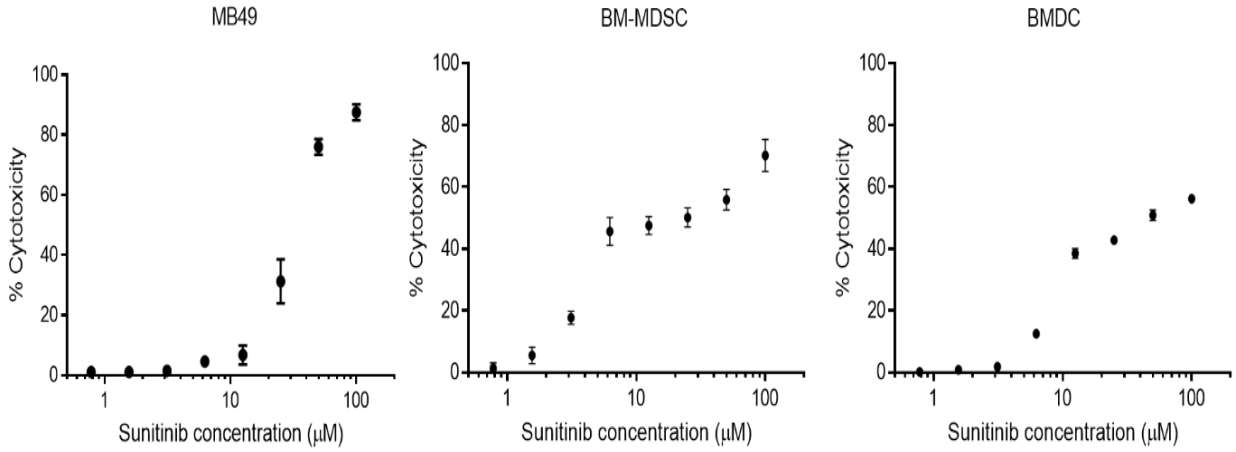

(B)

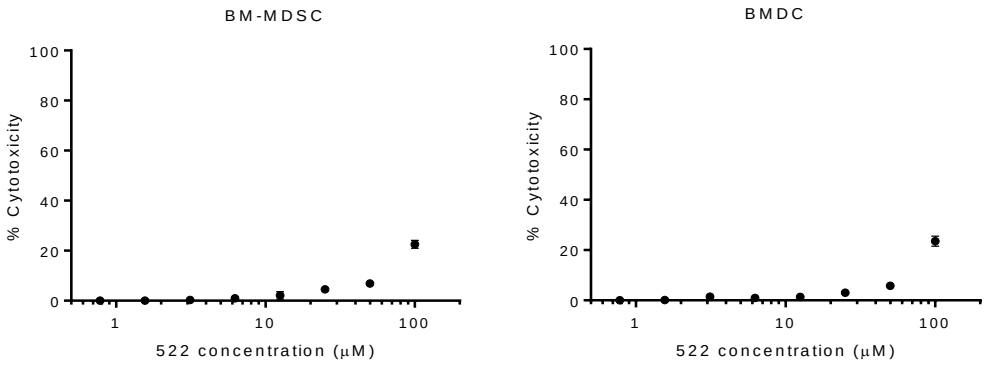

Figure 4.2. Cytotoxicity of sunitinib and 522

(A) Cytotoxicity of sunitinib against MB49 cells, BM-MDSCs, and BMDCs. Results are reported as mean ± SD, N=4 **(B)** Cytotoxicity of 522 was examined against BM-MDSCs and BMDCs. Results are reported as mean ± SD, N=4.

4.4.3. *Ex vivo* splenocytes IL-10 measurement

Based on the cytotoxicity profiles of sunitinib and 522, we chose 28 µM of 522 and 1.25, 2.5 and 5 µM of sunitinib for *ex vivo* cytokine assay. In both PBS treated and sunitinib treated splenocytes from MB49 tumor-bearing mice, we detected 41 pg/ml of IL-10 **(Figure 4.3A)**. Identical to that observed in BMDCs, 522 treatment significantly increased IL-10 expression (797 pg/ml) in splenocytes. However, addition of sunitinib resulted in a dose-dependent reduction in the amount of IL-10 produced by 522 treated splenocytes.

4.4.4. Effect of sunitinib on DCs

Consistent with **Figure 4.1A**, we detected high levels (603 pg/ml) of IL-10 when BMDCs were treated with 522 **(Figure 4.3B)** and negligible amount of IL-10 in PBS and sunitinib treated BMDCs. BMDCs treated with 522 and sunitinib showed significantly reduced IL-10 expression (89 pg/ml) compared to those that received only 522. We then investigated the effect of sunitinib on DC activation. Sunitinib alone did not activate DCs. However, 522 and sunitinib combination triggered increased co-stimulatory molecule (CD80, CD86) expression of BMDCs **(Figure 4.3C)**. Compared to PBS treated group, 522 treated BMDCs had 5-fold increased frequency of $CD80^{high}$ cells. When sunitinib was

added with 522, frequency of CD80^{high} cells increased 9-fold compared to that following PBS treatment. CD86^{high} cells also significantly increased from 14.7% in the PBS treatment group to 71% with 522 treatment and 81.4 % with sunitinib and 522 co-treatment.

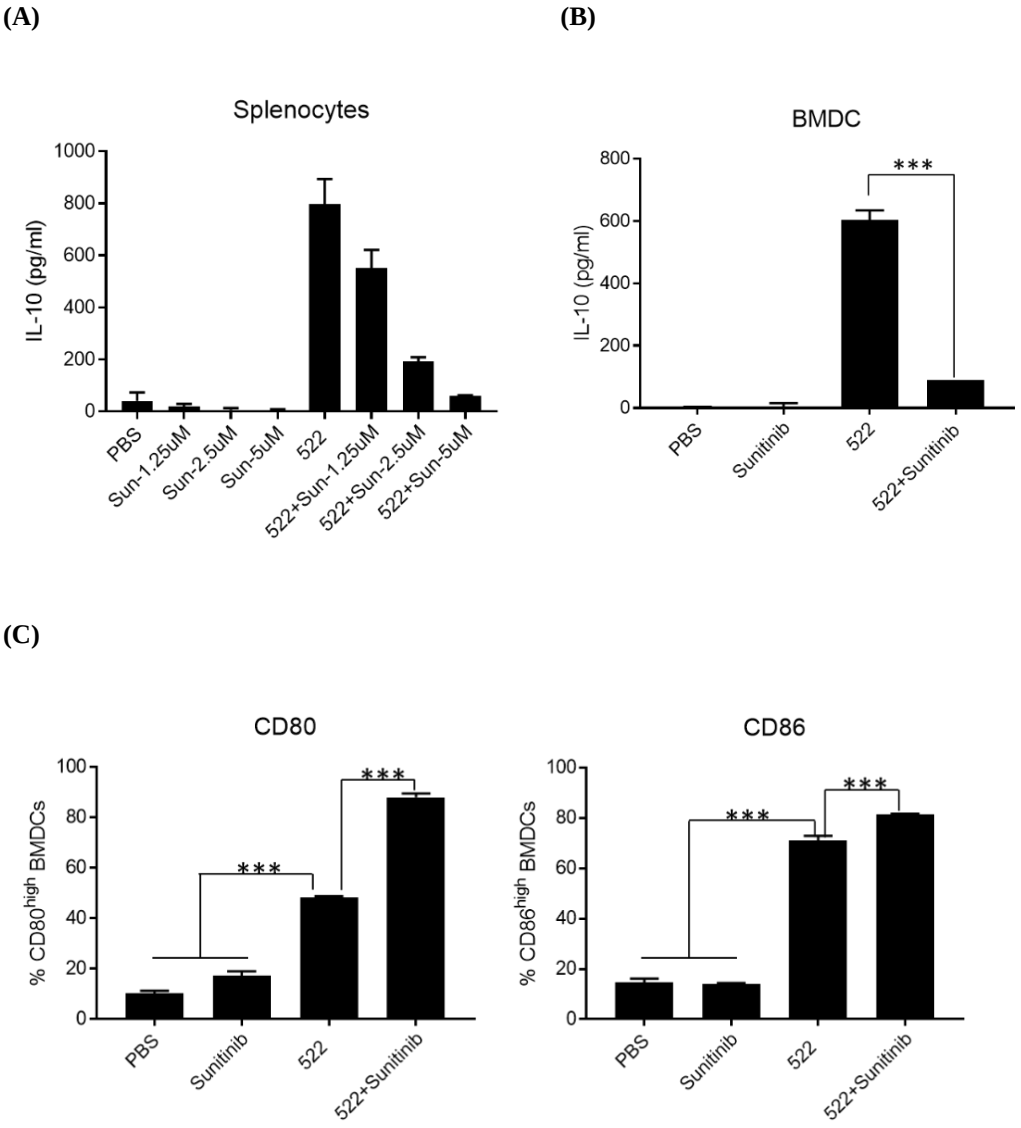

Figure 4.3. Cytokine assays and *In vitro* BMDC activation

(A) Splenocytes were collected from tumor-bearing mouse and incubated with 522 (28 µM) and sunitinib (1.25, 2.5 and 5 µM). IL-10 levels were measured from cell culture supernatants using ELISA. Results are reported as mean ± SD, N=3, One-way ANOVA with *post hoc* Tukey's test **(B)** BMDCs were incubated with 522 (28 µM) and sunitinib (5 µM). Cell culture supernatants were collected for IL-10 measurement. Results are reported as mean ± SD, N=3, ***p<0.001, One-way ANOVA with *post hoc* Tukey's test **(C)** Flow cytometry analysis of CD80 and CD86 expression on BMDCs after 24 h incubation with 522 (28 µM) and sunitinib (5 µM). Results are reported as mean ± SD, N=3, ***p<0.001, One-way ANOVA with *post hoc* Tukey's test

4.4.5. Effect of sunitinib on MDSC and Treg in vivo

We investigated the *in vivo* potency of sunitinib in reducing MDSCs and Tregs in the spleen and tumor. Tumor-free mice had 1.7% MDSCs in the spleen, while tumor-bearing mice had 2.7% MDSCs **(Figure 4.4A)**. When sunitinib was administered to tumor-bearing animals, MDSC population reduced to 1.6%, which is similar to that in the non-tumor bearing mice. Nanovaccine treated mice showed increased MDSCs (4.7%) in the spleen, but the combination of nanovaccine and sunitinib reduced the splenic MDSCs to 2.7%. A similar trend was observed for MDSCs in the tumor, where nanovaccine treated animals had 5.9% MDSCs while mice that received nanovaccine and sunitinib co-treatment had reduced (4.9%) tumor MDSC population.

Similar to MDSCs, Tregs also decreased when mice were treated with a combination of nanovaccine and sunitinib. Frequency of $Foxp3^+$ CD4 T cells in spleen of

tumor bearing mice was 12.6% compared to 9.4% in non-tumor bearing mice **(Figure 4.4B)**. Nanovaccine treated mice showed 11.9% of $Foxp^+$ CD4 T cells and nanovaccine and sunitinib co-treatment reduced the Treg population to 10.1%. In the tumor, frequency of $Foxp3^+$ CD4 T cells from untreated and nanovaccine treated animals were 29.1% and 30.8%, respectively. Sunitinib treatment reduced the frequency of $Foxp3^+$ CD4 T cells to 25.9% and nanovaccine and sunitinib co-treatment further reduced this population to 22.5%.

(A)

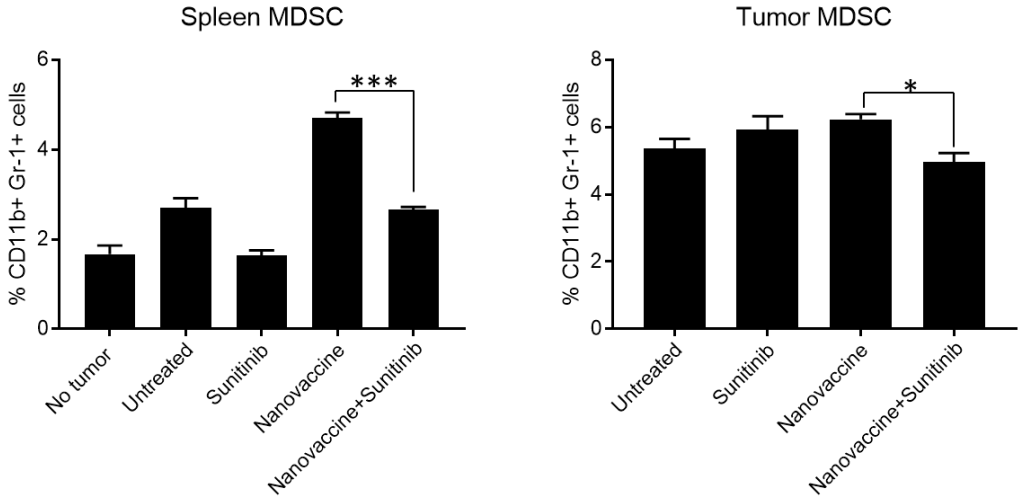

(B)

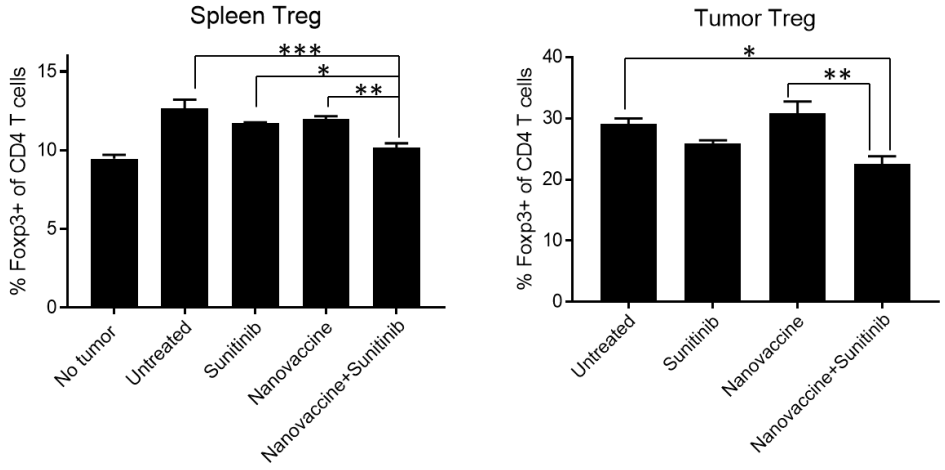

Figure 4.4. *In vivo* MDSCs and Tregs

MB49 tumor-bearing mice received nanovaccine and/or sunitinib as described in the Methods. Spleens and tumors were collected and analyzed by flow cytometry. **(A)** Frequency of MDSCs (Gr-1^{+}CD11b^{+}) in the spleen and tumor. **(B)** Frequency of Tregs (Foxp3^{+} of CD4 T cells) in the spleen and tumor. Results are reported as mean ± SEM, N=4, *p<0.05, **p<0.01, ***p<0.001, One-way ANOVA with *post hoc* Tukey's test

4.4.6. *In vivo* PD-L1^{high} M2 macrophage and MDSC

In the spleen of tumor-bearing mice, 41.6% of M2 macrophages expressed high level of PD-L1. Following treatment with nanovaccine and nanovaccine-sunitinib, this population decreased to 36.7% and 34.9%, respectively **(Figure 4.5A)**. When PD-L1 blockade was combined with nanovaccine, frequency of PD-L1^{high} M2 macrophages decreased to 23.1%, which was similar to that following treatment with just the PD-L1 blockade (25.5%). Animals treated with the triple combination of

nanovacine+sunitinib+PD-L1 blockade had the lowest frequency of PD-L1^{high} M2 macrophages (15.5%). M2 macrophages in the tumor (tumor-associated macrophages) also had high levels of PD-L1 (47.3%). Addition of sunitinib reduced this population somewhat (47% vs. 41% for nanovaccine and nanovaccine+sunitinib, respectively). Nanovaccine+PD-L1 blockade and PD-L1 blockade alone treatments reduced the PD-L1^{high} M2 macrophages to 9.9% and 12.1%, respectively. Similar to that observed in the spleen, nanovaccine+sunitinib+PD-L1 blockade treated animals had the lowest PD-L1^{high} M2 macrophages (9.4%).

PD-L1 expression levels on splenic MDSCs also showed similar trend as M2 macrophages. In the untreated group, 14.4% of MDSCs expressed high level of PD-L1. Nanovaccine and nanovaccine+sunitinib treatments reduced PD-L1^{high} MDSCs to 9.7% and 11.8%, respectively **(Figure 4.5B)**. Nanovaccine+PD-L1 blockade and PD-L1 blockade alone treatments reduced the PD-L1^{high} MDSCs by 7.6 % and 8.3 %, respectively. However, nanovaccine+sunitinib+PD-L1 blockade treated groups showed the lowest PD-L1^{high} MDSCs of 4.1%, which was the only treatment that showed a statistically significant reduction in PD-L1 expression compared to the untreated group. In the tumor, PD-L1 expression on MDSCs were higher than splenic MDSCs, where the untreated group had 34% of PD-L1^{high} MDSCs. Nanovaccine and nanovaccine+sunitinib treated groups also showed high frequencies of PD-L1^{high} MDSCs of 36.9% and 37.8%, respectively. PD-L1 blockade alone treatment reduced the PD-L1 high MDSCs to 31% while nanovaccine+PD-L1 blockade combination reduced this to 21.4%. Lowest PD-L1^{high} MDSCs were observed when animals were treated with nanovaccine+sunitinib+PD-L1 blockade (4.1%).

(A)

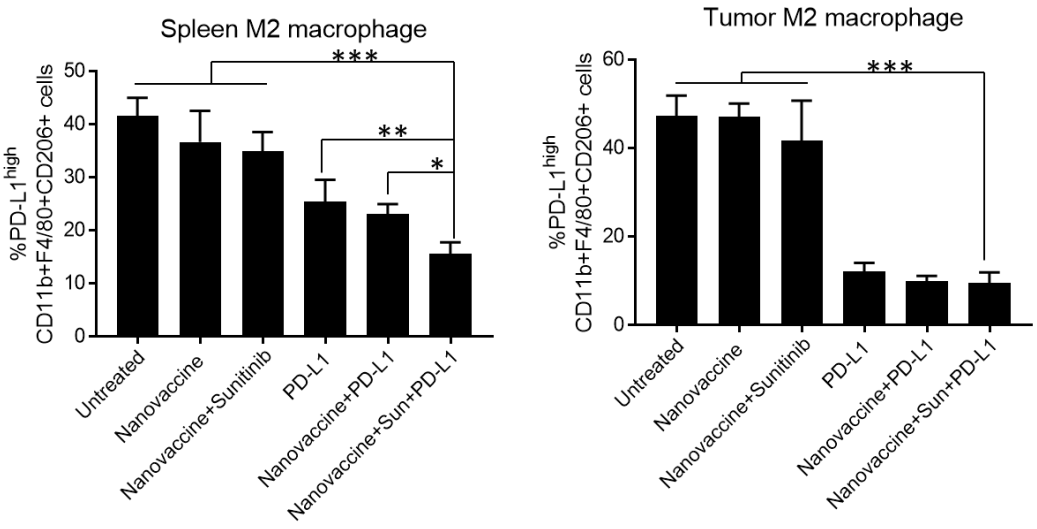

(B)

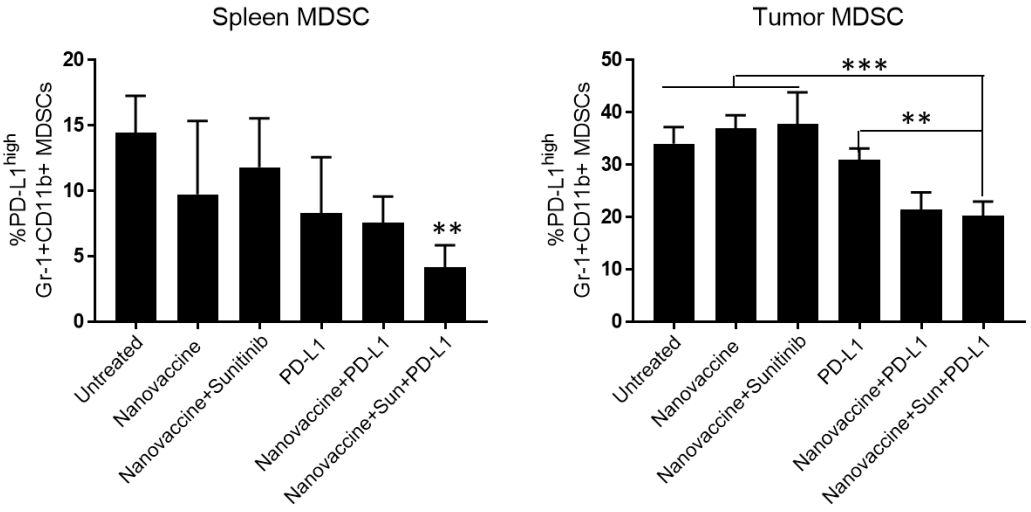

Figure 4.5. *In vivo* PD-L1^{high} M2 macrophages and MDSCs

MB49 tumor-bearing mice received combination treatments consisting of nanovaccine, sunitinib and anti-PD-L1 antibody. Spleens and tumors were collected and analyzed by flow cytometry. **(A)** Frequency of PD-L1^{high} M2 macrophages (CD11b^{+}F4/80^{+}CD206^{+}) in the spleen and tumor. **(B)** Frequency of PD-L1^{high} MDSCs (Gr-1^{+}CD11b^{+}) in the spleen and tumor. Results are reported as mean ± SEM, N=5, *p<0.05, **p<0.01, ***p<0.001, One-way ANOVA with *post hoc* Tukey's test

4.4.7. *In vivo* CD8 T cell activation

Activation of CD8 T cells in the spleen and tumor was examined by measuring CD44 expression on CD8 T cells [196]. In the spleen of untreated mice, CD44^{high} frequency was 11.9% **(Figure 4.6)**. Nanovaccine treatment increased the CD44^{high} CD8 T cells to 16.3% while nanovaccine+sunitinib treated animals had 15.5%. Nanovaccine+PD-L1 blockade treatment resulted in 17.6% of CD44^{high} CD8 T cells while PD-L1 blockade alone increased this population to 20.2%. Nanovaccine+sunitinib+PD-L1 blockade treatment increased the CD44^{high} CD8 T cells to 19.9%.

In the tumor, CD44^{high} CD8 T cells in untreated mice was 8.1% while nanovaccine and nanovaccine+sunitinib treatment increased this population to 10.9% and 12.4%, respectively. Nanovaccine+PD-L1 blockade and PD-L1 blockade alone treated animals had 11.1% and 14% of CD44^{high} CD8 T cells, respectively. Highest frequency (16.2%) of CD44^{high} CD8 T cells was observed in the animals treated with nanovaccine+sunitinib+PD-

L1 blockade, which was the only treatment that showed a statistically significant increase compared to the untreated group.

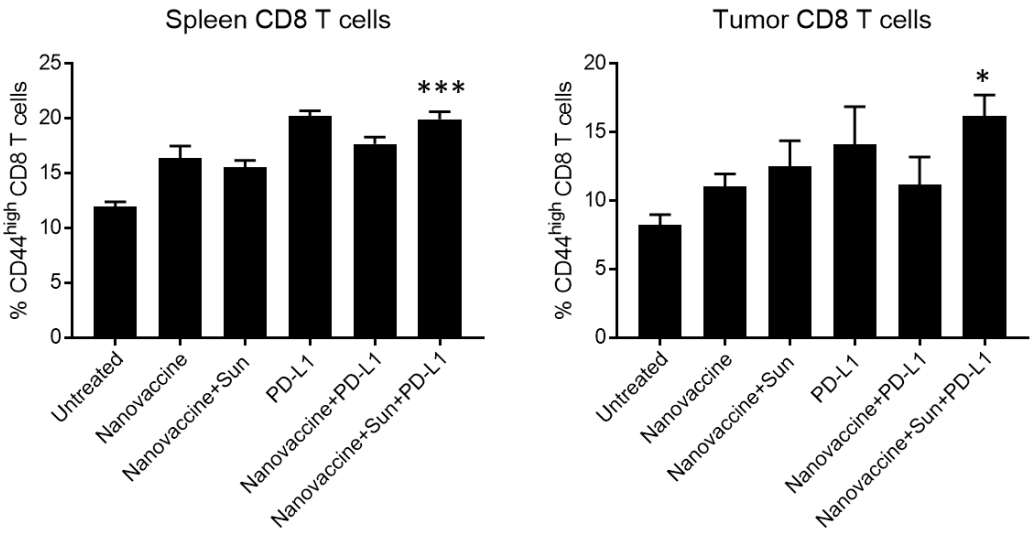

Figure 4.6. ***In vivo*** **CD8 T cell activation and IFN-ɣ response.**

MB49 tumor-bearing mice received combination treatments consisting of nanovaccine, sunitinib and anti-PD-L1 antibody. Spleens and tumors were collected and analyzed by flow cytometry and ELISA. Spleens and tumors were collected and analyzed by flow cytometry. Frequency of $CD44^{high}$ CD8 T cells in the spleen and tumor is shown. Results are reported as mean ± SEM, N=5. Statistical analysis indicates Untreated Vs Nanovaccine+sunitinib+PD-L1 blockade treatment group

4.4.8. Tumor specific CD8 T cell response

To measure tumor-specific immune response, we monitored $CD11a^{high}$ $CD8^{low}$ T cells, as these cells indicate the antigen-experienced CD8 T cells [197]. In the spleens of untreated animals, frequency of $CD11a^{high}$ $CD8^{low}$ T cell was 5.4% **(Figure 4.7A)**. When mice were immunized with nanovaccine, frequency of $CD11a^{high}$ $CD8^{low}$ T cells increased to 7.6% and nanovaccine+sunitinib showed similar frequency of 7.8%. However, when mice were immunized with nanovaccine+PD-L1 blockade, this frequency increased 2-fold (11.2 %) compared to that in untreated animals. PD-L1 blockade alone and nanovaccine+sunitinib+PD-L1 blockade also significantly increased the frequency of $CD11a^{high}$ $CD8^{low}$ T cells to ~13%.

We further examined tumor-specific memory response as previously reported [195]. Splenocytes from untreated mice secreted 13 pg/ml of IFN-ɣ when stimulated with MB49 cell lysate **(Figure 4.7B)**. Splenocytes from nanovaccine and nanovaccine+sunitinib treat groups secreted 44 pg/ml and 16.5 pg/ml of IFN-ɣ, respectively. Nanovaccine+PD-L1 blockade and PD-L1 blockade alone treated groups were characterized by significantly increased secretion of IFN-ɣ (110 pg/ml and 114 pg/ml, respectively). However, the highest IFN-ɣ response was observed from the nanovaccine+sunitinib+PD-L1 blockade group (325 pg/ml), which was 25-fold higher than untreated and 3-fold higher than nanovaccine+PD-L1 blockade group.

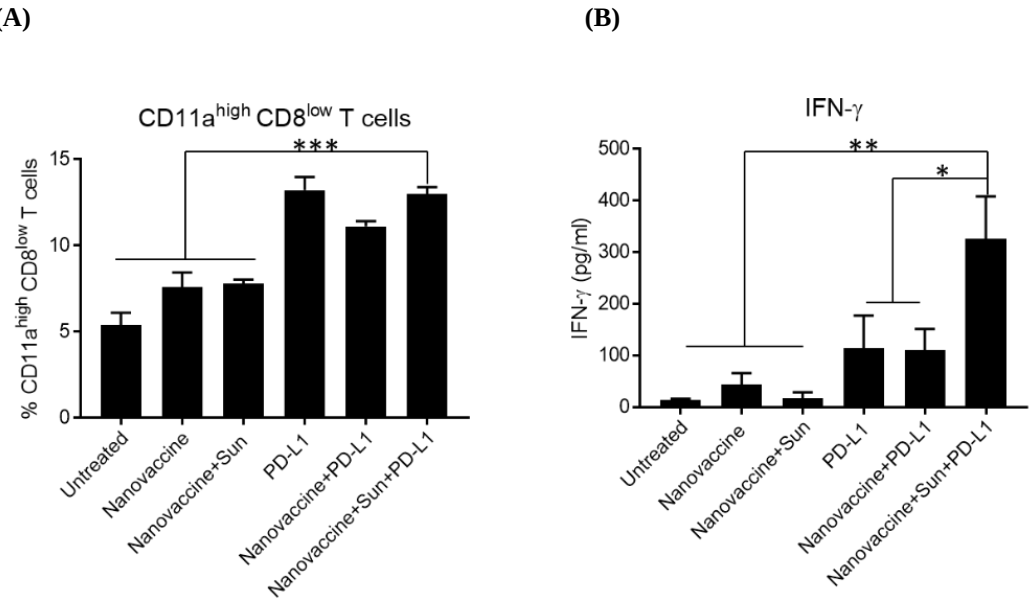

Figure 4.7. Antigen-specific CD8 T cell responses

MB49 tumor-bearing mice received combination treatment consisting of nanovaccine, sunitinib and anti-PD-L1 antibody and spleens were analyzed using flow cytometry and ELISA **(A)** Frequency of $CD11a^{high}$ $CD8^{low}$ T cells in the spleen **(B)** Splenocytes were pulsed with MB49 cell lysates for 24 h. Cell supernatants were collected to measure IFN-ɣ using ELISA. Results are reported as mean ± SEM, N=5, *p<0.05, **p<0.01, ***p<0.001, One-way ANOVA with *post hoc* Tukey's test

4.4.9. Tumor challenge

We investigated the therapeutic efficacy of nanovaccine based combination therapies in a murine bladder tumor model **(Figure 4.8AB)**. When MB49 tumors became palpable (~d 10 after injecting the tumor cells), treatments were initiated as described above. We observed rapid tumor growth in untreated group, in which the average tumor

volume reached 1392 mm^3 on d 32. Sunitinib treated animals also showed rapid tumor growth and had tumor volume of 1310 mm^3 on d 32. Consistent with our previous study, nanovaccine delayed the tumor growth. Average tumor volume of nanovaccine treated mice was 932 mm^3. However, nanovaccine+sunitinib failed to show any therapeutic efficacy and average tumor volume on d 32 was 1304 mm^3. In contrast, nanovaccine+PD-L1 blockade showed enhanced therapeutic efficacy than nanovaccine alone (663 mm^3). In nanovaccine+sunitinib+PD-L1 blockade treated mice, we observed significant therapeutic efficacy, where 2 out of 5 mice showed complete tumor eradication at d 34. Average tumor volume of 3 mice on d 34 was 165 mm^3. Interestingly, PD-L1 blockade alone treatment also showed dramatic tumor inhibition, where 3 out of 4 mice showed complete tumor eradication on d 34.

(A)

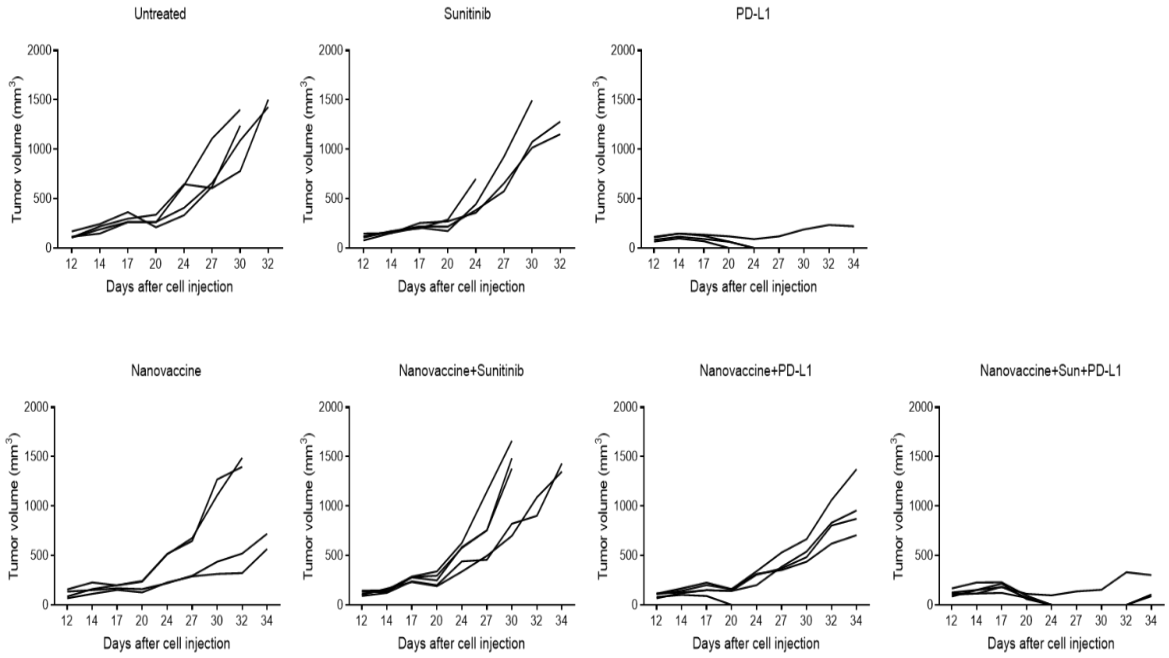

(B)

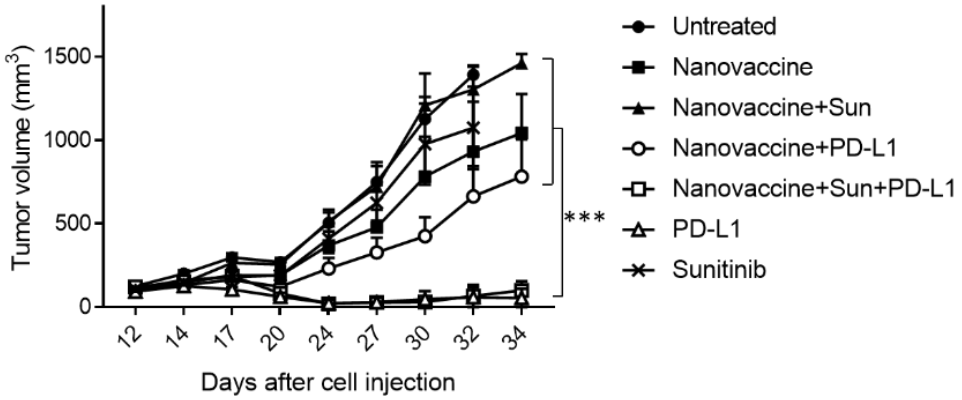

Figure 4.8. Tumor challenge using MB49 tumor model

MB49 tumor-bearing mice received combination treatments consisting of nanovaccine, sunitinib and anti-PD-L1 antibody. Tumor volume was monitored every 2~3 days using digital caliper. **(A)** Tumor volumes of individual mice are shown **(B)** Average tumor volume of mice per treatment are shown. Results are reported as mean ± SEM, N=4~5. Statistical analysis shown Nanovaccine+sunitinib+PD-L1 blockade treatment Vs other treatments, ***p<0.001, Two-way ANOVA with *post hoc* Tukey's test

4.5. Discussion

In vivo adjuvanticity of TLR agonists is often limited by rapid clearance from the injection site and inefficient delivery to lymphoid organs, resulting in sub-optimal efficacy of cancer vaccines [76]. Following S.C. injection, molecules with a molecular weight (MW) of 16 kDa or less or a size of 10 nm or less are preferentially absorbed by blood capillaries and enter the systemic circulation [61,62]. Additionally, the interstitial matrix, composed of

adipocytes, collagen and glycosaminoglycans (GAGs), in the hypodermis can contribute to biodegradation of injected molecules [60]. Encapsulation in polymeric NPs can protect the encapsulated TLR agonists from biodegradation [198]. In addition, size of the NPs can be fine-tuned to 200~300 nm to favor lymphatic drainage [57]. Due to their negative charge [53], PLGA NPs can rapidly pass the negatively charged interstitial matrix and drain into the lymphatic capillaries [199]. These aspects make PLGA NPs a suitable drug delivery platform of TLR agonists, particularly for synthetic TLR 7/8 agonists. Unlike other TLR agonists, synthetic TLR7/8 agonists are soluble in organic solvents and are sparingly soluble in normal saline or aqueous buffers [68], which limits their systemic use [69]. In our previous study [70], we were able to disperse PLGA NPs encapsulating TLR7/8 agonists in physiological saline and, could therefore combine the agonist NPs with tumor antigen in a single formulation for S.C. injection, which demonstrates that PLGA NPs can be suitable *in vivo* drug delivery platform of TLR7/8 agonists

MDSCs are key immunosuppressive cells in the tumor microenvironment that hamper the effectiveness of cancer immunotherapy. MDSCs express arginase 1 (ARG1) and inducible nitric oxide synthase (iNOS), both of which can inhibit T cell activation by impairing T cell receptor (TCR) signaling [200]. Furthermore, MDSCs secrete IL-10, which stimulates the induction of Tregs and deactivates T cells [201]. TLR7/8 ligation can activate MDSCs via NF-κB signaling and by inducing IL-10 secretion from DCs [201]. Thus, inhibition of MDSCs could be critical for the success of TLR7/8 agonist-based cancer immunotherapy. Sunitinib, a TKI that can selectively target signal transducer and activator of transcription 3 (STAT3), was utilized to eliminate MDSCs. Our results show that

TLR7/8 agonist triggers IL-10 secretion from splenocytes, but addition of sunitinib downregulates IL-10 significantly in dose-dependent manner. Based on the cytotoxicity of sunitinib against BM-MDSCs and BMDCs, it is possible that sunitinib selectively killed MDSCs and Tregs, which resulted in IL-10 reduction. *In vivo* studies showed that co-treatment of sunitinib with nanovaccine reduced the MDSCs in the spleen and tumor compared to vaccination alone, which was consistent with previous studies [202,203]. Furthermore, Tregs were also reduced when nanovaccine was combined with sunitinib treatment, which may be the consequence of sunitinib's effect on MDSCs. These results suggest that low oral doses of sunitinib is sufficient to reduce immunosuppressive cells. In addition to regulating MDSCs, sunitinib appeared to have favorable effects on DCs. In addition to reducing 522-induced IL-10 secretion, sunitinib also resulted in greater expression of co-stimulatory molecules CD80 and CD86 on DCs. It has been reported that TKI alone or combination with a TLR 7 agonist can induce detrimental effects on DCs [204,205]. One key difference in our study is that 522 is a dual TLR 7/8 agonist compared to the TLR 7-specific ligand used in the prior study. Pre-treatment of DCs with sunitinib can induce TH1 phenotype and downregulate TH2 phenotype [206], suggesting that sunitinib not only eliminates MDSC, but can also augment TH1 response.

PD-L1 is a inhibitory molecule expressed on various cells including tumor cells, monocytes, and macrophages [9]. PD-L1 can impair anti-tumor immune responses by inducing apoptosis, anergy and exhaustion of effector CD8 T cells and NK cells [13]. Consequently, PD-L1 expression is associated with poor prognosis in various tumors and, thus considered as a predictive marker of cancer immunotherapy [12]. Paradoxically, IFN-ɣ,

which enhances cancer immunotherapy by stimulating antigen-presenting machinery and sensitizing tumor cells to express MHC I, is a main inducer of PD-L1 upregulation on tumor cells [207]. As TLR agonists induce activation of CD8 T cells and NK cells that secrete IFN-ɣ, modulation of PD-L1^{high} suppressive cells can be beneficial for TLR7/8 agonist-based nanovaccine. In this regard, we combined PD-L1 blocking antibody with nanovaccine and investigated the efficacy of the combination in reducing PD-L1 expressing cells and augmenting CD8 T cell immunity. Interestingly, combination of sunitinib and nanovaccine did not downregulate PD-L1^{high} M2 macrophages, the triple combination of nanovaccine+sunitinib+PD-L1 blockade resulted in greater reduction of PD-L1^{high} splenic M2 macrophages compared to nanovaccine+PD-L1 blockade. This points to potential synergies between the three treatments. In the tumor, nanovaccine+sunitinib+PD-L1 blockade significantly reduced PD-L1^{high} M2 macrophages. A previous study reported that combination of TLR7 agonist with PD-1 blocking antibody polarizes immunosuppressive M2 macrophages to M1 phenotype in the tumor [134], which is similar to what we observed. In addition, nanovaccine+sunitinib+PD-L1 blockade significantly reduced PD-L1^{high} MDSCs [208] in the spleen and tumor. Interestingly, although sunitinib treatment reduced MDSCs and Tregs, it did not downregulate PD-L1 expression on MDSCs and M2 macrophages. Therefore, combining PD-L1 blockade with sunitinib can further neutralize immunosuppressive cells [209] and enhance the therapeutic efficacy of nanovaccine.

To determine whether inhibiting immunosuppressive cells leads to enhanced T cell response, we examined CD8 T cells in the spleen and tumor. CD44^{high} CD8 T cells were

investigated as these cells are in an activated state and can become memory cells [196]. In the spleen, nanovaccine+sunitinib+PD-L1 blockade treatment increased $CD44^{high}$ CD8 T cells compared to nanovaccine and nanovaccine+sunitinib treatments, but PD-L1 blockade alone and nanovaccine+PD-L1 blockade also showed similar CD8 T cell activation potency. However, in the tumor, only nanovaccine+sunitinib+PD-L1 blockade treatment promoted CD44 upregulation of CD8 T cells. These results suggest that PD-L1 blockade can lower the T cell exhaustion and augment overall T cell activation, but downregulation of MDSCs and Tregs is required to promote CD8 T cell activation in the tumor. Antigen-specific CD8 T cell responses were further examined to determine long-term memory response. Consistent with our previous study [70], nanovaccine increased $CD11a^{high}$ $CD8^{low}$ T cells in the spleen. While we detected no synergetic effect of sunitinib and nanovaccine, PD-L1 blockade alone significantly increased $CD11a^{high}$ $CD8^{low}$ T cells as single or combination therapy with nanovaccine and sunitinib. IFN-ɣ production showed a similar trend, where splenocytes from PD-L1 blockade alone and nanovaccine+PD-L1 blockade treated mice responded well to MB49 cell lysates. Interestingly, although nanovaccine+sunitinib+PD-L1 blockade induced similar induction of $CD11a^{high}$ $CD8^{low}$ T cells as PD-L1 blockade alone and nanovaccine+PD-L1 blockade, IFN-ɣ response was 3-fold greater than both treatments, which implies that nanovaccine+sunitinib+PD-L1 blockade treatment is effective in generating antigen-specific CD8 T cells and inducing long-term memory response.

Consistent with our previous study, nanovaccine was effective in delaying tumor growth compared to the untreated group. However, addition of sunitinib to nanovaccine

did not show any therapeutic advantages over nanovaccine treatment, which can be explained by the fact that sunitinib reduced MDSCs and Tregs, but did not directly promote CD8 T cell activation. Nanovaccine+PD-L1 blockade showed enhanced therapeutic efficacy compared to nanovaccine alone, which implies that promoting CD8 T cell response by blocking PD-L1/PD-1 signaling can enhance nanovaccine efficacy. We observed significant tumor regression from nanovaccine+sunitinib+PD-L1 blockade group, which demonstrates that eliminating MDSCs and Tregs as well as blocking PD-L1/PD-1 signaling promotes antigen-specific CD8 T cells and results in potent anticancer immunotherapy. Interestingly, PD-L1 blockade alone treated groups also showed significant therapeutic efficacy. Unlike TLR 7/8-based nanovaccine, PD-L1 blockade alone treatment does not stimulate immune-suppressive cell activation [210,211], which can explain the superior therapeutic efficacy of PD-L1 blockade alone treatment compared to nanovaccine+PD-L1 blockade. However, PD-L1 blockade alone treatment does not elicit long-term memory response, and previous studies report the development of resistance [11,212], which makes it a sub-optimal therapeutic for long-term therapy. Potent antigen-specific memory response induced by nanovaccine+sunitinib+PD-L1 blockade points to its potential for inducing long-term tumor growth inhibition.

In this study, we demonstrate that daily oral dosing of sunitinb reduces MDSCs and Tregs, and PD-L1 blockade further neutralizes PD-L1^{high} M2 macrophages and MDSCs. We also observed potent activation of antigen-specific CD8 T cells and induction of memory response. Combined, our results suggest that combination of sunitinib and PD-L1

blockade can modulate the tumor microenvironment and enhance the anticancer efficacy of TLR7/8 agonist-based nanovaccine.

Chapter 5.

TLR7/8 agonist encapsulating polymeric nanoparticles can promote NK cell activation and augment antibody-based cancer immunotherapy

5.1. Summary

Natural killer (NK) cells are cytotoxic cells that upon activation can kill malignant tumor cells via granule exocytosis and secrete IFN-ɣ, a key regulator of TH1 response. Thus, mobilization of NK cells can augment cancer immunotherapy, particularly mediated via antibody-dependent cellular cytotoxicity (ADCC). In the current study, we investigated synthetic toll-like receptor (TLR) 7/8 agonists to activate NK cells. TLR7/8 ligation of dendritic cells (DCs) promote NF-κB-mediated pro-inflammatory cytokine secretion and co-stimulatory molecule upregulation, both which potentiate NK cell activation. To enable subcutaneous delivery to antigen presenting cells, we encapsulated the agonists in polymeric nanoparticles (NPs). NP-encapsulated agonist induced enhanced co-stimulatory molecule expression on DCs and stronger pro-inflammatory cytokine response, compared to the soluble agonist. When injected into immunocompetent mice, NK cells from NP treated mice showed stronger cytotoxicity and prolonged activation compared to those from soluble agonist treated group. TLR7/8 agonist loaded NPs potentiated stronger NK cell degranulation, which resulted in enhanced ADCC efficacy of epidermal growth factor receptor (EGFR) targeting monoclonal antibody, cetuximab. These results suggest NPs encapsulating TLR7/8 agonist could be used as a potent immunostimulatory adjuvant for antibody-based cancer immunotherapy by promoting NK cell activation.

5.2. Introduction

Monoclonal antibodies targeting specific tumor cell surface receptors such as epidermal growth factor receptor (EGFR) and HER-2 are immunotherapeutics approved for the treatment of various solid tumors [6,213]. In addition to their direct inhibitory effects on these receptors, the antibodies also elicit natural killer (NK) cell-mediated antibody-dependent cell cytotoxicity (ADCC) responses to kill the tumor cells [5].

NK cells play multiple roles in cancer immunotherapy. NK cells can recognize and kill the tumor cells that are MHC I-deficient as well as those labeled by complement or antibodies via granule exocytosis [214]. In addition, NK cells secrete interferons that activate other immune cells including dendritic cells (DCs), B cells and T cells, which demonstrate their versatility in cancer immunotherapy [215]. Thus, stimulation of NK cells can augment therapeutic efficacy of antibody-based cancer immunotherapy.

Small molecules including toll-like receptor (TLR) agonists [216], lenalidomide [217], erlotinib [218], and NKG2D receptor ligands including histone deacetylase (HDAC) inhibitors [219] and retinoic acids [220] have been shown to activate NK cells and augment ADCC. Pro-inflammatory cytokines including IL-2, 12, 15, 18, IFN-α and IFN-ɣ are also modulators of NK cell activation [221]. As TLR agonists can stimulate diverse subsets of DCs to secrete pro-inflammatory cytokines and type I interferons [222], various TLR agonists including polysaccharide krestin (PSK; TLR2), polyinosinic:polycytidylic acid (poly I:C; TLR3), CpG oligodeoxynucleotides-derivatives (CpG; TLR9) have been shown to potentiate ADCC response in both pre-clinical and clinical studies [223–225].

Imidazoquinoline-based synthetic TLR7/8 agonists are potent pro-inflammatory cytokine inducers [35], and thus have the potential to improve the effectiveness of antibody-based cancer immunotherapy. Previously, our group reported a novel TLR7/8 agonist (termed '522'), which induces secretion of IL-12, IL-1β, TNF-α and IFN-ɣ from human peripheral blood mononuclear cells (PMBCs) [42], and upregulates co-stimulatory molecules expression on murine DCs. pointing to its potential as an NK cell stimulant. To enable *in vivo* use, we encapsulated the TLR7/8 agonist in an acid pH-responsive poly(lactide-co-glycolide) (PLGA) nanoparticles (NPs) [70]. In our previous study [70], we observed pH responsive agonist release and robust DC maturation and NK cell activation. In the present study, we investigated whether NP-encapsulated agonist can enhance ADCC against $EGFR^+$ human lung carcinoma using EGFR targeting monoclonal antibody, cetuximab [5]. Our results demonstrate that NPs encapsulating TLR7/8 agonist could be used as a potent immunostimulatory adjuvant for enhancing antibody-based cancer immunotherapy.

5.3. Materials and Methods

Chemicals and reagents

TLR7/8 agonist '522' and polymeric nanoparticle encapsulating 522 (522GGNP) were prepared as previously described [42]. Polyinosinic:polycytidylic acid (poly I:C) and sterile dimethyl sulfoxide (DMSO) were purchased from Sigma-Aldrich (St Louis, MO). Brefeldin A solution (BFA), carboxyfluorescein succinimidyl ester (CFSE) cell division tracker kit and fluorophore labeled antibodies (CD3, CD25, CD49b, CD56, CD69,

CD107a, IFN-ɣ, granzyme B) were purchased from Biolegend (San Diego, CA). Cetuximab was purchased from Merck KGaA (Darmstadt, Germany).

Animals and cell line

Athymic nude mice and TAP1-deficient ($Tap^{1tm1Arp}$) mice were purchased from Jackson Laboratories (Bar Harbor, ME). C57BL/6 mice were purchased from Charles River (Wilmington, MA). All mice were female and 6-7 weeks old at the time of arrival.

A549 cell line was purchased from ATCC. Cells were cultured in RPMI 1640 medium which contain fetal bovine serum, 100 µg/mL streptomycin, 100 U/mL penicillin (hereafter referred to as complete RPMI).

Bone marrow derived dendritic cells (BMDCs) activation and cytokine assay

BMDCs were cultured as previously reported [70] and one million BMDCs were plated in 24-well plate. Poly I:C (0.2 µg/ml), soluble form of 522 in DMSO (Free522)(0.2 µg/ml) and 522GGNPs (0.2 µg/ml of 522 equivalent) were added to the cells and incubated overnight. Next day, cells were harvested and pelleted down. Supernatants were collected and IL-12p70 was quantified by ELISA kit (Biolegend). Pelleted cells were washed and stained with fluorophore labeled antibody to measure co-stimulatory molecule expression (CD70, CD80, CD86) by flow cytometry (LSRFortessa H0081, BD Bioscience).

Cytokine and NK cell activation assay

Human peripheral blood mononuclear cells (PBMCs) were harvested from blood obtained from healthy donors. Heparinized blood was processed with standard density-gradient centrifugation using Ficoll-Paque media (GE healthcare). PBMCs (5 x 10^5 cells/well) were seeded at 24-well plate. Treatments used for BMDC assay were prepared at 10 µg/ml concentration and incubated with PBMCs for 18 h. After 18 h, cell culture supernatants were collected to measure IL-12p70 (Biolegend) and IL-18 (Raybiotech, Norcross, GA) using ELISA.

In a similar but separate experiment, BFA was added to the PBMCs for additional 6 h. Collected PBMCs were washed and stained with anti-CD3, anti-CD56, anti-CD25 and anti-CD69 antibodies (Biolegend). Intracellular IFN-γ staining was performed according to the manufacturer's protocol (Foxp3/Transcription Factor Staining Buffer Set, eBioscience). Stained cells were analyzed using flow cytometry.

***In vivo* NK cell cytotoxicity assay**

NK cell cytotoxicity was evaluated as previously described [226]. Spleens were collected from C57BL/6 and TAP1 ($Tap1^{tm1Arp}$)-deficient mice and were used to prepare single cell suspensions as previously reported [70]. Splenocytes from C57BL/6 and TAP-deficient mice were each labeled with 7 µM and 0.7 µM of CFSE, respectively. After staining, equal number of splenocytes from both mice were mixed and injected (total 1 x 10^7 cells) to recipient C57BL/6 mice via intravenous (I.V.) injection. Mice were then randomized and received different treatments. Free522 and 522GGNP (40 µg equivalent amount of 522) were prepared in PBS and injected subcutaneously (S.C.) in recipient mice.

After 18 h, spleens were harvested from recipient mice. Processed splenocytes were analyzed by flow cytometry to measure $CFSE^{low}$ (TAP1-deficient, target) to $CFSE^{high}$ (C57BL/6, control) ratio to determine in vivo NK cell cytotoxicity.

In vivo NK cell activation assay

Free522 and 522GGNP (40 µg equivalent amount of 522) were prepared in PBS and injected S.C. in C57BL/6 mice. After 3 d, spleens were harvested and single cell suspension of splenocytes were prepared as previously reported [70]. Cells were then stained with anti-CD3, anti-CD49b, anti-CD69 antibodies and intracellular staining of granyme B was performed as described above.

NK cell degranulation and T cell activation assay with cetuximab

NK cell degranulation assay was performed as previously reported [223,227]. Briefly, human PBMCs were treated with poly I:C, Free522 and 522GGNP as described above. After 18 h incubation, A549 cells (2.5×10^5 cells/well) and cetuximab (10 µg/ml) were added to the wells. Anti-CD107a antibody was then added to each well and after 1 h, BFA was added to the cells. After 6 h of incubation, cells were collected and stained with anti-CD3, anti-CD56 antibodies to label NK cells, and intracellular staining of IFN-γ and granzyme B was performed as described above. In a separate study, we stained the cells to label CD4 ($CD3^+CD56^-CD4^+$) and CD8 ($CD3^+CD56^-CD8^+$) T cells and determined the T cell activation by measuring CD69.

Antibody-dependent cell cytotoxicity (ADCC)

ADCC assay was performed as previously reported [224]. Briefly, human PBMCs were incubated with treatments as described above for 18 h, and used as effector cells. After 18 h, A549 cells were incubated with cetuximab (100 nM) for 1h. Effector PBMCs and cetuximab treated A549 cells (target cells) were seeded in 96-well plates in various effector to target (E:T) ratios and incubated overnight. The next day, supernatants were collected and cellular cytotoxicity was measured by LDH assay (Thermo) according to the manufacturer's protocol.

Statistical analyses

Results were reported as mean ± standard error of the mean (SEM) or mean ± standard deviation (SD). Statistical difference between the groups were analyzed by one-way analysis of variance (ANOVA), with a *post hoc* Tukey test. Data was analyzed using GraphPad 7 software (GraphPad software, La Jolla, CA). P-value less than 0.05 was valued as statistically significant; *$p<0.05$, **$p<0.01$, ***$p<0.001$, n.s = not significant ($p>0.05$).

5.4. Results

5.4.1. *In vitro* BMDC activation

We investigated the extent to which 522GGNP can induce DC maturation to express co-stimulatory molecules and secrete pro-inflammatory cytokines. TLR3 agonist poly I:C was utilized as a positive treatment in our studies, as previous studies report its strong potency to augment ADCC [224,227]. Similar to TLR7/8 agonist 522, poly I:C ligates

endo/lysosome-located TLR3, but triggers TRIF signaling pathway (TLR7/8: MyD88 signaling), which makes it an interesting control treatment. When treated with equimolar concentrations, Free522 increased co-stimulatory molecule relative to that with poly I:C and 522GGNP treated BMDCs showed greater DC activation than Free522 **(Figure 5.1A)**. CD70 expression increased from 6.5% for PBS treatment to 41% for 522GGNP treatment, while poly I:C and Free522 resulted in 9.8% and 20%, respectively. CD80 expression also increased from 12% for PBS treatment to 54% for 522GGNP treatment. Poly I:C and Free522 treatment induced 17% and 41% expression of CD86, respectively. We detected dramatic upregulation of CD86 on BMDCs treated with Free522 (73%) compared to PBS (15%) and poly I:C (27%) treatments. However, the highest CD86 expression was achieved with 522GGNP treatment (89%). In addition to co-stimulatory molecule upregulation, we also monitored increased pro-inflammatory cytokine secretion by 522GGNP **(Figure 5.1B)**. While PBS and poly I:C treated BMDCs did not have detectable levels of cytokines, we observed significant expression of IL-12p70 following Free522 treatment and even higher levels with 522GGNP treatment.

(A)

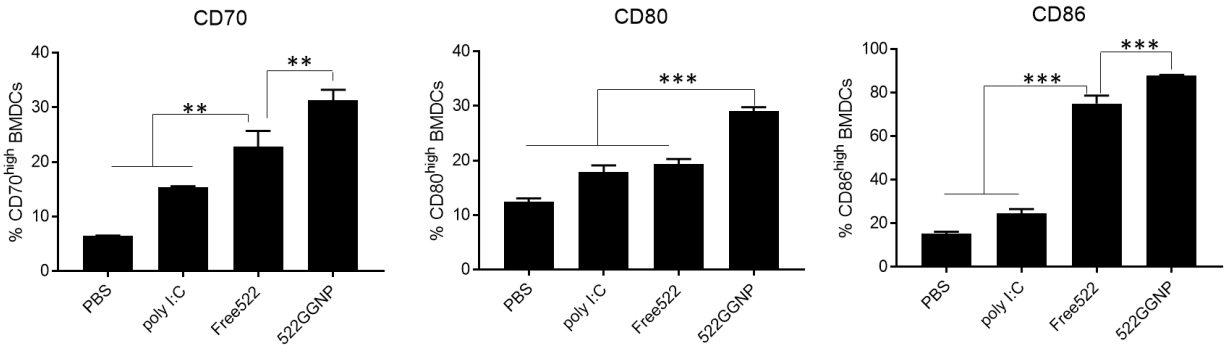

(B)

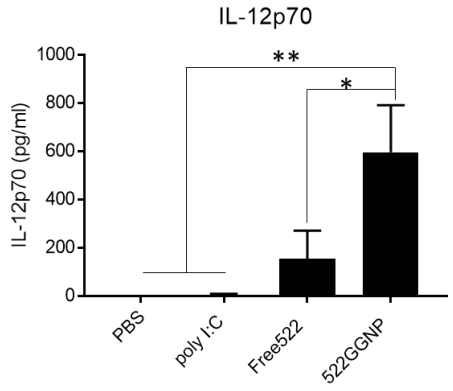

Figure 5.1. *In vitro* BMDC activation

BMDCs were incubated with treatments for 24 h. Cells were then analyzed by flow cytometry and cell culture supernatants were analyzed by ELISA **(A)** Flow cytometry analysis of CD70, CD80 and CD86 expression on $CD11c^+$ BMDCs. Results are reported as mean ± SD, n=3, **p<0.01, ***p<0.001, One-way ANOVA. **(B)** IL-12p70 levels were measured from cell culture supernatants using ELISA. Results are reported as mean ± SD, n=3, *p<0.05, **p<0.01, One-way ANOVA

5.4.2. Human PBMC cytokine assay

As pro-inflammatory cytokines secreted from DCs are key soluble factors in activating NK cells [228], we investigated whether 522GGNP treatment can trigger IL-12p70 and IL-18 secretion from human PBMCs **(Figure 5.2)**. Consistent with the data shown in **Figure 5.1B**, Free522 also induced IL-12p70 secretion (20 pg/ml) from human PBMCs, but 522GGNP treated PBMC showed significantly higher level of IL-12p70 (78 pg/ml)

than poly I:C and Free522. 522GGNP also induced significant IL-18 secretion (144 pg/ml) relative to poly I:C and Free522 (36 pg/ml and 80 pg/ml, respectively).

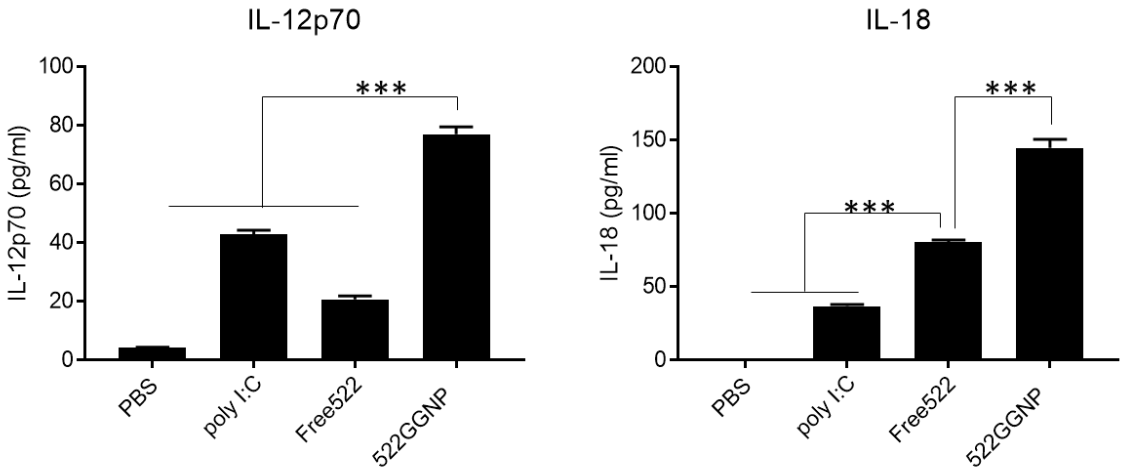

Figure 5.2. Human PBMC cytokine assay

Human PBMCs were incubated with treatments for 24 h. IL-12p70 and IL-18 levels in the cell culture supernatants were determined by ELISA. Results are reported as mean ± SD, n=3, ***p<0.001, One-way ANOVA.

5.4.3. *In vitro* NK cell activation assays

We further investigated whether 522GGNP is effective in activating NK cells by measuring NK cell activation markers (CD25, CD69) and IFN-ɣ using human PBMCs [229]. CD25 expression increased significantly when treated with 522GGNP (27%) compared to PBS treatment (1.2%). Poly I:C and Free522 also increased CD25 expression by 11% and

20%, respectively **(Figure 5.3A)**. Poly I:C increased CD69 expression from 15% observed for PBS treatment to 70%. However, Free522 and 522GGNP were more effective in increasing the CD69 expression (89% and 85%, respectively) **(Figure 5.3B)**. Consistent with CD25 and CD69 expression, 522GGNP was most effective in triggering IFN-ɣ expression of NK cells **(Figure 5.3C)**. IFN-ɣ expressing NK cells increased from 13% with vehicle treatment to 41% when treated with 522GGNP. Poly I:C and Free522 treated NK cells each resulted in 22% and 31% IFN-ɣ positive NK cells, respectively.

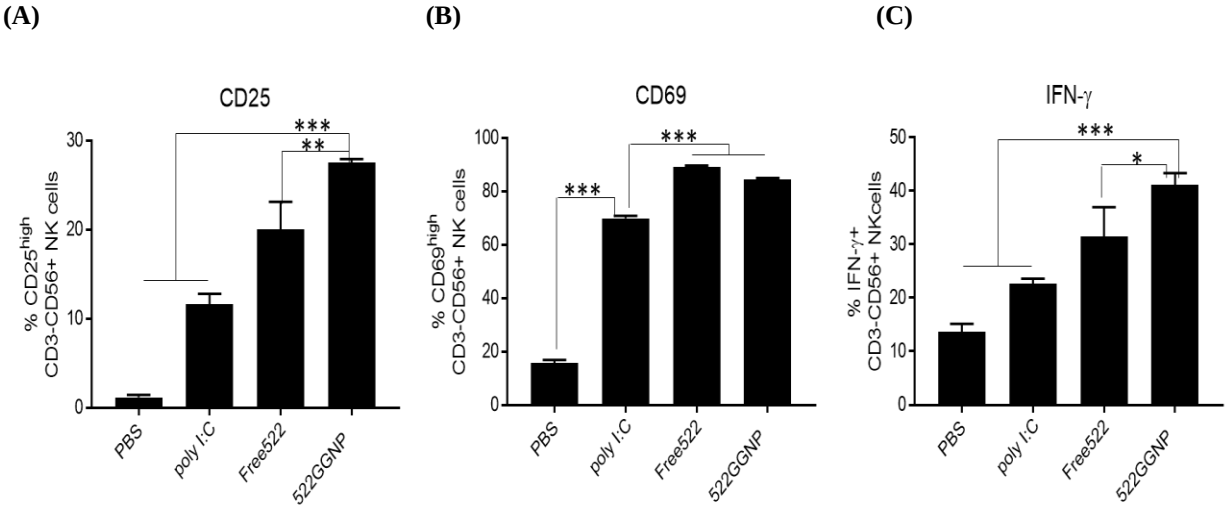

Figure 5.3. *In vitro* NK cell activation assay

Human PBMCs were incubated with treatments for 24 h and NK ($CD3^{-}CD56^{+}$) cells were analyzed by flow cytometry. **(A)** Frequency of $CD25^{high}$ NK cells. **(B)** Frequency of $CD69^{high}$ NK cells. **(C)** Frequency of IFN-$ɣ^{+}$ NK cells. Results are reported as mean ± SD, n=3, *p<0.05, **p<0.01, ***p<0.001, One-way ANOVA.

5.4.4. *In vivo* NK cell cytotoxicity

To assess the ability of 522GGNP to trigger *in vivo* NK cell cytotoxicity, splenocytes from TAP-deficient mice, which lack MHC I, were utilized. As seen in **Figure 5.4A,B**, untreated mice were only partially able to kill the target MHC I deficient splenocytes, resulting in a C57BL/6 (control; C) to TAP-deficient (Target; T) ratio of 3.7. When mice were treated with Free522, C:T ratio increased to 8.9. 522GGNP treatment was most effective as T:C ratio increased to 15.7, which demonstrates highly target-specific lysis by NK cells.

Activation of NK cells was investigated 3 d after a single dose immunization to assess long-term efficacy of 522GGNP. CD69 expression on NK cells in untreated and Free522 treated mice were 10.2% and 10.7%, respectively. However, 522GGNP treated mice showed 12.9% activation of CD69 **(Figure 5.4C)**. Granzyme B expressing NK cells showed similar trend where untreated and Free522 treated groups had 8.4% and 8.5%, respectively, while 522GGNP treatment resulted in 11 %.

(A) **(B)**

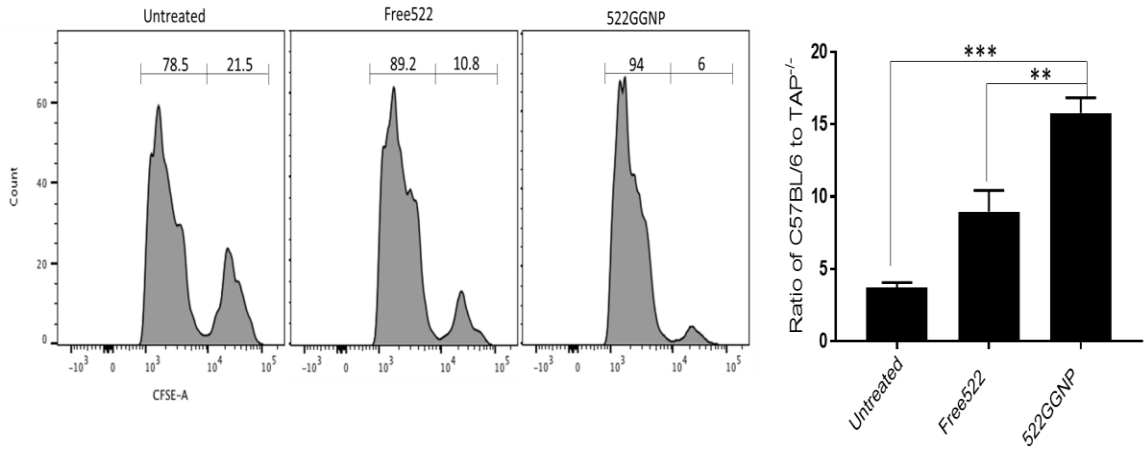

(C)

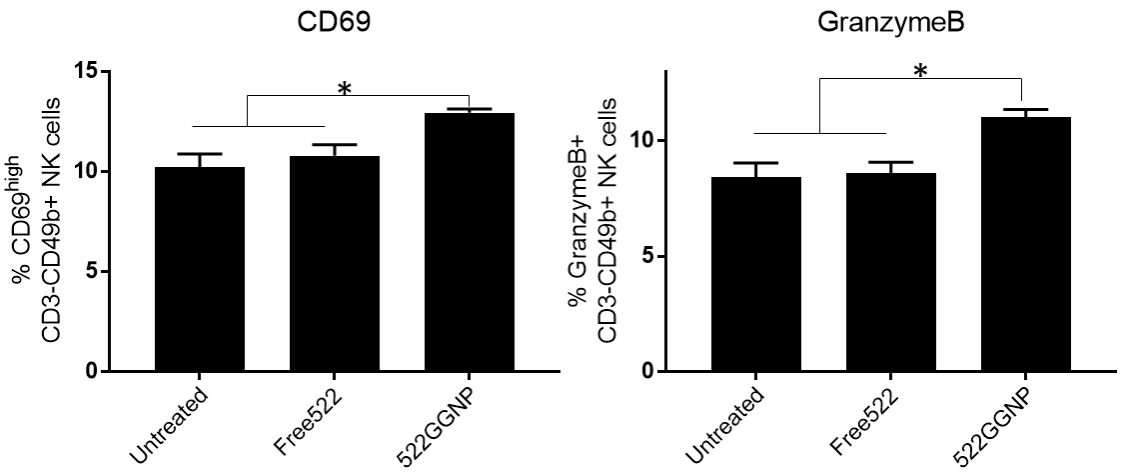

Figure 5.4. *In vivo* NK cell assays

(A-B) *In vivo* NK cell cytotoxicity assay – Recipient mice were injected with splenocytes stained with CFSE and were immunized immediately. **(A)** Representative flow cytometry plots for splenocytes from TAP-deficient mice ($CFSE^{high}$, target cells) and immunocompetent C57BL/6 mice ($CFSE^{low}$, control cells) **(B)** Ratio of number of $CFSE^{low}$ cells (*C*) to $CFSE^{high}$ cells (*T*) in the spleen of the receiver mice. Results are reported as mean ± SEM, n=4~5, **p<0.01, ***p<0.001, One-way ANOVA. **(C) *In vivo* NK cell activation assay** – Mice were euthanized 3 d after immunization and spleens were collected. Frequency of $CD69^{high}$ NK ($CD3^{-}CD49b^{+}$) cells and $GranzymeB^{+}$ NK cells are shown. Results are reported as mean ± SEM, n=4, *p<0.05, One-way ANOVA.

5.4.5. NK cell degranulation assay with cetuximab

As combined data demonstrate that 522GGNPs can efficiently activate NK cells both *in vitro* and *in vivo*, we investigated the potency of 522GGNP as vaccine adjuvant to enhance efficacy of therapeutic monoclonal antibodies.

NK cells release cytotoxic granules including perforin and granzyme to lyse target cells [230,231], which suggest that degranulation of NK cells is closely associated with cytotoxicity of NK cells. CD107a is a lysosomal membrane protein and considered a functional marker for NK cell degranulation [232,233]. Therefore, $CD107a^{+}GranzymeB^{+}$ NK cells were analyzed to examine NK cell cytotoxicity for ADCC. Compared to untreated PBMCs, we detected increased NK cell degranulation when A549 cells were co-incubated with PBMCs, which implies that NK cells undergo degranulation when they encounter foreign cells **(Figure 5.5A)**. NK cell degranulation significantly increased to 16% when cetuximab was added, compared to 5% in untreated group. Addition of Free522 further increased the NK cell degranulation to 27%, but 522GGNP treatment increased degranulated NK cell frequency to 32%, which is a 2-fold increase compared to cetuximab alone treatment. IFN-ɣ expressing NK cells also showed a similar trend. Cetuximab increased the frequency of IFN-ɣ expressing NK cells to 20% compared to 7% in the untreated group **(Figure 5.5B)**. Free522 treated NK cells showed higher IFN-ɣ (30%) than cetuximab alone and 522GGNP further increased IFN-ɣ positive cells to 33%.

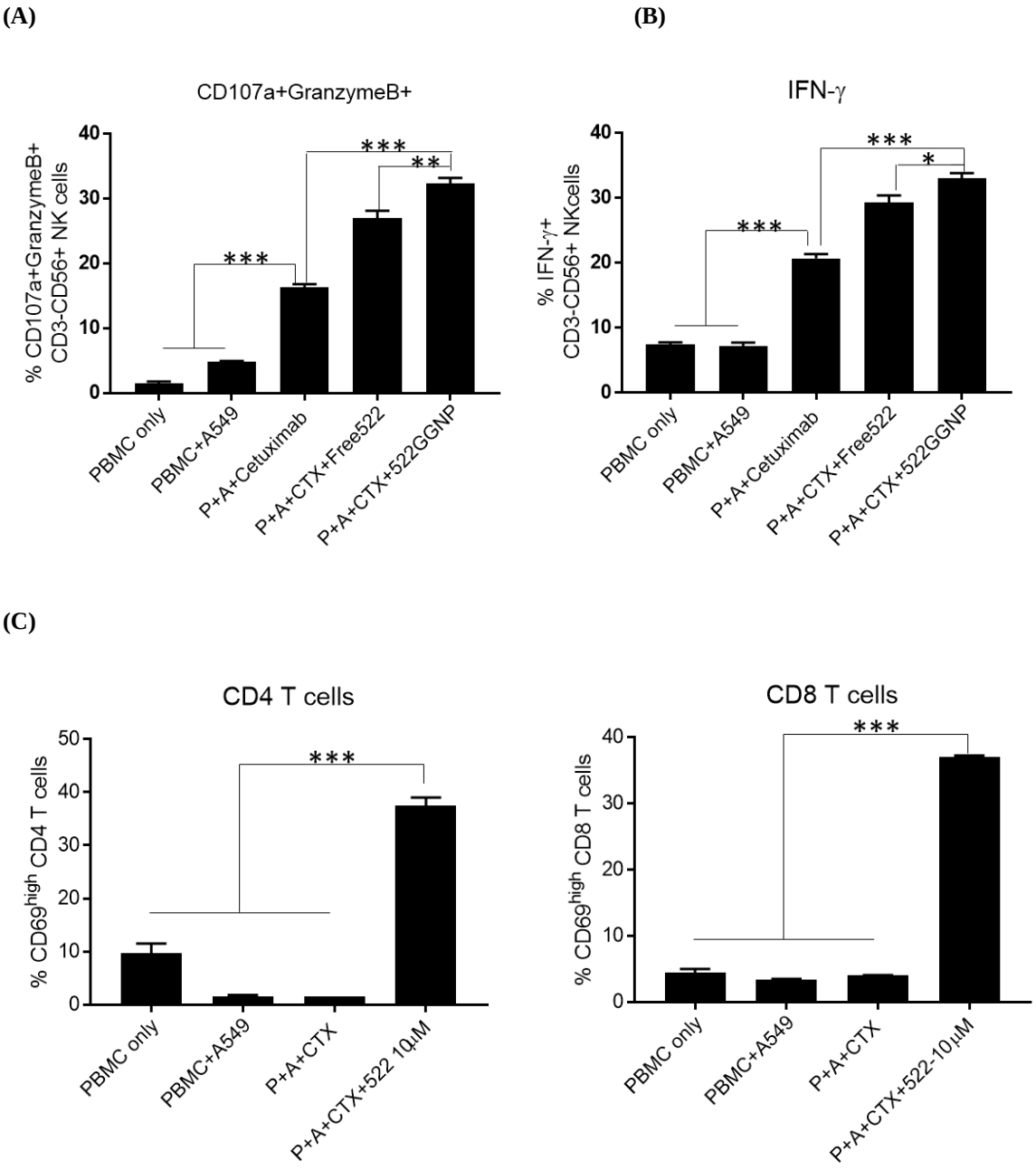

Figure 5.5. NK cell degranulation and T cell activation

Human PBMCs (*P*) were incubated with A549 (*A*) cells and other treatments for 24 h. NK cell degranulation was analyzed by flow cytometry. **(A)** Frequency of

$CD107a^{+}GranzymeB^{+}$ NK cells. **(B)** Frequency of IFN-ɣ$^{+}$ NK cells. Results are reported as mean ± SEM, n=3, *p<0.05, **p<0.01, ***p<0.001, One-way ANOVA. **(C)** CD4 ($CD3^{+}CD56^{-}CD4^{+}$) and CD8 T cells ($CD3^{-}CD56^{-}CD8^{+}$) were analyzed by flow cytometry. Frequency of $CD69^{high}$ T cells are shown. Results are reported as mean ± SEM, n=2, ***p<0.001, One-way ANOVA.

5.4.6. T cell activation assay with cetuximab

In addition to NK cell activation, we examined if 522 treatment can stimulate T cell activation. CD69, an early leukocyte activation molecule [234] was measured to determine the T cell activation **(Figure 5.5C)**. Interestingly, CD69 was downregulated (1.3 %) when PBMCs were co-incubated with A549 cells, compared to PBMC alone group (7.8 %). Cetuximab treated CD4 T cells also showed low CD69 expression (1. 5%). However, addition of Free522 (10 µM) significantly increased the $CD69^{high}$ CD 4 T cells (39 %). CD8 T cells showed similar trend, where PBMC only groups showed negligible CD69 expression on CD8 T cells (4.4 %). PMBCs incubated with A549 and A549+cetuximab also had low CD69high CD 8 T cells (3.4 % and 4 %, respectively). Similar to CD4 T cells, 522 significantly stimulated the CD8 T cell activation (39.9 %).

5.4.7. ADCC

We evaluated whether enhancement of NK cell degranulation and IFN-ɣ secretion induced by 522GGNP treatment can result in enhanced ADCC efficacy with cetuximab. Compared to cetuximab alone, both Free522 and 522GGNP improved the cytotoxicity of

cetuximab against A549 cells **(Figure 5.6)**. At an effector to target (E:T) ratio of 10:1, cetuximab treatment resulted in 17% cell kill, while Free522 and 522GGNP treatments increased the cytotoxicity to 21% and 26%, respectively. At an E:T ratio of 20:1, cetuximab treatment induced 17% cytotoxicity, which was similar to 10:1 ratio. However, Free522 and 522GGNP treatment significantly increased the cytotoxicity to 45 % and 41 %, respectively.

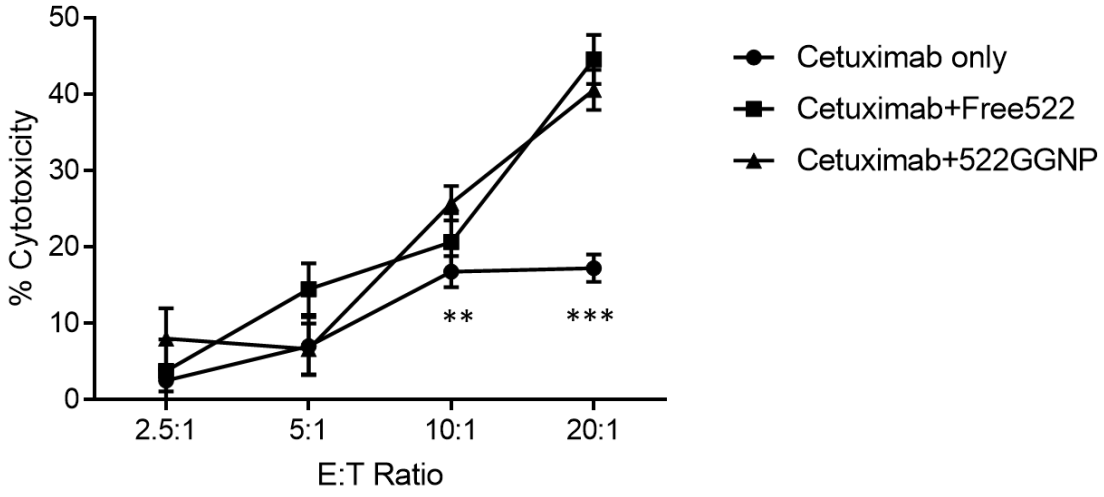

Figure 5.6. ADCC

Human PBMCs were incubated with A549 cells pre-labeled with cetuximab. ADCC was measured by LDH assay. Results are reported as mean ± SD, n=4, Statistical analysis for cetuximab alone Vs cetuximab+522GGNP treatment group. **p<0.01, ***p<0.001, One-way ANOVA.

Discussion

Despite their ability to effectively eliminate target cells, application of NK cells for cancer immunotherapy has been limited by their inability to recognize some tumor cells as well as their insufficient activation at the tumor site. Unlike CD8 T cells that selectively respond to antigens via major histocompatibility complex (MHC) I restriction, NK cells lack antigen-specificity and respond to MHC I-deficient cells [235]. However, tumors are highly heterogeneous and can exploit MHC I-signaling ligands including HLA-G and HLA-E to avoid the recognition [236]. Additionally, tumors secrete immune suppressive cytokines and ligands that neutralize NK cell stimulatory receptor NKG2D to impair NK cells [182].

Combination of tumor-targeting monoclonal antibodies and TLR7/8 agonist-induced activation can overcome some of the above challenges. Upon antibody binding to the tumor cells, NK cells can bind to Fc portion of the antibodies via its CD16 receptor [237]. This binding triggers NK cells to secrete IFN-ɣ and upregulate cytotoxic granules [238], which suggest that monoclonal antibodies can enhance tumor recognition by NK cells and mobilize NK cells to kill the tumor cells. Furthermore, TLR7/8 agonist can further augment ADCC by promoting NK cell activation indirectly by stimulating DC maturation. A previous study also suggests potential direct NK cell activation by TLR7/8 agonists [128].

DCs are the main modulators of NK cell activation. DC-NK cell contact signaling via co-stimulatory molecules and pro-inflammatory cytokines can induce NK cell mediated IFN-ɣ and ADCC responses [222]. In this study, we observed that TLR7/8 agonist 522 upregulates CD70 and CD80/86 on murine BMDCs, which ligate CD27 and CD28,

respectively, to stimulate NK cell activation [173]. In addition to co-stimulatory molecule expression, we observed upregulation of pro-inflammatory cytokines with 522 treatment. IL-12, a key promoter of NK cell activation [228], significantly increased with 522 treatment in both murine BMDCs and human PBMCs. We also observed increased IL-18 secretion from 522 treated human PBMCs. Previous studies report the synergetic effect of IL-12 and IL-18 in increasing IFN-ɣ production and consequent improvement in cytotoxicity of NK cells [228,239]. Interestingly, 522GGNP treatment triggered stronger immunostimulatory responses than Free522 in both BMDC and human PBMC assays. This is consistent with our previous study [70], where we observed that nanoparticle-encapsulated TLR7/8 agonist demonstrate superior *in vitro* DC maturation compared to the soluble form.

Activation associated markers CD25 and CD69 [229,240] were examined to investigate the extent to which 522-mediated DC maturation leads to NK cell activation. We observed drastically increased expression of CD25 on NK cells treated with both Free522 and 522GGNP, compared to PBS and poly I:C treatments. CD69 expression also significantly increased with both Free522 and 522GGNP treatment. As upregulation of CD25 and CD69 is associated with NKG2D activation [241], these results imply that TLR7/8 agonist can promote NK cell activation and cytotoxicity levels. Increased IFN-ɣ expression by 522-stimulated NK cells further demonstrates the potency of 522 for activating NK cells.

To determine *in vivo* efficacy of TLR7/8 agonist, we performed in vivo NK cell cytotoxicity assay using TAP-1 deficient mice model. Consistent with a previous study [226], we observed highly selective lysis of TAP-deficient cells even in the untreated group. Free522 treated animals showed enhanced cytotoxicity against target cells. In our study,

522GGNP treatment was highly effective in potentiating *in vivo* NK cell cytotoxicity compared to Free522, which demonstrates the advantage of nanoparticulate delivery of TLR7/8 agonist. Previous studies report that upon SC injection, small molecules with molecular weight of 16 kDa or less and/or size smaller than 10 nm, are rapidly cleared from the injection site either via drainage into the systemic circulation and through phagocytosis mediated by monocytes and macrophages [60,62]. Thus, a reasonable explanation for the stronger *in vivo* NK cell cytotoxicity with 522GGNPs is their ability to protect TLR7/8 agonist from rapid clearance and/or degradation at the injection site and to improve the delivery of the agonist to draining lymph nodes [61]. We also observed prolonged NK cell activation in mice treated with 522GGNPs compared to those treated with Free522. Together, these results suggest that nanoparticulate delivery will enhance the *in vivo* potency of TLR7/8 agonist.

ADCC studies showed that NK cell degranulation increased when PBMCs were incubated with A549 cells, which can be explained by partial NK cell degranulation against MHC I-deficient A549 cells. Consistent with previous studies, cetuximab alone induced enhanced NK cell degranulation compared to untreated NK cells, which may have resulted from CD16 ligation of cetuximab [242]. Co-treatment with 522GGNP significantly increased NK cell degranulation and IFN-ɣ production than cetuximab alone. Consistent with this data, 522GGNP co-treatment enhanced cetuximab-mediated ADCC against the tumor cells.

Several approaches have previously been examined to utilize NK cells for cancer immunotherapy. NK cells engineered to express chimeric antigen receptor (CAR) that

targets CD19, CS-1 and EGFR have been reported and shown to selectively kill the malignant tumor cells [243,244]. Bi-and tri-specific killer cell engagers (BiKEs, TriKEs) that bridge NK cell activation moieties including CD16, IL-15, and tumor-specific antigens (CD33, CD133) have shown to direct NK cells to tumor sites and induce cytotolysis of tumors [245]. Results of these studies imply that enhancing tumor cell recognition and activation of NK cells is critical for NK cell-mediated cancer immunotherapy. Therefore, combination of a therapeutic antibody and TLR7/8 agonist can be a potent immunotherapeutic to mobilize NK cells for cancer immunotherapy.

In addition to activating NK cells, TLR7/8 agonist can augment antibody-based cancer immunotherapy by their ability to elicit CD8 T cell immunity. Previous studies report that therapeutic efficacy of monoclonal antibodies is dependent on both innate and adaptive immunity [246], which suggest the importance of exploiting both NK cells and CD8 T cells. Combination of therapeutic antibodies and TLR agonists have shown to enhance not only NK cell activation, but also trigger the priming of antigen-specific CD8 T cells [242,247]. We also observed in our study that 522 treatment significantly upregulated CD69 on CD4 and CD8 T cells, which is consistent with previous findings. In our previous study, 522GGNP immunization triggered expansion of effector CD8 T cells, which further demonstrates the versatility of 522GGNP to promote both ADCC and CD8 T cell responses that can enhance anti-tumor efficacy of therapeutic antibodies.

In summary, we demonstrated the use of pH responsive nanoparticles encapsulating a potent TLR 7/8 agonist to activate NK cells for antibody-based cancer immunotherapy. Nanoparticle-encapsulated agonist augmented ADCC with cetuximab and demonstrated

superior *in vivo* NK cell activation efficacy over the free drug. Based on these results, we expect broad application of 522GGNPs as immunostimulatory adjuvant for combination therapies with checkpoint inhibitors [248], chemotherapeutics [249], and radiation therapies [195]. As the biocompatibility and safety profile of PLGA is well established [151], elucidating the pharmacokinetics of 522 after SC injection and potential adverse effects including systemic cytokine storm and auto-immunity will allow successful clinical translation of 522GGNPs.

Chapter 6.

Summary

Cancer immunology and immunotherapy is a highly complexed field, involving interrelated response where a single component modification can affect the overall immune response. Therefore, selective ligation of target cells is critical to promote anti-cancer immunity and to reduce undesired adverse effects. In this study, we used PLGA NPs as a drug delivery platform for TLR7/8 agonists. We demonstrated the advantages of PLGA NPs nanoparticulate delivery compared to soluble form of 522 to activate DCs using a novel TLR7/8 agonist 522 to elicit CD8 T cell response by performing *in vitro* DC assays, *in vivo* T cell assays and multiple tumor challenge studies with different vaccine designs and modalities. We then developed pH-responsive PLGA NP that potentiated stronger T cell immunity than conventional PLGA NPs. Modulation of tumor microenvironment by co-treatment of sunitinib and PD-L1 blockade significantly enhanced therapeutic efficacy of 522NP-based vaccine. Additionally, we suggest the application of 522 encapsulating NPs as NK cell stimulant for antibody-based cancer immunotherapy.

In chapter 2, we observed that 522NPs are similar or more effective in activating TLR7 and 8 reporter cells and inducing cytokines from human PBMCs. While 522NPs showed slightly enhanced upregulation of co-stimulatory molecules on BMDCs, antigen-presentation via MHC I, was significantly enhanced by antigen+522NP treatment compared to antigen+Free522, which can be explained by enhanced antigen uptake mediated by antigen absorption on NPs. More importantly, 522NP immunization showed significantly enhanced prophylactic and therapeutic efficacy compared to Free522 immunization. These findings imply that although 522 is a potent DC stimulant, *in vivo*

efficacy is limited in soluble form. Therefore, nanoparticulate delivery is a efficient drug delivery platform of TLR7/8 agonists.

In chapter 3, we achieved higher drug loading and acidic-pH responsive release kinetics by incorporating sodium bicarbonate within the PLGA NPs using double emulsion solvent evaporation method. In this study, new PLGA NP formulation showed enhanced *in vivo* T cell and NK cell response and augmented therapeutic efficacy in murine tumor model, compared to conventional PLGA NPs, which suggest that optimizing the NP formulation can enhance the efficacy of vaccine adjuvant.

In chapter 4, combination of nanovaccine and sunitinib reduced the MDSCs and Tregs population but did not show therapeutic advantage over nanovaccine as reduction of immune suppressive did not result in activation of CD8 T cells. Therefore, we further adapted anti-PD-L1 antibody to block the inhibitory PD-L1/PD-1 signaling. Combination of sunitinib and PD-L1 blockade not only reduced the immune suppressive cell population, but also increased the CD8 T cell activation at the tumor. Moreover, triple combination therapy triggered antigen-specific memory T cell response, which suggests the long-term efficacy against recurring tumors. Combined results indicate that modulating the tumor microenvironment can augment the therapeutic efficacy of nanovaccine by upregulating CD8 T cell responses at the tumor.

In chapter 5, when incubated with human PBMCs, 522GGNP significantly increased the NK cell activation markers. 522GGNP was also effective in potentiating *in vivo* NK cell cytotoxicity. Furthermore, 522GGNP co-treatment with cetuximab significantly increased the NK cell degranulation and induced IFN-ɣ secretion. These

results suggest that 522GGNPs are potent NK cell stimulant that can augment the ADCC of therapeutic antibodies.

Combined results suggest that nanoparticulate delivery of TLR7/8 agonist is a potent vaccine adjuvant for cancer vaccine therapy and antibody-based therapy. Additionally, recent studies show that combination of TLR agonists can promote synergetic effect with conventional oncology treatments including chemotherapeutics and radiation therapy, which suggest the versatility of TLR7/8 agonists as versatile immune adjuvants in a variety of cancer immunotherapy settings.

In our study, PLGA was utilized as polymer backbone as their biocompatibility and toxicity is well-established. Additionally, fabrication techniques to fine-tune the size and release kinetics was advantage of utilizing PLGA as drug carrier. However, other drug carriers including N-(2-hydroxypropyl)methacrylamide (HPMA), polyethyleneimine (PEI), chitosan, and liposomes are potent candidates for TLR7/8 agonist delivery platform.

For successful clinical translation of 522NP and 522GGNPs, further studies on safety is required. Although PLGA is a FDA-approved polymer, other formulation components including sodium bicarbonate, poly vinyl alcohol (PVA) and 522 need to be investigated. We expect negligible toxicity of sodium bicarbonate as concentration used in this study was comparable to that of buffered saline. A previous study reported that residual PVA on PLGA NPs affects their physical properties and cellular uptake, which suggest the need for investigating the effect of PVA on 522NPs and 522GGNPs in the future study. Currently, imidazoquinoline based TLR 7 agonists, imiquimod and resiquimod, are

approved only for topical treatments. Therefore, pharmacokinetics and potential adverse effects of 522 following SC and IM injection need to be investigated.

We also need to optimize the formulation of cancer vaccine and its immunization intervals. Here, we prepared the tumor cell lysates using repeated freeze-thaw cycle method, due to its simple preparation procedures and long-term stability of proteins. However, as TAA expression is highly heterogenic among the different tumor cell lines, examining the immunogenicity of tumor cell lysates prepared by different protocols is suggested.

Optimization of immunization interval is also required. In this study, we immunized the animals daily for five consecutive days. However, previous studies report 3~7 days as an optimal interval for T cell immunization and frequent antigen exposure may trigger T cell suppression. This will be particularly important for combination therapy with sunitinib as pre- or post- treatment of sunitinib appears to affect the antigen-presentation and T cell response of cancer vaccines. Therefore, mechanistic studies of immune cell responses following different doses and intervals of immunization is required to maximize the therapeutic efficacy and reduce the side effects of cancer vaccine.

With these issues addressed, we expect broad application of 522NP and 522GGNPs as vaccine adjuvant for cancer immunotherapy.

BIBILIOGRAPHY

1 S. A. Rosenberg, J. C. Yang and N. P. Restifo, *Nat. Med.*, 2004, 10, 909–915.

2 J. A. Berzofsky, M. Terabe, S. Oh, I. M. Belyakov, J. D. Ahlers, J. E. Janik and J. C. Morris, *J Clin Invest*, 2004, **113**, 1515–1525.

3 S. H. van der Burg, R. Arens, F. Ossendorp, T. van Hall and C. J. M. Melief, *Nat Rev Cancer*, 2016, **16**, 219–233.

4 L. M. Weiner, R. Surana and S. Wang, *Nat. Rev. Immunol.*, 2010, **10**, 317–327.

5 J. Kurai, H. Chikumi, K. Hashimoto, K. Yamaguchi, A. Yamasaki, T. Sako, H. Touge, H. Makino, M. Takata, M. Miyata, M. Nakamoto, N. Burioka and E. Shimizu, *Clin. Cancer Res.*, 2007, **13**, 1552–1561.

6 N. Robert, B. Leyland-Jones, L. Asmar, R. Belt, D. Llegbodu, D. Loesch, R. Raju, E. Valentine, R. Sayre, M. Cobleigh, K. Albain, C. McCullough, L. Fuchs and D. Slamon, *J. Clin. Oncol.*, 2006, **24**, 2786–2792.

7 C. G. Willett, Y. Boucher, E. Di Tomaso, D. G. Duda, L. L. Munn, R. T. Tong, D. C. Chung, D. V. Sahani, S. P. Kalva, S. V. Kozin, M. Mino, K. S. Cohen, D. T. Scadden, A. C. Hartford, A. J. Fischman, J. W. Clark, D. P. Ryan, A. X. Zhu, L. S. Blaszkowsky, H. X. Chen, P. C. Shellito, G. Y. Lauwers and R. K. Jain, *Nat. Med.*, 2004, **10**, 145–147.

8 A. M. Scott, J. D. Wolchok and L. J. Old, *Nat. Rev. Cancer*, 2012, **12**, 278–287.

9 W. Zou and L. Chen, *Nat. Rev. Immunol.*, 2008, **8**, 467–477.

10 E. I. Buchbinder and A. Desai, *Am. J. Clin. Oncol. Cancer Clin. Trials*, 2016, **39**, 98–106.

11 X. Zhao and S. Subramanian, *Cancer Res.*, 2017, **77**, 817–822.

12 S. P. Patel and R. Kurzrock, *Mol. Cancer Ther.*, 2015, **14**, 847–856.

13 L. Chen and X. Han, *J. Clin. Invest.*, 2015, **125**, 3384–3391.

14 N. P. Restifo, M. E. Dudley and S. a. Rosenberg, *Nat. Rev. Immunol.*, 2012, **12**, 269–281.

15 S. A. Rosenberg, N. P. Restifo, J. C. Yang, R. A. Morgan and M. E. Dudley, *Nat. Rev. Cancer*, 2008, **8**, 299–308.

16 a Lanzavecchia and F. Sallusto, *Cell*, 2001, **106**, 263–266.

17 D. Berd, H. C. Maguire Jr., P. McCue and M. J. Mastrangelo, *J. Clin. Oncol.*, 1990, **8**, 1858–1867.

18 V. K. Sondak and J. A. Sosman, *Semin. Cancer Biol.*, 2003, **13**, 409–415.

19 F. O. Nestle, S. Alijagic, M. Gilliet, Y. Sun, S. Grabbe, R. Dummer, G. Burg and D. Schadendorf, *Nat. Med.*, 1998, **4**, 328–332.

20 M. Scanlan, A. Gure, A. Jungbluth and L. Old, *Immunol. Rev.*, 2002, **188**, 22–32.

21 T. J. De Vries, A. Fourkour, T. Wobbes, G. Verkroost, D. J. Ruiter and G. N. P. Van Muijen, *Cancer Res.*, 1997, 3223–3230.

22 J. Dannull, P. A. Diener, L. Prikler, G. Furstenberger, T. Cerny, U. Schmid, D. K. Ackermann and M. Groettrup, *Cancer Res.*, 2000, **60**, 5522–5528.

23 D. Raina, Y. Uchida, A. Kharbanda, H. Rajabi, G. Panchamoorthy, C. Jin, S. Kharbanda, M. Scaltriti, J. Baselga and D. Kufe, *Oncogene*, 2014, **33**, 3422–3431.

24 M. Shinozaki, A. Fujimoto, D. L. Morton and D. S. B. Hoon, *Clin. Cancer Res.*,

2004, **10**, 1753–1757.
25 A. M. Pullen, J. W. Kappler and P. Marrack, *Immunol. Rev.*, 1989, **107**, 125–140.
26 M. Lehner, P. Morhart, A. Stilper, D. Petermann, P. Weller, D. Stachel and W. Holter, *J. Immunother.*, 2007, **30**, 312–322.
27 J. W. Simons and N. Sacks, *Urol. Oncol. Semin. Orig. Investig.*, 2006, **24**, 419–424.
28 G. Napolitani, A. Rinaldi, F. Bertoni, F. Sallusto and A. Lanzavecchia, *Nat. Immunol.*, 2005, **6**, 769–776.
29 C. Reis E Sousa, *Semin. Immunol.*, 2004, **16**, 27–34.
30 M. Gilliet, W. Cao and Y.-J. Liu, *Nat. Rev. Immunol.*, 2008, **8**, 594–606.
31 M. Torisu, Y. Hayashi, T. Ishimitsu, T. Fujimura, K. Iwasaki, M. Katano, H. Yamamoto, Y. Kimura, M. Takesue, M. Kondo and K. Nomoto, *Cancer Immunol. Immunother.*, 1990, **31**, 261–268.
32 A. M. Didierlaurent, S. Morel, L. Lockman, S. L. Giannini, M. Bisteau, H. Carlsen, A. Kielland, O. Vosters, N. Vanderheyde, F. Schiavetti, D. Larocque, M. Van Mechelen and N. Garcon, *J. Immunol.*, 2009, **183**, 6186–6197.
33 P. Sabbatini, T. Tsuji, L. Ferran, E. Ritter, C. Sedrak, K. Tuballes, A. A. Jungbluth, G. Ritter, C. Aghajanian, K. Bell-McGuinn, M. L. Hensley, J. Konner, W. Tew, D. R. Spriggs, E. W. Hoffman, R. Venhaus, L. Pan, A. M. Salazar, C. M. Diefenbach, L. J. Old and S. Gnjatic, *Clin. Cancer Res.*, 2012, **18**, 6497–6508.
34 C. S. Zent, B. J. Smith, Z. K. Ballas, J. E. Wooldridge, B. K. Link, T. G. Call, T. D. Shanafelt, D. A. Bowen, N. E. Kay, T. E. Witzig and G. J. Weiner, *Leuk. Lymphoma*, 2012, **53**, 211–217.
35 D. Wang, M. Precopio, T. Lan, D. Yu, J. X. Tang, E. R. Kandimalla and S. Agrawal, *Mol. Cancer Ther.*, 2010, **9**, 1788–1797.
36 Stanley MA., *Clin Exp Dermatol*, 2002, **27**, 12464152.
37 S. J. Gibson, J. M. Lindh, T. R. Riter, R. M. Gleason, L. M. Rogers, A. E. Fuller, J. L. Oesterich, K. B. Gorden, X. Qiu, S. W. McKane, R. J. Noelle, R. L. Miller, R. M. Kedl, P. Fitzgerald-Bocarsly, M. A. Tomai and J. P. Vasilakos, *Cell. Immunol.*, 2002, **218**, 74–86.
38 A. Iwasaki and R. Medzhitov, *Nat. Immunol.*, 2004, **5**, 987–995.
39 V. Durand, S. Y. C. Wong, D. F. Tough and A. Le Bon, *Immunol. Cell Biol.*, 2004, **82**, 596–602.
40 M. Schön, A. B. Bong, C. Drewniok, J. Herz, C. C. Geilen, J. Reifenberger, B. Benninghoff, H. B. Slade, H. Gollnick and M. P. Schön, *J. Natl. Cancer Inst.*, 2003, **95**, 1138–1149.
41 C. Shi, Z. Xiong, P. Chittepu, C. C. Aldrich, J. R. Ohlfest and D. M. Ferguson, *ACS Med. Chem. Lett.*, 2012, **3**, 501–504.
42 P. Larson, T. A. Kucaba, Z. Xiong, M. Olin, T. S. Griffith and D. M. Ferguson, *ACS Med. Chem. Lett.*, 2017, **8**, 1148–1152.
43 C. E. Schia, C. Shi, Z. Xiong, M. Olin, J. R. Ohlfest, C. C. Aldrich and D. M. Ferguson, *J. Med. Chem.*, 2014, **57**, 339–347.
44 A. Larange, D. Antonios, M. Pallardy and S. Kerdine-Romer, *J. Leukoc. Biol.*, 2009, **85**, 673–683.

45 B. R. James, E. L. Brincks, T. A. Kucaba, L. Boon and T. S. Griffith, *Cancer Immunol. Immunother.*, 2014, **63**, 685–697.
46 A. Kumari, S. K. Yadav and S. C. Yadav, *Colloids Surfaces B Biointerfaces*, 2010, **75**, 1–18.
47 J. Fang, H. Nakamura and H. Maeda, *Adv. Drug Deliv. Rev.*, 2011, **63**, 136–151.
48 Y. Barenholz, *J. Control. Release*, 2012, **160**, 117–134.
49 J. P. Micha, B. H. Goldstein, C. L. Birk, M. A. Rettenmaier and J. V. Brown, *Gynecol. Oncol.*, 2006, **100**, 437–438.
50 K. Shao, S. Singha, X. Clemente-Casares, S. Tsai, Y. Yang and P. Santamaria, *ACS Nano*, 2015, **9**, 16–30.
51 J. M. Silva, M. Videira, R. Gaspar, V. Préat and H. F. Florindo, *J. Control. Release*, 2013, **168**, 179–199.
52 R. Dinarvand, N. Sepehri, S. Manoochehri, H. Rouhani and F. Atyabi, *Int. J. Nanomedicine*, 2011, **6**, 877–895.
53 H. K. Makadia and S. J. Siegel, *Polymers (Basel).*, 2011, **3**, 1377–1397.
54 C. E. Astete and C. M. Sabliov, *J. Biomater. Sci. Polym. Ed.*, 2006, **17**, 247–289.
55 N. Benne, J. Van Duijn, J. Kuiper, W. Jiskoot and B. Slütter, *J. Control. Release*, 2016, **234**, 124–134.
56 S. Hamdy, A. Haddadi, R. W. Hung and A. Lavasanifar, *Adv. Drug Deliv. Rev.*, 2011, **63**, 943–955.
57 M. F. Bachmann and G. T. Jennings, *Nat. Rev. Immunol.*, 2010, **10**, 787–96.
58 C. Foged, B. Brodin, S. Frokjaer and A. Sundblad, *Int. J. Pharm.*, 2005, **298**, 315–322.
59 J. Panyam and V. Labhasetwar, *Pharm. Res.*, 2003, **20**, 212–220.
60 W. Wang, N. Chen, X. Shen, P. Cunningham, S. Fauty, K. Michel, B. Wang, X. Hong, C. Adreani, C. N. Nunes, C. V. Johnson, K. C. Yin, M. Groff, Y. Zou, L. Liu, L. Hamuro and T. Prueksaritanont, *Drug Metab. Dispos.*, 2012, **40**, 952–962.
61 M. A. Swartz, *Adv. Drug Deliv. Rev.*, 2001, **50**, 3–20.
62 A. Supersaxo, W. R. Hein and H. Steffen, *Pharm. Res.*, 1990, **7**, 167–169.
63 J. Panyam, M. M. Dali, S. K. Sahoo, W. Ma, S. S. Chakravarthi, G. L. Amidon, R. J. Levy and V. Labhasetwar, *J. Control. Release*, 2003, **92**, 173–187.
64 V. Manolova, A. Flace, M. Bauer, K. Schwarz, P. Saudan and M. F. Bachmann, *Eur. J. Immunol.*, 2008, **38**, 1404–1413.
65 L. Jeanbart, M. Ballester, A. de Titta, P. Corthesy, P. Romero, J. A. Hubbell and M. A. Swartz, *Cancer Immunol. Res.*, 2014, **2**, 436–447.
66 M. Kovacsovics-Bankowski, K. Clark, B. Benacerraf and K. L. Rock, *Proc. Natl. Acad. Sci. U. S. A.*, 1993, **90**, 4942–6.
67 M. Diwan, M. Tafaghodi and J. Samuel, *J. Control. Release*, 2002, **85**, 247–262.
68 A. D. Duong, S. Sharma, K. J. Peine, G. Gupta, A. R. Satoskar, E. M. Bachelder, B. E. Wyslouzil and K. M. Ainslie, *Mol. Pharm.*, 2013, **10**, 1045–1055.
69 A. H. Rook, J. C. Gelfand, M. Wysocka, A. B. Troxel, B. Benoit, C. Surber, R. Elenitsas, M. A. Buchanan, D. S. Leahy, R. Watanabe, I. R. Kirsch, E. J. Kim and R. A. Clark, *Blood*, 2015, **126**, 1452–1461.
70 H. Kim, L. Niu, P. Larson, T. A. Kucaba, K. A. Murphy, B. R. James, D. M.

Ferguson, T. S. Griffith and J. Panyam, *Biomaterials*, 2018, **164**, 38–53.
71 I. Melero, G. Gaudernack, W. Gerritsen, C. Huber, G. Parmiani, S. Scholl, N. Thatcher, J. Wagstaff, C. Zielinski, I. Faulkner and H. Mellstedt, *Nat. Rev. Clin. Oncol.*, 2014, **11**, 509–24.
72 H. Kanzler, F. J. Barrat, E. M. Hessel and R. L. Coffman, *Nat. Med.*, 2007, **13**, 552–559.
73 K. B. Gorden, K. S. Gorski, S. J. Gibson, R. M. Kedl, W. C. Kieper, X. Qiu, M. A. Tomai, S. S. Alkan and J. P. Vasilakos, *J. Immunol.*, 2005, **174**, 1259–1268.
74 J. P. Vasilakos and M. A. Tomai, *Expert Rev. Vaccines*, 2013, **12**, 809–819.
75 C. E. Schiaffo, C. Shi, Z. Xiong, M. Olin, J. R. Ohlfest, C. C. Aldrich and D. M. Ferguson, *J. Med. Chem.*, 2014, **57**, 339–347.
76 G. M. Lynn, R. Laga, P. A. Darrah, A. S. Ishizuka, A. J. Balaci, A. E. Dulcey, M. Pechar, R. Pola, M. Y. Gerner, A. Yamamoto, C. R. Buechler, K. M. Quinn, M. G. Smelkinson, O. Vanek, R. Cawood, T. Hills, O. Vasalatiy, K. Kastenmüller, J. R. Francica, L. Stutts, J. K. Tom, K. A. Ryu, A. P. Esser-Kahn, T. Etrych, K. D. Fisher, L. W. Seymour and R. A. Seder, *Nat. Biotechnol.*, 2015, **33**, 1201–1210.
77 S. Hamdy, O. Molavi, Z. Ma, A. Haddadi, A. Alshamsan, Z. Gobti, S. Elhasi, J. Samuel and A. Lavasanifar, *Vaccine*, 2008, **26**, 5046–5057.
78 U. S. Toti, B. R. Guru, M. Hali, C. M. McPharlin, S. M. Wykes, J. Panyam and J. A. Whittum-Hudson, *Biomaterials*, 2011, **32**, 6606–6613.
79 Y. Patil and J. Panyam, *Int. J. Pharm.*, 2009, **367**, 195–203.
80 D. F. Nixon, C. Hioe, P. De Chen, Z. Bian, P. Kuebler, M. L. Li, H. Qiu, X. M. Li, M. Singh, J. Richardson, P. McGee, T. Zamb, W. Koff, C. Y. Wang and D. O'Hagan, *Vaccine*, 1996, **14**, 1523–1530.
81 Y. R. Lee, Y. H. Lee, S. A. Im, I. H. Yang, G. W. Ahn, K. Kim and C. K. Lee, *Arch. Pharm. Res.*, 2010, **33**, 1859–1866.
82 M. D. Chavanpatil, Y. Patil and J. Panyam, *Int. J. Pharm.*, 2006, **320**, 150–156.
83 J. Xiang, L. Xu, H. Gong, W. Zhu, C. Wang, J. Xu, L. Feng, L. Cheng, R. Peng and Z. Liu, *ACS Nano*, 2015, **9**, 6401–6411.
84 J. Davda and V. Labhasetwar, *Int. J. Pharm.*, 2002, **233**, 51–59.
85 K. A. Murphy, B. R. James, A. Wilber and T. S. Griffith, *J. Vis. Exp.*, , DOI:doi:10.3791/55080.
86 G. Trinchieri and A. Sher, *Nat. Rev. Immunol.*, 2007, **7**, 179–90.
87 S. W. Van Gool, P. Vandenberghe, M. de Boer and J. L. Ceuppens, *Immunol. Rev.*, 1996, **153**, 47–83.
88 L. Delamarre, H. Holcombe and I. Mellman, *J. Exp. Med.*, 2003, **198**, 111–122.
89 C. D. Pham, M.-Y. Woo, Y.-S. Kim, S. Park and M.-H. Kwon, *J. Immunol.*, 2012, **189**, 5755–5763.
90 T. R. Mempel, S. E. Henrickson and U. H. von Andrian, *Nature*, 2004, **427**, 154–159.
91 K. A. Casey, K. A. Fraser, J. M. Schenkel, A. Moran, M. C. Abt, L. K. Beura, P. J. Lucas, D. Artis, E. J. Wherry, K. Hogquist, V. Vezys and D. Masopust, *J. Immunol.*, 2012, **188**, 4866–4875.
92 B. S. Parker, J. Rautela and P. J. Hertzog, *Nat. Rev. Cancer*, 2016, **16**, 131–144.

93 L. Martínez-Lostao, A. Anel and J. Pardo, *Clin. Cancer Res.*, 2015, **21**, 5047–5056.
94 F. Aranda, D. Llopiz, N. Díaz-Valdés, J. I. Riezu-Boj, J. Bezunartea, M. Ruiz, M. Martínez, M. Durantez, C. Mansilla, J. Prieto, J. J. Lasarte, F. Borrás-Cuesta and P. Sarobe, *Cancer Res.*, 2011, **71**, 3214–3224.
95 W. W. Overwijk and N. P. Restifo, *Curr Protoc Immunol*, 2001, **Chapter 20**, Unit 20 1.
96 S. M. Kaech, E. J. Wherry and R. Ahmed, *Nat. Rev. Immunol.*, 2002, **2**, 251–262.
97 M. Bellone, D. Cantarella, P. Castiglioni, M. C. Crosti, A. Ronchetti, M. Moro, M. P. Garancini, G. Casorati and P. Dellabona, *J. Immunol.*, 2000, **165**, 2651–2656.
98 S. N. Khleif, S. I. Abrams, J. M. Hamilton, E. Bergmann-Leitner, A. Chen, A. Bastian, S. Bernstein, Y. Chung, C. J. Allegra and J. Schlom, *J. Immunother.*, 1999, 22, 155–65.
99 K. L. Knutson, K. Schiffman and M. L. Disis, *J Clin Invest*, 2001, **107**, 477–484.
100 F. E. Gonzalez, A. Gleisner, F. Falcon-Beas, F. Osorio, M. N. Lopez and F. Salazar-Onfray, *Hum. Vaccin. Immunother.*, 2014, **10**, 3261–3269.
101 D. Coe, C. Addey, M. White, E. Simpson, J. Dyson and J. G. Chai, *Immunology*, 2010, **131**, 556–569.
102 B. Duncan, *J Immunother.*, 2013, **36**, 1–21.
103 D. Rai, N.-L. L. Pham, J. T. Harty and V. P. Badovinac, *J. Immunol.*, 2009, **183**, 7672–7681.
104 M. H. M. G. M. Den Brok, R. P. M. Sutmuller, R. Van Der Voort, E. J. Bennink, C. G. Figdor, T. J. M. Ruers and G. J. Adema, *Cancer Res.*, 2004, **64**, 4024–4029.
105 J. D. Brody, W. Z. Ai, D. K. Czerwinski, J. A. Torchia, M. Levy, R. H. Advani, Y. H. Kim, R. T. Hoppe, S. J. Knox, L. K. Shin, I. Wapnir, R. J. Tibshirani and R. Levy, *J. Clin. Oncol.*, 2010, **28**, 4324–4332.
106 L. A. Norian, T. P. Kresowik, H. M. Rosevear, B. R. James, T. R. Rosean, A. J. Lightfoot, T. A. Kucaba, C. Schwarz, C. J. Weydert, M. D. Henry and T. S. Griffith, *PLoS One*, , DOI:10.1371/journal.pone.0031085.
107 A. Kugler, G. Stuhler, P. Walden, G. Zoller, A. Zobywalski, P. Brossart, U. Trefzer, S. Ullrich, C. A. Muller, V. Becker, A. J. Gross, B. Hemmerlein, L. Kanz, G. A. Muller and R. H. Ringert, *Nat. Med.*, 2003, **9**, 332–336.
108 H. Harlin, Y. Meng, A. C. Peterson, Y. Zha, M. Tretiakova, C. Slingluff, M. McKee and T. F. Gajewski, *Cancer Res.*, 2009, **69**, 3077–3085.
109 P.-L. Lollini, F. Cavallo, P. Nanni and G. Forni, *Nat. Rev. Cancer*, 2006, **6**, 204–216.
110 G. Schuler, B. Schuler-Thurner and R. M. Steinman, *Curr. Opin. Immunol.*, 2003, **15**, 138–147.
111 J. Banchereau and R. M. Steinman, *Nature*, 1998, **392**, 245–252.
112 T. S. Lim, J. K. H. Goh, A. Mortellaro, C. T. Lim, G. J. Hämmerling and P. Ricciardi-Castagnoli, *PLoS One*, , DOI:10.1371/journal.pone.0045185.
113 K. Kastenmüller, U. Wille-reece, R. W. B. Lindsay, L. R. Trager, P. A. Darrah, B. J. Flynn, M. R. Becker, M. C. Udey, B. E. Clausen, B. Z. Igyarto, D. H. Kaplan, W. Kastenmüller, R. N. Germain and R. A. Seder, *J. Clin. Invest.*, 2011, **121**, 23–

25.
114 R. Audran, K. Peter, J. Dannull, Y. Men, E. Scandella, M. Groettrup, B. Gander and G. Corradin, *Vaccine*, 2003, **21**, 1250–1255.
115 P. Nair-Gupta, A. Baccarini, N. Tung, F. Seyffer, O. Florey, Y. Huang, M. Banerjee, M. Overholtzer, P. A. Roche, R. Tampé, B. D. Brown, D. Amsen, S. W. Whiteheart and J. M. Blander, *Cell*, 2014, **158**, 506–521.
116 E. Schlosser, M. Mueller, S. Fischer, S. Basta, D. H. Busch, B. Gander and M. Groettrup, *Vaccine*, 2008, **26**, 1626–1637.
117 S. L. Demento, S. C. Eisenbarth, H. G. Foellmer, C. Platt, M. J. Caplan, W. Mark Saltzman, I. Mellman, M. Ledizet, E. Fikrig, R. A. Flavell and T. M. Fahmy, *Vaccine*, 2009, **27**, 3013–3021.
118 D. M. Smith, J. K. Simon and J. R. Baker, *Nat. Rev. Immunol.*, 2013, **13**, 592–605.
119 P. M. Sondel, I. N. Buhtoiarov and K. DeSantes, *J. Clin. Invest.*, 2003, **112**, 25–27.
120 D. A. Thomas and J. Massagué, *Cancer Cell*, 2005, **8**, 369–380.
121 F. Vianello, N. Papeta, T. Chen, P. Kraft, N. White, W. K. Hart, M. F. Kircher, E. Swart, S. Rhee, G. Palu, D. Irimia, M. Toner, R. Weissleder and M. C. Poznansky, *J. Immunol.*, 2006, **176**, 2902–2914.
122 G. Parmiani, C. Castelli, P. Dalerba, R. Mortarini, L. Rivoltini, F. M. Marincola and A. Anichini, *J. Natl. Cancer Inst.*, 2002, **94**, 805–818.
123 W. Zou, *Nat. Rev. Cancer*, 2005, **5**, 263–274.
124 C. L. L. Chiang, F. Benencia and G. Coukos, *Semin. Immunol.*, 2010, **22**, 132–143.
125 J. H. Günther, A. Jurczok, T. Wulf, S. Brandau, I. Deinert, D. Jocham and A. Böhle, *Cancer Res.*, 1999, **59**, 2834–2837.
126 I. Le Mercier, D. Poujol, A. Sanlaville, V. Sisirak, M. Gobert, I. Durand, B. Dubois, I. Treilleux, J. Marvel, J. Vlach, J. Y. Blay, N. V. Bendriss, C. Caux, I. Puisieux and N. Goutagny, *Cancer Res.*, 2013, **73**, 4629–4640.
127 A. Marabelle, H. Kohrt, C. Caux and R. Levy, *Clin. Cancer Res.*, 2014, **20**, 1747–1756.
128 O. M. Hart, V. Athie-Morales, G. M. O'Connor and C. M. Gardiner, *J. Immunol.*, 2005, **175**, 1636–1642.
129 H. Lu, G. N. Dietsch, M. A. H. Matthews, Y. Yang, S. Ghanekar, M. Inokuma, M. Suni, V. C. Maino, K. E. Henderson, J. J. Howbert, M. L. Disis and R. M. Hershberg, *Clin. Cancer Res.*, 2012, **18**, 499–509.
130 A. Tristram, C. N. Hurt, T. Madden, N. Powell, S. Man, S. Hibbitts, P. Dutton, S. Jones, A. J. Nordin, R. Naik, A. Fiander and G. Griffiths, *Lancet Oncol.*, 2014, **15**, 1361–1368.
131 L. G. Salazar, H. Lu, J. L. Reichow, J. S. Childs, A. L. Coveler, D. M. Higgins, J. Waisman, K. H. Allison, Y. Dang and M. L. Disis, *JAMA Oncol.*, 2017, **8050**, 1–6.
132 J. H. Cho, H. Lee, H. Ko, B. Yoon, K. Kim, T. Hahn, J. A. Han, S. S. Choi, M. Jung, K. Lee, Y. Lee and Y. Jung, *Oncotarget*, 2017, **8**, 24932–24948.
133 S. J. Dovedi, M. H. M. Melis, R. W. Wilkinson, A. L. Adlard, I. J. Stratford, J. Honeychurch and T. M. Illidge, *Blood*, 2013, **121**, 251–259.
134 F. Sato-Kaneko, S. Yao, A. Ahmadi, S. S. Zhang, T. Hosoya, M. M. Kaneda, J. A. Varner, M. Pu, K. S. Messer, C. Guiducci, R. L. Coffman, K. Kitaura, T.

Matsutani, R. Suzuki, D. A. Carson, T. Hayashi and E. E. W. Cohen, *JCI Insight*, , DOI:10.1172/JCI.INSIGHT.93397.
135 A. Wicki, D. Witzigmann, V. Balasubramanian and J. Huwyler, *J. Control. Release*, 2015, **200**, 138–157.
136 D. Bobo, K. J. Robinson, J. Islam, K. J. Thurecht and S. R. Corrie, *Pharm. Res.*, 2016, **33**, 2373–2387.
137 J. M. Anderson and M. S. Shive, *Adv. Drug Deliv. Rev.*, 2012, **64**, 72–82.
138 X. Q. Zhang, C. E. Dahle, N. K. Baman, N. Rich, G. J. Weiner and A. K. Salem, *J. Immunother.*, 2007, **30**, 469–478.
139 Y. Qian, H. Jin, S. Qiao, Y. Dai, C. Huang, L. Lu, Q. Luo and Z. Zhang, *Biomaterials*, 2016, **98**, 171–183.
140 G.-N. Shi, C.-N. Zhang, R. Xu, J.-F. Niu, H.-J. Song, X.-Y. Zhang, W.-W. Wang, Y.-M. Wang, C. Li, X.-Q. Wei and D.-L. Kong, *Biomaterials*, 2017, **113**, 191–202.
141 S. Adams, L. Kozhaya, F. Martiniuk, T. C. Meng, L. Chiriboga, L. Liebes, T. Hochman, N. Shuman, D. Axelrod, J. Speyer, Y. Novik, A. Tiersten, J. D. Goldberg, S. C. Formenti, N. Bhardwaj, D. Unutmaz and S. Demaria, *Clin. Cancer Res.*, 2012, **18**, 6748–6757.
142 C. Primard, J. Poecheim, S. Heuking, E. Sublet, F. Esmaeili and G. Borchard, *Mol. Pharm.*, 2013, **10**, 2996–3004.
143 M. B. Heo and Y. T. Lim, *Biomaterials*, 2014, **35**, 590–600.
144 R. D. Weeratna, S. R. Makinen, M. J. McCluskie and H. L. Davis, *Vaccine*, 2005, **23**, 5263–5270.
145 K. Kastenmüller, U. Wille-Reece, R. W. B. Lindsay, L. R. Trager, P. A. Darrah, B. J. Flynn, M. R. Becker, M. C. Udey, B. E. Clausen, B. Z. Igyarto, D. H. Kaplan, W. Kastenmüller, R. N. Germain and R. A. Seder, *J. Clin. Invest.*, 2011, **121**, 1782–1796.
146 Y. Kawarada, R. Ganss, N. Garbi, T. Sacher, B. Arnold and G. J. Hammerling, *J. Immunol.*, 2001, **167**, 5247–5253.
147 S. Akira and K. Takeda, *Nat. Rev. Immunol.*, 2004, **4**, 499–511.
148 N. Grabowski, H. Hillaireau, J. Vergnaud, N. Tsapis, M. Pallardy, S. Kerdine-Römer and E. Fattal, *Int. J. Pharm.*, 2015, **482**, 75–83.
149 C. J. Ke, W. L. Chiang, Z. X. Liao, H. L. Chen, P. S. Lai, J. S. Sun and H. W. Sung, *Biomaterials*, 2013, **34**, 1–10.
150 J. Panyam, S. K. Sahoo, S. Prabha, T. Bargar and V. Labhasetwar, *Int. J. Pharm.*, 2003, **262**, 1–11.
151 J. Panyam and V. Labhasetwar, *Adv. Drug Deliv. Rev.*, 2003, **55**, 329–347.
152 M. a Dobrovolskaia, P. Aggarwal, J. B. Hall and S. E. Mcneil, *Mol. Pharm.*, 2009, **5**, 487–495.
153 R. J. Ulevitch, *Nat. Rev. Immunol.*, 2004, **4**, 512–20.
154 C. B. Thompson, T. Lindsten, J. A. Ledbetter, S. L. Kunkel, H. A. Young, S. G. Emerson, J. M. Leiden and C. H. June, *Proc. Natl. Acad. Sci.*, 1989, **86**, 1333–1337.
155 P. Guermonprez, J. Valladeau, L. Zitvogel, C. Théry and S. Amigorena, *Annu. Rev. Immunol.*, 2002, **20**, 621–667.

156 D. Dudziak, A. Kampfhorst, G. Heidkamp, V. Buhcholz, C. Trumpfheller, S. Yamazaki, C. Cheong, K. Liu and H. Lee, *Science (80-.).*, 2007, **315**, 107–112.
157 J. M. Schenkel, K. A. Fraser, V. Vezys and D. Masopust, *Nat. Immunol.*, 2013, **14**, 509–513.
158 S. E. Macatonia, N. A. Hosken, M. Litton, P. Vieira, C. S. Hsieh, J. A. Culpepper, M. Wysocka, G. Trinchieri, K. M. Murphy and A. O'Garra, *J. Immunol.* , 1995, **154**, 5071–5079.
159 D. J. Shedlock, *Science (80-.).*, 2003, **300**, 337–339.
160 C. A. Klebanoff, L. Gattinoni, P. Torabi-Parizi, K. Kerstann, A. R. Cardones, S. E. Finkelstein, D. C. Palmer, P. A. Antony, S. T. Hwang, S. A. Rosenberg, T. A. Waldmann and N. P. Restifo, *Proc. Natl. Acad. Sci.*, 2005, **102**, 9571–9576.
161 C. A. Klebanoff, L. Gattinoni and N. P. Restifo, *Immunol. Rev.*, 2006, **211**, 214–224.
162 S. Huet, H. Groux, B. Caillou, H. Valentin, A. M. Prieur, S. Huet, H. Groux, H. Valentin, M. Prieur and A. Bernard, *J. Immunol.*, 1989, **143**, 798–801.
163 F. C. Yang, K. Agematsu, T. Nakazawa, T. Mori, S. Ito, T. Kobata, C. Morimoto and A. Komiyama, *Immunology*, 1996, **88**, 289–293.
164 M. Iqbal, N. Zafar, H. Fessi and A. Elaissari, *Int. J. Pharm.*, 2015, **496**, 173–190.
165 K. F. Pistel, T. Kissel, *J. Microencapsul.*, 2000, **17**, 467–483.
166 Q. Liu, X. Chen, J. Jia, W. Zhang, T. Yang, L. Wang and G. Ma, *ACS Nano*, 2015, **9**, 4925–4938.
167 C. J. Ke, T. Y. Su, H. L. Chen, H. L. Liu, W. L. Chiang, P. C. Chu, Y. Xia and H. W. Sung, *Angew. Chemie - Int. Ed.*, 2011, **50**, 8086–8089.
168 S. Jost, P. J. Tomezsko, K. Rands, I. Toth, M. Lichterfeld, R. T. Gandhi and M. Altfeld, *J. Virol.*, 2014, **88**, 8349–8354.
169 S. J. Szabo, B. M. Sullivan, C. Stemmann, A. R. Satoskar, B. P. Sleckman and L. H. Glimcher, *Science (80-.).*, 2002, **295**, 338–343.
170 S. P. Schoenberger, R. E. M. Toes, E. I. H. Van der Voort, R. Offringa and C. J. M. Melief, *Nature*, 1998, **393**, 480–483.
171 D. L. Farber, M. Luqman, O. Acute and K. Bottomly, *Cell*, 1995, **2**, 249–259.
172 C. H. M. J. Van Elssen, T. Oth, W. T. V Germeraad, G. M. J. Bos and J. Vanderlocht, *Clin. Cancer Res.*, 2014, **20**, 1095–1103.
173 M. A. Degli-Esposti and M. J. Smyth, *Nat. Rev. Immunol.*, 2005, **5**, 112–124.
174 F. Borrego, M. J. Robertson, J. Ritz, J. Peña and R. Solana, *Immunology*, 1999, **97**, 159–165.
175 S. Jung, D. Unutmaz, P. Wong, G. I. Sano, K. De Los Santos, T. Sparwasser, S. Wu, S. Vuthoori, K. Ko, F. Zavala, E. G. Pamer, D. R. Littman and R. A. Lang, *Immunity*, 2002, **17**, 211–220.
176 N.-L. L. Pham, L. L. Pewe, C. J. Fleenor, R. A. Langlois, K. L. Legge, V. P. Badovinac and J. T. Harty, *Proc. Natl. Acad. Sci.*, 2010, **107**, 12198–12203.
177 G. Kroemer, L. Galluzzi, O. Kepp and L. Zitvogel, *Annu. Rev. Immunol.*, 2013, **31**, 51–72.
178 L. Aymeric, L. Apetoh, F. Ghiringhelli, A. Tesniere, I. Martins, G. Kroemer, M. J. Smyth and L. Zitvogel, *Cancer Res.*, 2010, **70**, 855–858.

179 A. Martín-Fontecha, L. L. Thomsen, S. Brett, C. Gerard, M. Lipp, A. Lanzavecchia and F. Sallusto, *Nat. Immunol.*, 2004, **5**, 1260–1265.
180 R. L. Sabado, A. Pavlick, S. Gnjatic, C. Cruz, I. Vengco, F. Hasan, F. Darvishian, L. Chiriboga, R. Holman, J. Escalon, C. Muren, C. Escano, E. Yepes, D. Sharpe, S. Adams, P. Ott, A. Jungbluth, L. Pan, R. Venhaus and N. Bhardwaj, *Cancer Immunol. Res.*, 2015, **3**, 278–287.
181 H. Lu, W. M. Wagner, E. Gad, Y. Yang, H. Duan, L. M. Amon, N. Van Denend, E. R. Larson, A. Chang, H. Tufvesson and M. L. Disis, *J. Immunol.*, 2010, **184**, 5360–5367.
182 T. L. Whiteside, *Oncogene*, 2008, **27**, 5904–5912.
183 Z. Granot and Z. G. Fridlender, *Cancer Res.*, 2015, **75**, 4441–4445.
184 C. Blank, T. F. Gajewski and A. Mackensen, *Cancer Immunol. Immunother.*, 2005, **54**, 307–314.
185 R. Adelaiye, E. Ciamporcero, K. M. Miles, P. Sotomayor, J. Bard, M. Tsompana, D. Conroy, L. Shen, S. Ramakrishnan, S.-Y. Ku, A. Orillion, J. Prey, G. Fetterly, M. Buck, S. Chintala, G. A. Bjarnason and R. Pili, *Mol. Cancer Ther.*, 2015, **14**, 513–522.
186 J. S. Ko, A. H. Zea, B. I. Rini, J. L. Ireland, P. Elson, P. Cohen, A. Golshayan, P. A. Rayman, L. Wood, J. Garcia, R. Dreicer, R. Bukowski and J. H. Finke, *Clin. Cancer Res.*, 2009, **15**, 2148–2157.
187 H. Xin, C. Zhang, A. Herrmann, Y. Du, R. Figlin and H. Yu, *Cancer Res.*, 2009, **69**, 2506–2513.
188 K. Abiko, N. Matsumura, J. Hamanishi, N. Horikawa, R. Murakami, K. Yamaguchi, Y. Yoshioka, T. Baba, I. Konishi and M. Mandai, *Br. J. Cancer*, 2015, **112**, 1501–1509.
189 S. M. Mangsbo, L. C. Sandin, K. Anger, A. J. Korman, A. Loskog and T. H. Tötterman, *J. Immunother.*, 2010, **33**, 225–235.
190 P. Loke and J. P. Allison, *Proc. Natl. Acad. Sci.*, 2003, **100**, 5336–5341.
191 T. Spinetti, L. Spagnuolo, I. Mottas, C. Secondini, M. Treinies, C. Rüegg, C. Hotz and C. Bourquin, *Oncoimmunology*, 2016, **5**, 1–8.
192 B. K. Jha, B. Dong, C. T. Nguyen, I. Polyakova and R. H. Silverman, *Mol. Ther.*, 2013, **21**, 1749–1757.
193 N. Nishii, H. Tachinami, Y. Kondo, Y. Xia, Y. Kashima, T. Ohno, S. Nagai, L. Li, W. Lau, H. Harada and M. Azuma, *Oncotarget*, 2018, **9**, 13301–13312.
194 A. J. Vandeveer, J. K. Fallon, R. Tighe, H. Sabzevari, J. Schlom and J. W. Greiner, *Cancer Immunol. Res.*, 2016, **4**, 452–462.
195 M. Z. Dewan, C. Vanpouille-Box, N. Kawashima, S. DiNapoli, J. S. Babb, S. C. Formenti, S. Adams and S. Demaria, *Clin. Cancer Res.*, 2012, **18**, 6668–6678.
196 B. J. G. Baaten, C. R. Li, M. F. Deiro, M. M. Lin, P. J. Linton and L. M. Bradley, *Immunity*, 2010, **32**, 104–115.
197 D. Rai, N.-L. L. Pham, J. T. Harty and V. P. Badovinac, *J. Immunol.*, 2009, **183**, 7672–7681.
198 J. Panyam, D. William, A. Dash, D. Leslie-Pelecky and V. Labhasetwar, *J. Pharm. Sci.*, 2004, **93**, 1804–1814.

199 J. C. Parker, S. Gilchrist and J. T. Cartledge, *J. Appl. Physiol.*, 1985, **59**, 1128–1136.
200 G. T. Ğoŕgun, G. Whitehill, J. L. Anderson, T. Hideshima, C. Maguire, J. Laubach, N. Raje, N. C. Munshi, P. G. Richardson and K. C. Anderson, *Blood*, 2013, **121**, 2975–2987.
201 D. I. Gabrilovich and S. Nagaraj, *Nat. Rev. Immunol.*, 2009, **9**, 162–174.
202 A. Bose, J. L. Taylor, S. Alber, S. C. Watkins, J. A. Garcia, B. I. Rini, J. S. Ko, P. A. Cohen, J. H. Finke and W. J. Storkus, *Int. J. Cancer*, 2011, **129**, 2158–2170.
203 O. Draghiciu, H. W. Nijman, B. N. Hoogeboom, T. Meijerhof and T. Daemen, *Oncoimmunology*, 2015, **4**, 1–11.
204 N. Gao, J. Zhong, X. Wang, Z. Jin, W. Li, Y. Liu, Y. Diao, Z. Wang, W. Jiang and G. Jin, *Sci. Rep.*, 2016, **6**, 39598.
205 M. M. Hipp, N. Hilf, S. Walter, D. Werth, K. M. Brauer, M. P. Radsak, T. Weinschenk, H. Singh-jasuja and P. Brossart, *Blood*, 2008, **111**, 5610–5620.
206 A. Wongkajornsilp, V. Wamanuttajinda, K. Kasetsinsombat, S. Duangsa-ard, K. Sa-ngiamsuntorn and K. M. Suradej Hongeng, *PLoS One*, 2013, **8**, 1–9.
207 M. Mandai, J. Hamanishi, K. Abiko, N. Matsumura, T. Baba and I. Konishi, *Clin. Cancer Res.*, 2016, **22**, 2329–2334.
208 T. Iwata, Y. Kondo, O. Kimura, T. Morosawa, Y. Fujisaka, T. Umetsu, T. Kogure, J. Inoue, Y. Nakagome and T. Shimosegawa, *Sci. Rep.*, 2016, **6**, 1–11.
209 R. J. Davis, E. C. Moore, P. E. Clavijo, J. Friedman, H. Cash, Z. Chen, C. Silvin, C. Van Waes and C. Allen, *Cancer Res.*, 2017, **77**, 2607–2619.
210 J. R. Brahmer, S. S. Tykodi, L. Q. M. Chow, W.-J. Hwu, S. L. Topalian, P. Hwu, C. G. Drake, L. H. Camacho, J. Kauh, K. Odunsi, H. C. Pitot, O. Hamid, S. Bhatia, R. Martins, K. Eaton, S. Chen, T. M. Salay, S. Alaparthy, J. F. Grosso, A. J. Korman, S. M. Parker, S. Agrawal, S. M. Goldberg, D. M. Pardoll, A. Gupta and J. M. Wigginton, *N. Engl. J. Med.*, 2012, **366**, 2455–2465.
211 J. Naidoo, D. B. Page, B. T. Li, L. C. Connell, K. Schindler, M. E. Lacouture, M. A. Postow and J. D. Wolchok, *Ann. Oncol.*, 2015, **26**, 2375–2391.
212 R. W. Jenkins, D. A. Barbie and K. T. Flaherty, *Br. J. Cancer*, 2018, **118**, 9–16.
213 R. Pirker, J. R. Pereira, J. Von Pawel, M. Krzakowski, R. Ramlau, K. Park, F. De Marinis, W. E. E. Eberhardt, L. Paz-Ares, S. Störkel, K. M. Schumacher, A. Von Heydebreck, I. Celik and K. J. O'Byrne, *Lancet Oncol.*, 2012, **13**, 33–42.
214 M. Cheng, Y. Chen, W. Xiao, R. Sun and Z. Tian, *Cell. Mol. Immunol.*, 2013, **10**, 230–252.
215 M. J. Smyth, Y. Hayakawa, K. Takeda and H. Yagita, *Nat. Rev. Cancer*, 2002, **2**, 850.
216 M. Moreno, B. M. Mol, S. von Mensdorff-Pouilly, R. H. M. Verheijen, B. M. E. von Blomberg, A. J. M. van den Eertwegh, R. J. Scheper and H. J. Bontkes, *Cancer Lett.*, 2008, **272**, 70–76.
217 E. M. Bertino, E. L. McMichael, X. Mo, P. Trikha, M. Davis, B. Paul, M. Grever, W. E. Carson and G. A. Otterson, *Mol. Cancer Ther.*, 2016, **15**, 2244–2250.
218 J. J. Wheler, A. M. Tsimberidou, G. S. Falchook, R. G. Zinner, D. S. Hong, J. Y. Fok, S. Fu, S. A. Piha-Paul, A. Naing and R. Kurzrock, *Mol. Cancer Ther.*, 2013,

12, 2167–2175.
219 R. Shimizu, J. Kikuchi, T. Wada, K. Ozawa, Y. Kano and Y. Furukawa, *Leukemia*, 2010, **24**, 1760–1768.
220 I. S. Nijhof, R. W. J. Groen, H. M. Lokhorst, B. van Kessel, A. C. Bloem, J. van Velzen, R. de Jong-Korlaar, H. Yuan, W. A. Noort, S. K. Klein, A. C. M. Martens, P. Doshi, K. Sasser, T. Mutis and N. W. C. J. van de Donk, *Leukemia*, 2015, **29**, 2039–2049.
221 L. Zamai, C. Ponti, P. Mirandola, G. Gobbi, S. Papa, L. Galeotti, L. Cocco and M. Vitale, *J. Immunol.*, 2007, **178**, 4011–4016.
222 N. C. Fernandez, A. Lozier, C. Flament, P. Ricciardi-Castagnoli, D. Bellet, M. Suter, M. Perricaudet, T. Tursz, E. Maraskovsky and L. Zitvogel, *Nat. Med.*, 1999, **5**, 405–411.
223 H. Lu, Y. Yang, E. Gad, C. Inatsuka, C. A. Wenner, M. L. Disis and L. J. Standish, *Clin. Cancer Res.*, 2011, **17**, 6742–6753.
224 R. Charlebois, B. Allard, D. Allard, L. Buisseret, M. Turcotte, S. Pommey, P. Chrobak and J. Stagg, *Cancer Res.*, 2017, **77**, 312–319.
225 R. Houot, H. E. Kohrt, A. Marabelle and R. Levy, *Trends Immunol.*, 2011, **32**, 510–516.
226 K. S. Gorski, E. L. Waller, J. Bjornton-Severson, J. A. Hanten, C. L. Riter, W. C. Kieper, K. B. Gorden, J. S. Miller, J. P. Vasilakos, M. A. Tomai and S. S. Alkan, *Int. Immunol.*, 2006, **18**, 1115–1126.
227 C. M. Lim, R. Stephenson, A. M. Salazar and R. L. Ferris, *Oncoimmunology*, , DOI:10.4161/onci.24677.
228 B. R. Lauwerys, N. Garot, J.-C. Renauld and F. A. Houssiau, *J. Immunol.*, 2000, **165**, 1847–1853.
229 J. Clausen, B. Vergeiner, M. Enk, A. L. Petzer, G. Gastl and E. Gunsilius, *Immunobiology*, 2003, **207**, 85–93.
230 Y. T. Bryceson, M. E. March, D. F. Barber, H.-G. Ljunggren and E. O. Long, *J. Exp. Med.*, 2005, **202**, 1001–1012.
231 L. Fischer, O. Penack, C. Gentilini, A. Nogai, A. Muessig, E. Thiel and L. Uharek, *Exp. Hematol.*, 2006, **34**, 753–759.
232 G. Alter, J. M. Malenfant and M. Altfeld, *J. Immunol. Methods*, 2004, **294**, 15–22.
233 K. Krzewski, A. Gil-krzewska, V. Nguyen, G. Peruzzi, J. E. Coligan, W. Dc, K. Krzewski, A. Gil-krzewska, V. Nguyen, G. Peruzzi and J. E. Coligan, *Immunobiology*, 2013, **121**, 4672–4683.
234 D. Sancho, M. Gómez and F. Sánchez-Madrid, *Trends Immunol.*, 2005, **26**, 136–140.
235 A. Thielens, E. Vivier and F. Romagné, *Curr. Opin. Immunol.*, 2012, **24**, 239–245.
236 A. Garcia-Lora, I. Algarra and F. Garrido, *J. Cell. Physiol.*, 2003, **195**, 346–355.
237 W. H. Yeap, K. L. Wong, N. Shimasaki, E. C. Y. Teo, J. K. S. Quek, H. X. Yong, C. P. Diong, A. Bertoletti, Y. C. Linn and S. C. Wong, *Sci. Rep.*, , DOI:10.1038/srep34310.
238 E. Hatjiharissi, L. Xu, D. D. Santos, Z. R. Hunter, B. T. Ciccarelli, M. Modica, Y. Cao, R. J. Manning, X. Leleu, E. a Dimmock, A. Kortsaris, C. Mitsiades, K. C.

Anderson, E. a Fox, P. Steven, S. Verselis and S. P. Treon, *Blood*, 2012, **110**, 2561–2564.
239 W. Walker, M. Aste-Amezaga, R. a Kastelein, G. Trinchieri and C. A. Hunter, *J. Immunol.*, 1999, **162**, 5894–901.
240 S. Sivori, M. Falco, M. D. Chiesa, S. Carlomagno, M. Vitale, L. Moretta and A. Moretta, *Proc. Natl. Acad. Sci.*, 2004, **101**, 10116–10121.
241 P. André, R. Castriconi, M. Espéli, N. Anfossi, T. Juarez, S. Hue, H. Conway, F. Romagné, A. Dondero, M. Nanni, S. Caillat-Zucman, D. H. Raulet, C. Bottino, E. Vivier, A. Moretta and P. Paul, *Eur. J. Immunol.*, 2004, **34**, 961–971.
242 R. M. Srivastava, S. C. Lee, P. A. Andrade Filho, C. A. Lord, H. B. Jie, H. C. Davidson, A. López-Albaitero, S. P. Gibson, W. E. Gooding, S. Ferrone and R. L. Ferris, *Clin. Cancer Res.*, 2013, **19**, 1858–1872.
243 J. Chu, Y. Deng, D. M. Benson, S. He, T. Hughes, J. Zhang, Y. Peng, H. Mao, L. Yi, K. Ghoshal, X. He, S. M. Devine, X. Zhang, M. A. Caligiuri, C. C. Hofmeister and J. Yu, *Leukemia*, 2014, **28**, 917–927.
244 K. Schönfeld, C. Sahm, C. Zhang, S. Naundorf, C. Brendel, M. Odendahl, P. Nowakowska, H. Bönig, U. Köhl, S. Kloess, S. Köhler, H. Holtgreve-Grez, A. Jauch, M. Schmidt, R. Schubert, K. Kühlcke, E. Seifried, H. G. Klingemann, M. A. Rieger, T. Tonn, M. Grez and W. S. Wels, *Mol. Ther.*, 2015, **23**, 330–338.
245 Z. B. Davis, D. A. Vallera, J. S. Miller and M. Felices, *Semin. Immunol.*, 2017, **31**, 64–75.
246 S. G. Park, Z. Jiang, E. D. Mortenson, L. Deng, O. Radkevich-Brown, X. Yang, H. Sattar, Y. Wang, N. K. Brown, M. Greene, Y. Liu, J. Tang, S. Wang and Y. X. Fu, *Cancer Cell*, 2010, **18**, 160–170.
247 R. M. Stephenson, C. M. Lim, M. Matthews, G. Dietsch, R. Hershberg and R. L. Ferris, *Cancer Immunol. Immunother.*, 2013, **62**, 1347–1357.
248 B. Boyerinas, C. Jochems, M. Fantini, C. R. Heery, J. L. Gulley, K. Y. Tsang and J. Schlom, *Cancer Immunol. Res.*, 2015, **3**, 1148–1157.
249 L. Ding, J. Ren, D. Zhang, Y. Li, X. Huang, J. Ji, Q. Hu, H. Wang, Y. Ni and Y. Hou, *Mol. Cancer Ther.*, 2017, **16**, 1068–1079.